Summer 2014

Light off temperature based approach to determine diesel oxidation catalyst effectiveness level and the corresponding outlet NO and NO2 characteristics

Prateek Tayal
Purdue University

Graduate School ETD Form 9
(Revised 01/14)

PURDUE UNIVERSITY
GRADUATE SCHOOL
Thesis/Dissertation Acceptance

This is to certify that the thesis/dissertation prepared

By Prateek Tayal

Entitled
Light-Off Temperature Based Approach to Determine Diesel Oxidation Catalyst Effectiveness Level and the Corresponding Outlet NO and NO2 Characteristics.

For the degree of Master of Science in Mechanical Engineering

Is approved by the final examining committee:

Peter H. Meckl

Galen B. King

Gregory M. Shaver

To the best of my knowledge and as understood by the student in the *Thesis/Dissertation Agreement. Publication Delay, and Certification/Disclaimer (Graduate School Form 32)*, this thesis/dissertation adheres to the provisions of Purdue University's "Policy on Integrity in Research" and the use of copyrighted material.

Peter H. Meckl

Approved by Major Professor(s): _____

_____

Approved by: David Anderson 06/27/2014

Head of the Department Graduate Program Date

LIGHT OFF TEMPERATURE BASED APPROACH TO DETERMINE DIESEL OXIDATION CATALYST EFFECTIVENESS LEVEL AND THE CORRESPONDING OUTLET NO AND NO_2 CHARACTERISTICS

A Thesis

Submitted to the Faculty

of

Purdue University

by

Prateek Tayal

In Partial Fulfillment of the

Requirements for the Degree

of

Master of Science in Mechanical Engineering

August 2014

Purdue University

West Lafayette, Indiana

This thesis is dedicated to my Family for their never ending support.

ACKNOWLEDGEMENTS

Dr. Meckl, I thank you for your guidance and perseverance towards me and the project, even when I was lagging behind. Keqin Zhou, I thank you for your confidence in my experimenting abilities and for enriching my knowledge base regarding the project material. I thank Kyle Wright for letting us use the facilities at Alcoa in Lafayette multiple times for the project purpose, free of charge. I thank Raymond Sutjiono and Ryan Schultz for being great sources of information regarding the project. I would also like to thank James Burrell and Mark Peckham of Cambustion, Inc. for patiently listening to my queries and concerns, and answering them every time. Lastly, this effort would not have been a success without help from the wonderful guys at the Herrick Labs shop: Bob Brown, Frank Lee, Gilbert Gordon and Ron. Thank you for sharing your experience with me, it definitely helped me perform better.

TABLE OF CONTENTS

Page

LIST OF TABLES vii

LIST OF FIGURES ix

LIST OF ABBREVIATIONS xvi

ABSTRACT xviii

CHAPTER 1. INTRODUCTION 1
1.1 Motivation 1
1.2 Diesel Engine Fundamentals 2
1.3 After-Treatment System Introduction 4
1.3.1 Three-Way Catalyst (TWC) for Gasoline Engines 5
1.3.2 Diesel Engine After-Treatment Systems 6
1.4 Effect of Vehicular Emission on the Environment 7
1.4.1 Carbon Monoxide 7
1.4.2 Oxides of Nitrogen (NO and NO_2) 8
1.4.3 Unburnt Hydrocarbons (UHC) 8
1.4.4 Particulate Matter 8
1.5 Emission Regulations 9
1.6 Diesel Engine After-treatment System Configuration 11
1.7 Fundamentals of Catalysts and Catalysis 12
1.7.1 Reactions with Catalysis 12
1.7.2 Catalytic Convertors: Structure and Construction 15
1.7.3 Heterogeneous Catalysis 19
1.7.4 Catalyst Light Off 20
1.7.5 Catalyst Deactivation 21
1.8 The Diesel Oxidation Catalyst (DOC) 24
1.8.1 Functionality 25
1.8.2 Design and Operation 26
1.9 Catalyzed Diesel Particulate Filter (CDPF) 28
1.10 Selective Catalytic Reduction (SCR) System 29

Page

1.11 Problem Definition 32
1.11.1 NOx Regulation 32
1.11.2 Purpose of the Project 32
1.12 Document Organization 33
1.13 Contributions to the Project 34

CHAPTER 2. LITERATURE REVIEW 35
2.1 SCR Performance Dependence on NO_x Content 35
2.2 Aging Effect on DOC Performance 38
2.2.1 Substantiating DOC Aging Level 40
2.3 Light Off Based Strategies to Understand DOC Effectiveness Level .. 41

CHAPTER 3. EXPERIMENTAL SETUP 44
3.1 Overview of the Hardware Setup 44
3.2 Data Measurement and Acquisition 48
3.3 Emissions Analyzers 50
3.3.1 Cambustion HFR500 HC Analyzer 51
3.3.2 fNO_X 400 NO_x Measurement System 52
3.4 DOC Aging Procedure 54

CHAPTER 4. DIRECT AND INDIRECT HYDROCARBON LIGHT OFF TEMPERATURE DETERMINATION FOR A DOC AND EFFECT OF AGING ON LIGHT OFF 55
4.1 Experimental Method to Determine HC Light Off for a DOC 55
4.1.1 Introduction 55
4.1.2 Procedure 56
4.1.3 Results and Analysis 57
4.2 Indirect Method to Determine Light Off Temperature for a DOC 61
4.2.1 Introduction 61
4.2.2 Development of the Model 62
4.2.3 Reducing Input Parameters for Practicality 73
4.3 Effect of Thermal Aging on Light Off Temperature and Conversion .75
4.3.1 Aging Level 2 vs. Aging Level 3 76
4.3.2 Aging Level 2 vs. Aging Level 4 77
4.3.3 Aging level 3 vs. Aging level 4 79
4.4 Validation of Assumptions 85
4.4.1 Assumption of NO Conversion Being Minimal for the Light Off Experiments 85
4.4.2 HC Adsorption in the DOC at Cold Start of the Engine 87

CHAPTER 5. DOC OUTLET NO AND NO2 CHARACTERISTICS AND THE EFFECT OF THERMAL AGING ON CONCENTRATION 90

Page
5.1 Experimental Method to Determine NO and NO2 Concentration ... 90
5.1.1 Introduction ... 90
5.1.2 Design of Experiments ... 91
5.2 Development of Model to Determine DOC out NO and NO_2 Concentration ... 92
5.2.1 Modeling Procedure ... 92
5.2.2 Modeling Applied to Aging Level 4 ... 96
5.2.3 Effect of Aging on Kp ... 109
5.2.4 Effect of Using Engine Out Oxygen sensor for Calculations ... 109

CHAPTER 6. CONCLUSIONS AND FUTURE WORK ... 111
6.1 Conclusions ... 114
6.2 Future Work ... 115

LIST OF REFERENCES ... 117

LIST OF TABLES

Table Page

Table 1.1US Emission Standard for Heavy Duty Diesel Engines [10] 10

Table 3.1 Engine Specifications 46

Table 3.2 Dynamometer Specifications 46

Table 3.3 DOC Properties 46

Table 3.4 Cambustion HFR500 Specifications 51

Table 3.5. DOC Aging Procedure 54

Table 4.1Engine Operating Points for DOC Light-off Temperature Experiments. 57

Table 4.2Direct and Indirect Light Off Temperature Comparison between Aging Levels 2 and 3 77

Table 4.3Direct and Indirect Light Off Temperature Comparison between Aging Levels 2 and 4 78

Table 4.4Direct and Indirect Light Off Temperature Comparison between Aging Levels 3 and 4 81

Table 5.1Table showing the data points used to develop the model for the second aging level DOC Table 5.1 continued. 94

Table 5.2 Parameters Obtained for the Second Aging Level Model 95

Table Page

Table 5.3 Data Points used to develop the model for the fourth aging level DOC 97

Table 5.4 Parameters Obtained for the Fourth Aging Level Model 98

LIST OF FIGURES

Figure Page

Figure 1.1. A Three Way Catalyst (TWC) Schematic [9]. 5

Figure 1.2. General Aftertreatment Configuration for a Diesel Engine. 12

Figure 1.3. Activation Energy for Oxidation Of CO To CO_2 with Catalytic Reaction [9]. 14

Figure 1.4. Conversion of CO Comparison with and without a Catalyst [9]..... 15

Figure 1.5. Automotive Packed Bed Reactor. 16

Figure 1.6. Schematic of Catalytic Sites Dispersed on a High Surface Area Al_2O_3 Carrier Bonded to a Monolith Support [9].....17

Figure 1.7. An Actual Microscopic side view Picture of the Catalyst [27]. 17

Figure 1.8. The Step Diagram of Catalytic Heterogeneous Reaction in Catalyst [14]. 20

Figure 1.9. Decay by Sintering Causing Pore Closure [14]. 21

Figure 1.10. Decay by Sintering Resulting in Agglomeration of Deposited Metal Sites. This is the TEM of Fresh and Sintered Pt on Al_2O_3. The Left Picture Shows Very Small and Dispersed Pt, and in the Right Picture, the Pt Experiences Crystalline Growth [9]. 22

Figure 1.11. Schematic of Decay by Coking [14].....22

Figure Page

Figure 1.12. DOC Schematic. 24

Figure 1.13. Schematic of a CDPF Depicting Gas Flow from the Inlet to the Outlet Channel through Pores in the DPF Substrate, while the Soot Particles are Accumulated in the Inlet Channels. 28

Figure 1.14. Schematic of a Single CDPF Channel Showing the Alternate Open and Closed Pathways. 29

Figure 1.15. Schematic of a Selective Catalytic Reduction System. 30

Figure 2.1. Experimental Results of NO_2 /NO_x vs NO_x. The Model Illustrates An Exponential Decay Between NO_2/NO_x and NO_x Concentration [33]. 37

Figure 2.2. Continuous Stirred Tank Reactor (CSTR) Model [34]. 38

Figure 2.3. Comparison of CO, NO and HC oxidation rates for a typical Diesel Oxidation Catalyst[34]. 39

Figure 4.1. Figure showing the upstream and downstream HC concentration as the reaction proceeds for Aged level 3, 1200 RPM-150 lb-ft. 59

Figure 4.2. Figure showing the temperature values at inlet and outlet of the DOC as well as averaged temperature at the three axial locations as the reaction proceeds for Aged level 3, 1200 RPM-150 lb-ft. 60

Figure 4.3. Figure showing the Direct conversion efficiency trend for the DOC at Aged level 3, 1200 RPM-150 lb-ft. Notice the negative value of conversion at start of fuel injection. 61

Figure 4.4. 1D Differential Control Volume for the solid [46]. 63

Figure Page

Figure 4.5. 1D Differential Control Volume for Exhaust Gas Flow [46]. 65

Figure 4.6. Plug Flow Reactor (PFR) Model. 67

Figure 4.7. Figure showing the direct and indirect conversion efficiencies for the DOC at Aged level 3, 1200 RPM-150 lb-ft. 70

Figure 4.8. Figure showing the direct and indirect conversion efficiencies for the DOC at Aged level 3, 1400 RPM-300 lb-ft. 71

Figure 4.9. Figure showing the heat rate comparison for the DOC at Aged level 3, 1200 RPM-150 lb-ft. 72

Figure 4.10. Figure showing the heat rate comparison for the DOC at Aged level 3, 1400 RPM-300 lb-ft. 73

Figure 4.11. Figure showing the axial locations of the thermocouples. 74

Figure 4.12. Indirect Conversion Efficiency Calculated Using Reduced Number of TCs. 75

Figure 4.13. Figure showing the conversion efficiency comparison between the DOC at aged level 2 and aged level 3 for the 1200 rpm 300 lb-ft case. 76

Figure 4.14. Figure showing the conversion efficiency comparison between the DOC at aged level 2 and aged level 3 for the 1400 rpm 300 lb-ft case. 77

Figure 4.15. Figure showing the conversion efficiency comparison between the DOC at aged level 2 and aged level 4 for the 1200 rpm 300 lb-ft case. 78

Figure 4.16. Figure showing the conversion efficiency comparison between the DOC at aged level 3 and aged level 4 for the 1200 rpm 300 lb-ft case. 79

Figure Page

Figure 4.17. Figure showing the conversion efficiency comparison between the DOC at aged level 3 and aged level 4 for the 1400 rpm 300 lb-ft case. 80

Figure 4.18. Figure showing the conversion efficiency comparison between the DOC at aged level 3 and aged level 4 for the 1800 rpm 300 lb-ft case. 81

Figure 4.19. Figure showing the comparison between the Direct light off temperatures from the degreened DOC to aging level 4. Numbers 1-7 denote engine set points according to Table 4.4. 82

Figure 4.20. Figure showing the comparison between the Indirect light off temperatures from the degreened DOC to aging level 4. Numbers 1-7 denote engine set points according to Table 4.4. 83

Figure 4.21. Indirect Light Off Temperature vs. Direct Light Off Temperature Error plot for the Aging Level 2 DOC. 84

Figure 4.22Indirect Light Off Temperature vs. Direct Light Off Temperature Error plot for the Aging Level 3 DOC. 84

Figure 4.233. Indirect Light Off Temperature vs. Direct Light Off Temperature Error plot for the Aging Level 4 DOC. 85

Figure 5.1. Figure Showing the Overall Functionality of the Mathematical Model.....93

Figure 5.2. Figure Showing Gaussian Distribution Fitting the Measured Data.....

.....95

Figure Page

Figure 5.3. Figure Showing Gaussian Distribution Fitting the Measured Data for Aging Level 4. 98

Figure 5.4. NO real vs. NO model for the DOC at aging level 4, 1200 rpm case. 99

Figure 5.5. NO model vs. NO real at Aging Level 4, 1200 rpm, error plot. 99

Figure 5.6. NO2 real vs. NO_2 model for the DOC at aging level 4, 1200 rpm case. 100

Figure 5.7. NO_2 model vs. NO_2 real at Aging Level 4, 1200 rpm, error plot. 100

Figure 5.8. NO real vs. NO model for the DOC at aging level 4, 1350 rpm case. 101

Figure 5.9. NO model vs. NO real at Aging Level 4, 1350 rpm, error plot. 101

Figure 5.10. NO_2 real vs. NO_2 model for the DOC at aging level 4, 1350 rpm case. 102

Figure 5.11. NO_2 model vs. NO_2 real at Aging Level 4, 1350 rpm, error plot. 102

Figure 5.12. NO real vs. NO model for the DOC at aging level 4, 1500 rpm case. 103

Figure 5.13. NO real vs. NO model for the DOC at aging level 4, 1500 rpm case, error plot. 103

Figure 5.14. NO_2 real vs. NO_2 model for the DOC at aging level 4, 1500 rpm case. 104

Figure Page

Figure 5.15. NO_2 real vs. NO_2 model for the DOC at aging level 4, 1500 rpm case, error plot. 104

Figure 5.16. NO real vs. NO model for the DOC at aging level 4, 1650 rpm case. 105

Figure 5.17. NO real vs. NO model for the DOC at aging level 4, 1650 rpm case, error plot. 105

Figure 5.18. NO_2 real vs. NO_2 model for the DOC at aging level 4, 1650 rpm case. 106

Figure 5.19. NO_2 real vs. NO_2 model for the DOC at aging level 4, 1650 rpm case, error plot. 106

Figure 5.20. NO real vs. NO model for the DOC at aging level 4, 1800 rpm case. 107

Figure 5.21. NO real vs. NO model for the DOC at aging level 4, 1800 rpm case, error plot. 107

Figure 5.22. NO_2 real vs. NO_2 model for the DOC at aging level 4, 1800 rpm case. 108

Figure 5.23. NO_2 real vs. NO_2 model for the DOC at aging level 4, 1800 rpm case, error plot. 108

Figure 5.24. Comparison of K_P Values between the Three Aging Levels of the DOC. 109

Figure Page

Figure 5.25. Comparison between the NO concentration results obtained by assuming constant O_2 concentration (Left) and by using the O_2 sensor values (Right) for the 1200 rpm set point. 110

LIST OF ABBREVIATIONS

ADC	Analog to Digital Conversion
CAN	Controller Area Network
CARB	California Air Resources Board
CDPF	Catalyzed Diesel Particulate Filter
CI	Compression Ignition
CO	Carbon Monoxide
CSTR	Continuous Stirred-Tank Reactor
DOC	Diesel Oxidation Catalyst
ECM	Engine Control Module
EGR	Exhaust Gas Recirculation
EPA	Environmental Protection Agency
GWR	Gross Weight Rating
H_2O	Water
HC	Hydrocarbon
HD	Heavy Duty
ISB	Cummins Interact System B Engine
LDD	Light-Duty Diesel
LHDDE	Light Heavy Duty Diesel Engine
N_2	Nitrogen
NH_3	Ammonia
NO	Nitric Oxide
NO_2	Nitric Dioxide
NO_x	Nitrogen Oxide ($NO+NO_2$)

Pd	Palladium
PFR	Plug-Flow Reactor
PGM	Platinum Group Metal
PM	Particulate Matter
Pt	Platinum
Rh	Rhodium
RPM	Rotation Per Minute
SCR	Selective Catalytic Reduction
TWC	Three-Way Catalyst
VGT	Variable-Geometry Turbocharger

ABSTRACT

Tayal, Prateek M.S.M.E., Purdue University, August 2014. Light-Off Temperature Based Approach to Determine Diesel Oxidation Catalyst Effectiveness Level and the Corresponding Outlet NO and NO_2 Characteristics. Major Professor: Peter H. Meckl, School of Mechanical Engineering.

According to the latest EPA emission regulations, the NO_x (Nitrogen oxide compounds) emissions from heavy duty compression ignition engines need to see a dramatic reduction. The current technology used for this purpose is the selective catalytic reduction (SCR) system, which achieves NO_x reduction of around 90% [9]. This involves urea injection which is influenced by the NO: NO2 ratio at the inlet to the SCR. Thus, the role of the DOC (Diesel Oxidation Catalyst) where most of the oxidation of the NO_x compounds takes place, comes to fore. The focus is also on the effectiveness of the catalyst as it thermally ages. Therefore, the aim of this research project is to correlate the aging in the DOC with the light off temperature of the catalyst and subsequent variation in the NO and NO_2 concentration at the outlet of the DOC. This shall be achieved through means of a model developed after extensive experimental procedures. Also, further exhaustive experiments to validate the model over multiple aging cycles of the catalyst shall be undertaken.

The DOC was subjected to 2 rigorous kinds of experiments aimed at determining the light off temperature shift as the catalyst aged and to determine the NO and NO2 concentrations at the DOC outlet as it aged. Exhaust stream compounds were measured

using exhaust analyzers and DOC temperatures were determined using thermocouples installed inside the DOC and at its inlet and outlet.

The data thus obtained was then analyzed and 2 separate models were developed, one for the light off experiments, and the other for the NO_x experiments. Aging procedures were carried out at an oven according to prescribed techniques and the DOC was subjected to similar experiments again. Analysis was carried out on the data. From the light off experiments and the model analysis, a clear positive shift in light off temperatures was observed from one aging level to another across the range of set points. It was also observed that even after subjecting the DOC to three thermal aging exercises, its conversion efficiency went up to 90%. Also, as the DOC aged, the NO concentration at the DOC outlet showed a downward trend which was observed across the spectrum of engine set points and aging levels. These experiments were repeated for consistency so that the models could be rendered more useful.

CHAPTER 1. INTRODUCTION

1.1 Motivation

The Diesel Oxidation Catalyst (DOC) is responsible for reducing the carbon monoxide and unburnt hydrocarbons by oxidizing them as well as to convert NO to NO_2 in order to provide feed gas for the Selective Catalytic Reduction (SCR) system downstream of the DOC and the Diesel Particulate Filter (DPF). The SCR system reduces the NO and NO_2 in the exhaust stream to N_2 before the emissions exit out into the environment through the tailpipe. The DOC is also responsible for the regeneration of the DPF at a lower temperature. However, the DOC ages thermally with extended use, just like other oxidation catalysts. This leads to a reduced conversion of CO and unburnt hydrocarbons. In addition, the NO: NO_2 ratio at the DOC outlet starts to get skewed such that NO_x reduction in the SCR system starts getting affected. This also means that a higher temperature or a different urea injection strategy is required in the SCR to carry out NO_x reduction.

This calls for an efficient mechanism to determine aging in the DOC. Aging in a DOC can be detected from the shift in its light off temperature. Here, light off temperature refers to the temperature at which the upstream Hydrocarbons (HCs) undergo 50% conversion at DOC exit. This light off temperature increases as the DOC ages. This temperature shift can help in determining the oxidation efficiency of a DOC at a particular instant, and further help in substantiating the NO and NO_2 concentration at the DOC exit.

This project aims at validating an indirect model that determines the light off temperature of a DOC as it thermally ages. This shall be done by carrying out direct HC conversion measurement experiments at different aging levels of the DOC. This shall further be extended to validation of a model that shall estimate the NO and NO_2 concentration downstream of the DOC which shall involve the use of a different measurement strategy. Also, an effort shall be made to pre-empt any potential issues in the models and important assumptions shall also be validated.

1.2 Diesel Engine Fundamentals

A diesel engine falls in the category of a Compression Ignition (CI) Engine. It has a piston-cylinder mechanism with a two-stroke or four-stroke configuration. A four-stroke configuration is commonly used in small and medium sized engines and is comprised of 4 phases namely, Intake, Compression, Power, and Exhaust Stroke in that order. Two-stroke configurations (Compression and Power stroke) are widely used in the applications of large sized engines [1].

Compression Ignition engines have a much higher compression ratio in general (range of 12-24) than their counterpart spark ignition engines and the corresponding heat of compression is used to ignite and carry out combustion of the non-premixed air-fuel mixture, where the fuel is injected at the end of the compression stroke. Spark Ignition engines (Gasoline Engines generally), on the other hand use a spark plug to ignite the premixed air-fuel mixture in the combustion chamber. The higher compression ratio in a CI engine leads to a higher fuel efficiency than a typical SI engine and that leads to the popularity of diesel engines.

The air intake system of a diesel engine can be either of or a combination of the following three types of air induction systems- naturally aspirated, turbocharged induction, supercharged induction. A naturally aspirated engine inducts atmospheric air into the cylinder by the vacuum generated by the receding piston during the intake stroke. In a turbocharged system, the hot exhaust flow rotates the turbine of the turbocharger, which compresses inlet air into the cylinder using an axial or radial compressor attached on the common shaft. In a supercharged system, air is fed into the cylinders using a compressor that is belt or chain driven off the engine crankshaft. Turbocharging and supercharging processes increase air flow which leads to a corresponding increase in fuel flow thus increasing the engine power output.[1]

Although diesel engines combust fuel more efficiently and emit less carbon dioxide than gasoline engines, since fuel burns at a higher temperature, the problem of increased NOx emissions comes to fore. Also, diesel fuels often don't combust completely, leading to the formation of soot, since they consist of a mixture of hydrocarbons with 14 carbon chains, which makes them less volatile and heavier than gasoline (7 to 11 carbon chains). This soot can be generally seen in the exhaust of buses and heavy-duty trucks. [2]

Traditionally, diesel engines have been incorporated in heavy-duty applications like construction, mining and power generation equipment as well as commercial trucks, buses and off road vehicles and military applications. The fact that diesel engines are more efficient, durable and generate less carbon pollution has played a major role in this. Diesel engine passenger cars are also attracting more attention than ever globally.

Traditionally diesel engine vehicles are seen as being loud, polluting and unpleasant. However, modern diesel engine powered vehicles are equipped with sophisticated

technologies to check the production of pollutants. Stricter greenhouse gas emission regulations are also fuelling the improvements in these technologies. Some of these technological improvements envisaged for the future are- a focus on reduction of cold start emissions for Light Duty Diesel (LDD) applications, late cycle fuel injections, cylinder deactivation, and an advanced Diesel Oxidation Catalyst (DOC) due to which the urea injection event happens earlier than that for a normal system. For heavy-duty diesel engines, the focus is on obtaining higher fuel efficiency and lower emissions. The focus is also on reducing NOx emissions, for which after-treatment systems are being optimized [5].

1.3 After-Treatment System Introduction

An after-treatment system is installed in the tailpipe of an internal combustion engine and its purpose is to reduce the environmentally harmful products of combustion such as unburned Hydrocarbons (HC), Carbon Monoxide (CO), Nitric Oxide (NO), Nitrogen Dioxide (NO_2), some Nitrous Oxide (N_2O) and particulate matter (PM or soot) through various chemical reactions. The chemical reactions happen inside the 'flow reactor'. These reactions, which convert the pollutants into less hazardous components (H_2O, CO_2 and N_2), proceed through catalytic processes inside the reactor. These processes increase the rate of a reaction by providing a lower energy pathway for the reaction to proceed. Since the reaction temperature also decreases, the conversion processes are able to occur at the engine's exhaust operating temperature. A brief description of a gasoline engine after-treatment configuration and a diesel engine after-treatment configuration is given in the following sections.

1.3.1 Three-Way Catalyst (TWC) for Gasoline Engines

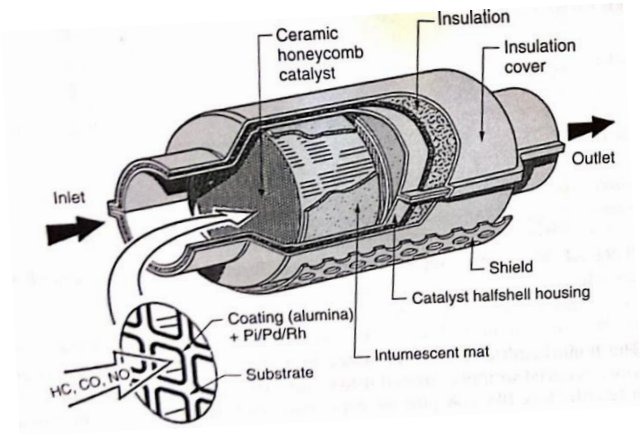

Figure 1.1. A Three Way Catalyst (TWC) Schematic [9].

The three main types of pollutants emitted from a gasoline engine are NO_x, HC and CO, and all three are in the gaseous state with a high prevailing exhaust temperature of nearly 400°C. The most commonly used emission control system for converting these harmful pollutants is the Three-Way Catalyst (TWC) which converts NO_x, HC and CO to nitrogen, carbon dioxide and water using a single device. The device is built from an inert monolith structure on which the catalyst is coated. Cordierite ($Mg_2Al_4Si_5O_{18}$) is one of the most common materials used to make the monolith. A coating of an oxide ceramide ("washcoat") is coated onto the monolith and this is what contains the precious metals (platinum, palladium and rhodium) which carry out the catalysis. In a TWC, the optimal conversion of all the three pollutants occurs only if the air-to-fuel ratio lies in a narrow band. As a result, precision metering of fuel is required prior to injection, which gives rise to the need for closed loop control. Usually, a Heated Exhaust Gas Oxygen (HEGO) sensor

is used for this purpose [6]. In a TWC, NO_x gets reduced to nitrogen and HC and CO gets oxidized to carbon dioxide and water simultaneously according to the following reactions:

Reduction of NOx to nitrogen,

$$2NOx \rightarrow xO_2 + N_2. \tag{1.1}$$

Oxidation of HCs to water and carbon dioxide,

$$C_xH_{2x+2} + \frac{(3x+1)}{2}O_2 \rightarrow xCO_2 + (x+1)H_2O. \tag{1.2}$$

Oxidation of carbon monoxide to carbon dioxide,

$$2CO + O_2 \rightarrow 2CO_2. \tag{1.3}$$

1.3.2 Diesel Engine After-Treatment Systems

The four primary pollutants emitted from a diesel engine are CO, HCs, NOx and PM (soot). Traditionally, diesel engines have been using only an oxidation catalyst to remove CO and HC. However, the other two major constituents of diesel engine emissions, namely NO_x and soot, are left unaddressed as a result of using only an oxidative catalyst. Also, since the exhaust temperatures are generally lower than those for a gasoline engine, the chemistry is always oxidative. Therefore, in order to address this problem, more and more diesel engine manufacturers are adding Diesel Particulate Filters (DPF) for the reduction of soot, and Selective Catalytic Reduction (SCR) systems for the conversion of NO_x into nitrogen, N_2. With emission norms getting more and more strict by the year, it is getting almost impossible to meet the emission limits only by making the combustion and fuel metering systems more advanced, and an additional treatment of the exhaust before being let out into the atmosphere has almost become the order of the day.

An added advantage of having the engine and after-treatment system separate is that with the after-treatment system focusing on treatment of harmful exhaust, engine combustion efficiency need not be sacrificed for that purpose [6].

1.4 Effect of Vehicular Emission on the Environment

Environmental pollution caused by vehicular exhaust emission was not considered a serious issue until the late 1950s and early 1960s. By the early 1960s, serious air quality concerns were starting to come up, especially in big urban areas such as Tokyo, Los Angeles, Mexico City and other urban areas in Europe [7]. Recent reports from cities in developing countries such as China and India also suggest that the number of motor vehicles seems to have a direct correlation with the decline in air quality. Research in this area during the same period and thereafter suggests that the "photochemical smog" that contains harmful ozone and other pollutants, which is so clearly visible in a majority of these areas, is formed due to photochemical reactions of hydrocarbons (HCs) and nitric oxide (NO)[6].

The four main internal combustion engine emissions, i.e. Hydrocarbons (HC), Nitrogen Oxide (NOx), Carbon Monoxide (CO), and Particular Matter (soot), are described in the following subsections briefly.

1.4.1 Carbon Monoxide

Carbon Monoxide (CO) is a colorless and odorless gas. This makes it difficult to detect. What makes it poisonous is the fact that it has a much higher binding capacity to the haemoglobin in our blood than the oxygen we breathe. As a result of this, victims who

breathe in CO get asphyxiated rapidly. At low concentrations (approximately 200- 300 ppm) effects such as impairment of judgment, headaches and nausea might be caused. At high concentrations (> 1000 ppm), it might be lethal.

1.4.2 Oxides of Nitrogen (NO and NO_2)

Oxides of nitrogen, primarily NO and NO2 can be poisonous even at low concentrations (1 ppm). Upon inhalation, these may cause damage in lung tissues. Nitrogen oxides can also form acid rain and photochemical smog through various atmospheric reactions. They are also considered to be greenhouse gases which ultimately lead to global warming. Acid rain is formed via the following reaction:

$$2NO_2 + H_2O \rightarrow HNO_2 + HNO_3. \quad (1.4)$$

Nitrous acid and nitric acid are the main constituents of acid rain formed from the oxides of nitrogen.

1.4.3 Unburnt Hydrocarbons (UHC)

Unburnt hydrocarbons constitute hundreds of different carbon-containing compounds that are present in the gaseous state: alkynes, alkenes, alkanes, and aromatics. Harmful effects from UHCs include irritation in the mucous membrane, coughing, sneezing and drowsiness. Some HC chains combine to form carcinogens. Environmental effects include formation of tropospheric ozone and photochemical smog which are formed when the UHCs react with nitrogen oxides in the atmosphere.

1.4.4 Particulate Matter

Particulate Matter consists of micro-sized particles which are mostly carbon particles. They pose a health hazard since they can penetrate through the respiratory system upon

inhalation. Particles of size < 5 microns can enter the trachea and primary bronchi. Particles of size smaller than these can enter the alveoli, thus seriously hindering the exchange of oxygen and carbon dioxide in the respiratory system. PM can also cause cardiovascular diseases and can even be carcinogenic in certain cases. PM is a sophisticated emission component and it cannot be described solely on a total mass basis.

1.5 Emission Regulations

Emission regulations to control environmental pollution and prevent subsequent health and environmental problems are being seriously pursued all over the globe. Up until the 1960s, regulations were not given serious thought. However, due to observations of vehicular pollution related problems, regulations to control emissions were begun to be framed. In the US, serious legislation in this regard began with the Clean Air Act of 1970 [9]. The Environmental Protection Agency (EPA) was set up in that year and since then, it has set emission standards for various kinds of internal combustion engine applications, including for on-road Heavy Duty (HD) diesel engines. Table 1.1 shows how emission standards have evolved through the years by the EPA. A CO (carbon monoxide) standard and a combined HC and NOx standard were added in the 1974 model year, and in 1979, the EPA maintained the HC+NOx standard while adding a HC standard. The combined HC+NOx standard was removed in 1985 and a PM standard was added in 1988. However, the combined standard for HC and NOx was brought back in 2004 and had an even lower requirement in terms of NMHC. NMHC stands for 'Non-Methane Hydrocarbons'. These are alkanes, alkenes and alkynes which have 1 to 5 carbon atoms and have an influence on the oxidizing capacity of the atmosphere [6].

These reducing trends in emission standards impose a pressure on the automotive industry to rapidly adapt to the changing requirements [6].

Changes in emission levels have been more or less gradual except for in the year 2007 where the acceptable NOx and PM levels were reduced by a factor of 10 compared to the previous year (Table 1.1). This led to an increased effort by all major automotive companies to develop emission after-treatment control systems, and therefore, scope for research increased in this field.

Except for California, where the California Air Resource Board (CARB) sets standards for emissions, all the US states emission regulations are governed by the EPA. Many major cities in California had very high levels of pollution and this led to the establishment of CARB. California's automotive market is also one of the world's largest and therefore, CARB has a huge influence over the emission requirements that major automakers follow.

Table 1.1. US Emission Standard for Heavy Duty Diesel Engines [10].

Model year	Pollutant (g/bhp-hr)				
	HC	CO	NO_x	HC + NO_x	Particulate (PM) t=truck, b=bus, ub=urban bus
1970	—	—	—	—	—
1974	—	40	—	16[b]	—
1979	1.5	25	—	10[b]	—
1985[c]	1.3	15.5	10.7	—	—
1988	1.3	15.5	10.7	—	0.60
1990	1.3	15.5	6.0	—	0.60
1991	1.3	15.5	5.0	—	0.25
1993	1.3	15.5	5.0	—	0.25 t, 0.10 b
1994	1.3	15.5	5.0	—	0.10 t, 0.07 ub
1996	1.3	15.5	5.0	—	0.10 t, 0.05 ub
1998	1.3	15.5	4.0	—	0.10 t, 0.05 ub
2004	1.3	15.5	—	2.4 NMHC[d]	0.10 t, 0.05 ub
2007		15.5	0.2	0.14 NMHC	0.01

EPA legislation defines emission regulations based on a vehicle's gross weight rating (GWR). For example, the regulation for a 3000 lb passenger car will be different from that of a 10,000 lb truck. According to this standard, passenger cars and light trucks belong to the category of vehicles with GWR < 6000 lbs., while heavy duty trucks are defined as vehicles with GWR > 8500 lbs.

It is required by law for car manufacturers to comply with the emission standards implemented for a particular model year. Failure to do so results in a penalty per non-compliant vehicle. The vehicle emission rate is checked by a standard test, i.e. the "steady state European 13 stage test" cycle and the "dynamic/transient test" cycle [12]. In addition to this, heavy duty vehicles are tested to a certain end of useful life based on their specific applications. For example, for a Light Heavy Duty Diesel Engine (LHDDE), the useful life is 10 years or 110,000 miles, whichever occurs first. The vehicles are expected to meet the emission standards within this useful life period [13].

1.6 Diesel Engine After-Treatment System Configuration

As briefly discussed earlier, the after-treatment systems for diesel engines are designed to oxidize, reduce and filter the wide variety of gaseous components in the exhaust. In the most common layout for a diesel engine after-treatment system, the first component downstream of the engine is called the Diesel Oxidation Catalyst, which uses the remaining oxygen in the exhaust to oxidize HC, CO and NO. However, there is no quick way to oxidize the Particulate Matter. A Diesel particulate filter (DPF) is then installed downstream of the DOC to trap PM. The last component of this after-treatment setup is called the Selective Catalytic Reduction (SCR) unit. The SCR system was introduced to

meet the tighter emission regulations on Nitrogen Oxides. Figure 1.1 shows the schematic of a typical diesel engine aftertreatment system.

In all of the preceding sections as well as this one, catalysts have been mentioned where ever after treatment systems have been mentioned. Therefore, the following section will describe in reasonable detail the basic functioning and theoretical principles related to the typical catalysts used in the mentioned after-treatment systems.

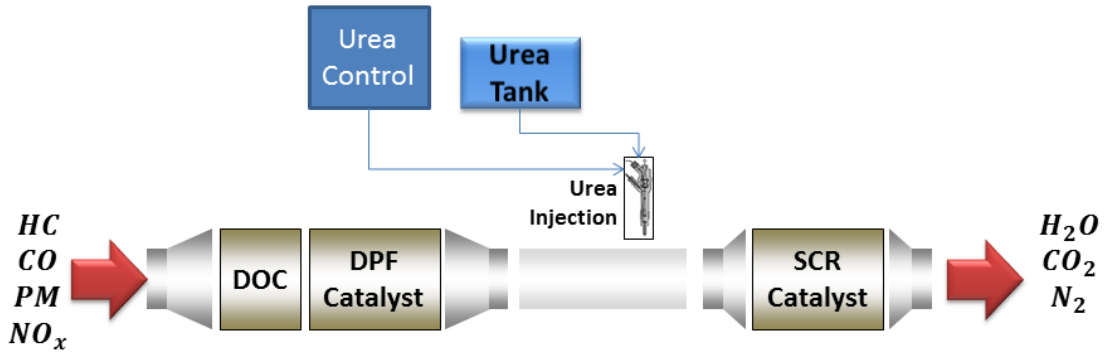

Figure 1.2. General Aftertreatment Configuration for a Diesel Engine.

1.7 Fundamentals of Catalysts and Catalysis

This section will discuss in brief the fundamentals of the reactions involved in the chemistry regarding the conversion of exhaust emissions, and also discuss the basics of the typically used catalysts in a diesel engine after-treatment system.

1.7.1 Reactions with Catalysis

Catalysis improves the production efficiency of a process and therefore, it is used for a variety of industrial processes involving numerous chemical reactions. Precious metals, which are elements located in the group VIIIB of the periodic table and include elements

like Rubidium (Ru), Rhodium (Rh), Palladium (Pd), Iridium (Ir), Platinum (Pt) and Osmium (Os) are constituents of a variety of catalysts. For exhaust emission control applications, the commonly used elements are Pt, Pd and Rh, which are used individually or in combination with one another. Catalysts expedite homogeneous reactions by providing a lower energy path for the reaction to proceed from (thereby lowering the reactant's activation temperature). In heterogeneous reactions, more than one phase is involved and catalysis involves interactions between components of the gaseous phase and the metal catalyst through chemisorption.

We know that catalysts accelerate a reaction by lowering the activation energy of the reaction. Here, activation energy is defined as the minimum amount of energy required by a system to initiate a chemical reaction. The reaction rate of the reaction also increases consequently. We can see from Figure 1.2 that the reaction in the presence of a catalyst is faster due to a lowered activation energy, whereas the enthalpy generated as a result of the exothermic reaction remains the same.

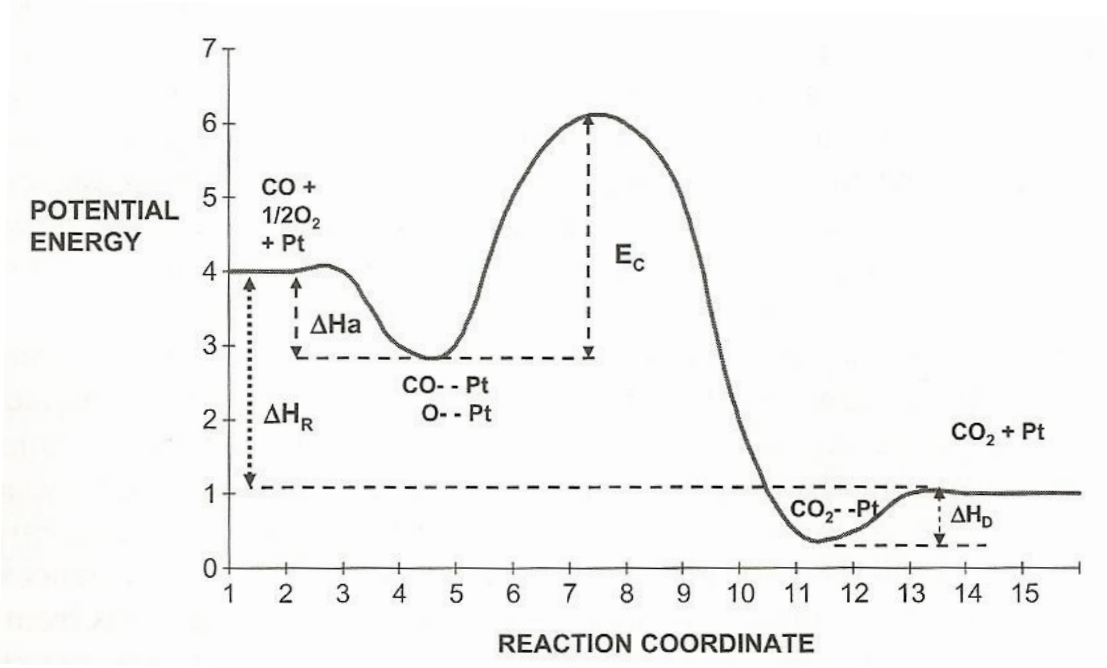

Figure 1.3. Activation Energy for Oxidation Of CO To CO2 with Catalytic Reaction [9].

A lower activation energy suggests that a lower temperature than an uncatalyzed reaction is necessary to carry out the reaction. The chemical kinetics for a catalyzed reaction can be explained using the Arrhenius equation:

$$k = A\, e^{-\frac{E_a}{RT}}, \tag{1.5}$$

where A is a simple pre-factor (or frequency factor), E_a is the activation energy, R is the universal gas constant, T is the system temperature and k is the reaction rate constant. From this equation, we can infer that the lower the activation energy, the higher is the reaction rate constant and vice-versa. From Figure 1.3, we can see that the oxidation of CO to CO2 can be carried out at a much lower temperature in the presence of a Platinum (Pt) catalyst than without it. The conversion here is taking place in an automotive convertor. Majority of after-treatment reactions are also exothermic and therefore, the internal temperature of the reactor also increases as the reaction proceeds. The S curve of

conversion depicts this. At a particular activation temperature, called the “light off temperature”, the conversion rate rises rapidly and levels off at a certain maximum conversion rate depending on the conversion reaction.

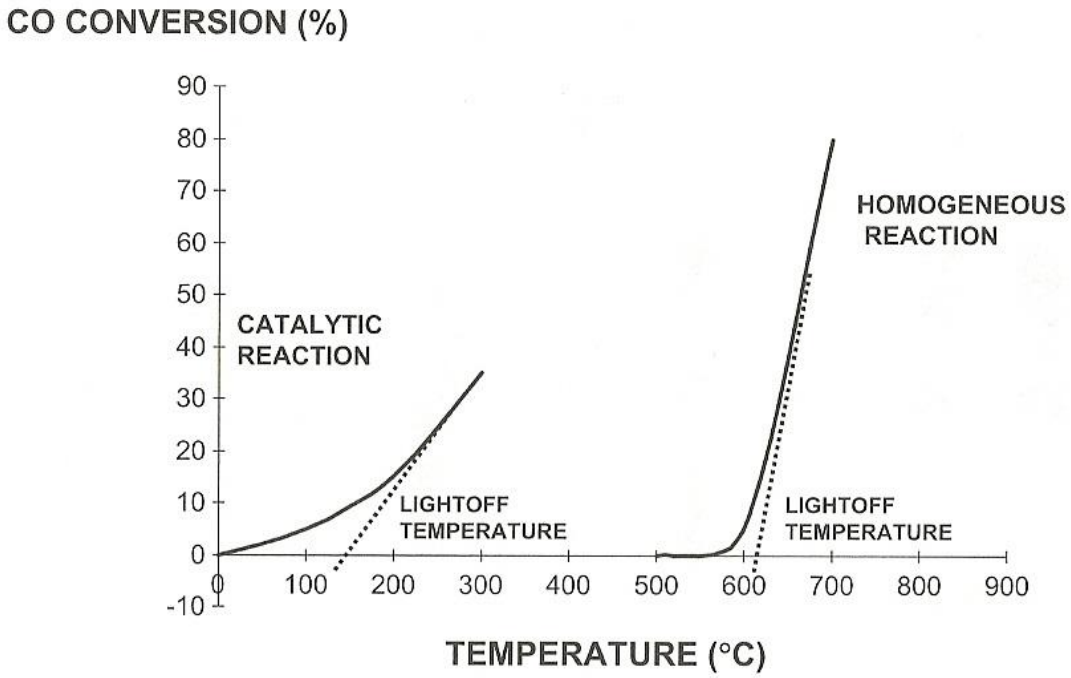

Figure 1.4. Conversion of CO Comparison with and without a Catalyst [9].

1.7.2 Catalytic Convertors: Structure and Construction

Figure 1.4 shows an automotive packed bed reactor which is similar in construction to the general design of a packed bed reactor where the catalytic reactions take place. These are built from 'monoliths' which form the skeleton of the convertor on which the succeeding layers, including the sites on which actual catalysis takes place, are added. Monoliths are usually ceramics or metals. The precious metal constituents which provide the active sites are added on an intermediate layer called 'washcoat' which is an oxide ceramic material [6].

Figure 1.5. Automotive Packed Bed Reactor.

The basic aim of the catalyst is to speed up the reaction and this is also attained by increasing the surface area available inside the reactor. In light of this requirement, the construction is done in such a way as to provide a number of flow-through passages for the exhaust gas, and the flow rate depends on the exit pressure from the engine.

From Figure 1.5, we can see a general schematic of the catalyst surface. This section is extended to the length, breadth and height of the reactor. It clearly shows the three important sections of the catalyst, i.e. the monolithic substrate, the washcoat layer on top of it and the Platinum Group Metal (PGM) layer on the washcoat. Figure 1.6 shows more clearly how the catalyst surface would look if seen under a microscope. As we can see, the channel has a square-shaped cross section monolith with a thin layer of the washcoat layered on top of it. The important sections of the catalyst will now be discussed in detail in the following sections.

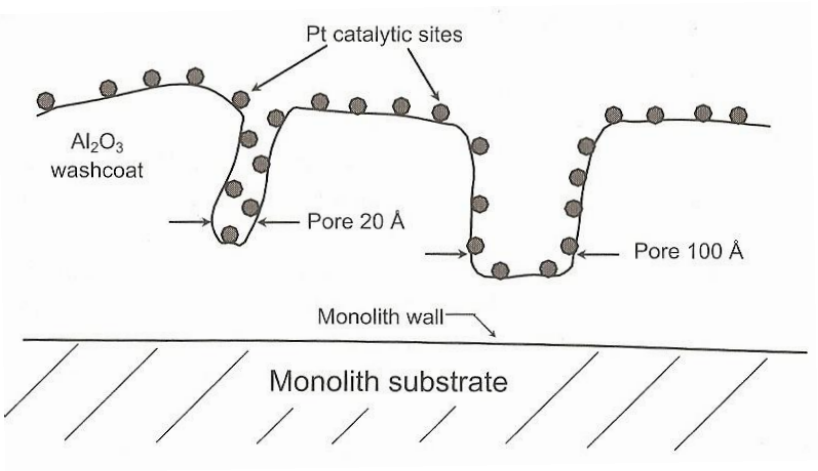

Figure 1.6. Schematic of Catalytic Sites Dispersed on a High Surface Area Al2O3 Carrier Bonded to a Monolith Support [9].

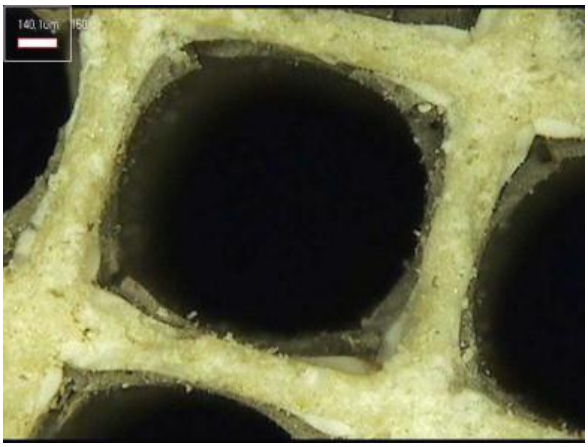

Figure 1.7. An Actual Microscopic side view Picture of the Catalyst [27].

1.7.2.1 Monolithic Substrate

The monolithic substrate acts as the basic framework which provides an inert substrate for the actual catalytic coat. This structure is widespread in the automotive industry. It is constituted generally out of inorganic oxides (cordierite) although metal monoliths are also gaining popularity. It is generally made in a squared cross section with parallel channels in a honeycomb design. The design can also be optimized by using a

circular, triangular or hexagonal shape as per the application. The ceramic monolithic substrate such as the one used in this project requires an extremely low thermal shock resistance, i.e. very little dimensional change should occur during large axial temperature gradients, and a large surface area. Automotive catalyst monoliths also need to withstand high acceleration shaking forces as well as gas pulsations. Therefore, these ceramic monoliths are made to tolerate axial pressures of over 3000 psi. Also, they are made to have a high melting point of over 1300°C [9].

1.7.2.2 Washcoat

A washcoat is layered onto the substrate and it is here that the PGM elements lie. It provides a large surface which has a complex pore structure. The large surface area amounts to a higher amount of catalyst dispersion, thus providing a higher reaction rate. A washcoat can maintain high reaction selectivity, activity, and durability in terms of the catalyst deposited onto it. Most commonly, the base component of a washcoat is alumina (Al_2O_3) to which ceria (CeO_2) is added at different percentages. Components called 'stabilizers' are also added to slow the thermal aging process and 'promoters' are added to enhance the PGM performance regarding catalysis [9].

1.7.2.3 Precious Metal Catalysts

Elements from the Precious Group Metals (PGM) or the Platinum Group Metals are the metals used in automotive catalytic reactors. These are responsible for the actual catalysis in the reactor. They are positioned in group VIIIB of the periodic table and include metals such as Rubidium, Rhodium, Palladium, Iridium, Platinum and Osmium.

The exhaust flow from the engine requires a rapid conversion into less harmful constituents. Therefore, these PGMs facilitate this by allowing the gaseous exhaust components to adsorb and react on top of them. The most commonly used PGMs as automotive catalysts include Platinum (Pt), Rhodium (Rh) and Palladium (Pd) [9]. PGMs have been shown to be resistant to oxidation, some degree of poisoning, and high temperature damage. In addition to these advantages, PGMs have high chemisorption rates, which make them highly active as catalysts. However, as a result of being rare in the environment, these are expensive to obtain. Recycling, reusing and purification processes of these metals when their performance degrades helps in addressing this issue to some degree.

1.7.3 Heterogeneous Catalysis

Since the type of catalysis taking place inside the catalyst we use is a heterogeneous type, we shall be describing that in brief.

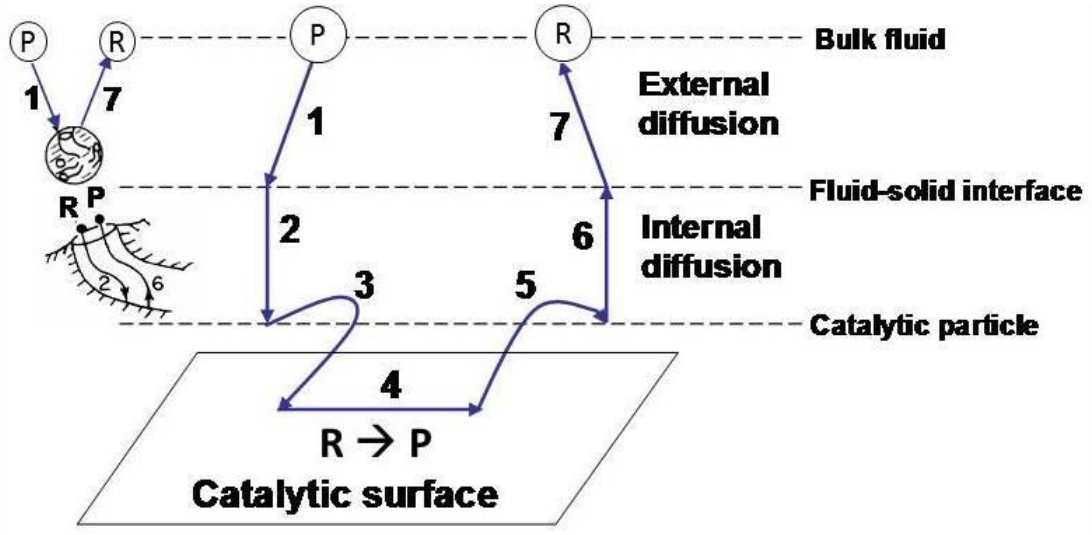

Figure 1.8. The Step Diagram of Catalytic Heterogeneous Reaction in Catalyst [14].

Heterogeneous Catalysis goes through several steps in order to complete a reaction. These are:

1. Bulk mass transport of the reactants occurs from the bulk fluid to the outside surface of the catalyst.
2. Diffusion of reactants to active sites through the pore structure of the catalyst occurs.
3. Reactants then adsorb onto the active sites through chemisorption.
4. The chemisorbed species convert into products.
5. Consequently, these products desorb from the active sites.
6. The products diffuse through the pore structure.
7. The products diffuse from the outside surface of the washcoat to the bulk fluid.

1.7.4 Catalyst Light-Off

Catalyst light off or Light off temperature is defines as the temperature or range of temperatures at which the catalytic reactions initiate and the reaction rate increases

exponentially as the temperature increases. The light off temperature is typically referred to as the catalyst inlet temperature at which 50% concentration of a gas species gets converted.

Light off temperature has been explored as an indicator of catalyst effectiveness. Light off temperature varies according to engine speed and torque since the exhaust flow rate changes and this can change the light off temperature.

1.7.5 Catalyst Deactivation

Catalyst effectiveness does not remain constant in throughout and decays with use due to numerous factors. This ultimately leads to catalyst deactivation. Catalyst deactivation is caused due to three main factors, i.e. sintering or aging, fouling or coking, and poisoning. Sintering is defined as the loss of catalytic activity as a result of reduced active surface area resulting from a clumping together of the active metal particles due to prolonged exposure to excessive heat. Since the pores close as a result of this, the number of active sites decreases. Figure 1.8 shows a schematic of sintering and Figure 1.9 shows an actual picture of a sintered catalyst.

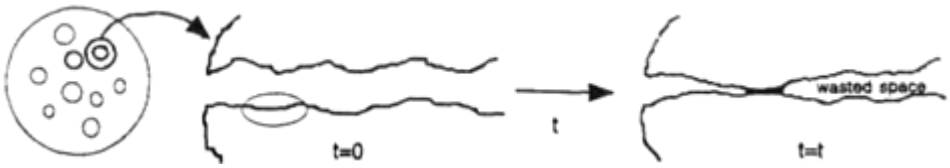

Figure 1.9. Decay by Sintering Causing Pore Closure [14].

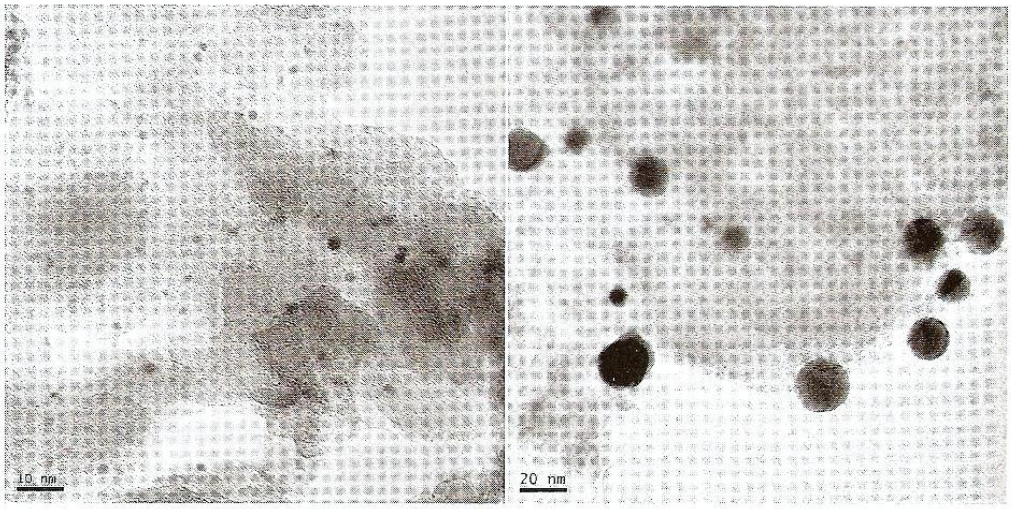

Figure 1.10. Decay by Sintering Resulting in Agglomeration of Deposited Metal Sites. This is the TEM of Fresh and Sintered Pt on Al_2O_3. The Left Picture Shows Very Small and Dispersed Pt, and in the Right Picture, the Pt Experiences Crystalline Growth [9].

Coking or fouling, as shown in Figure 1.10, occurs as a result of carbonaceous particles being deposited on the catalyst surface, usually at the inlet of the reactor bed. This is very common in reactions involving unburnt HCs. With greater accumulation, catalyst effectiveness starts to decrease. However, coking can be decreased by allowing a hydrogen-rich stream to pass through at elevated pressures.

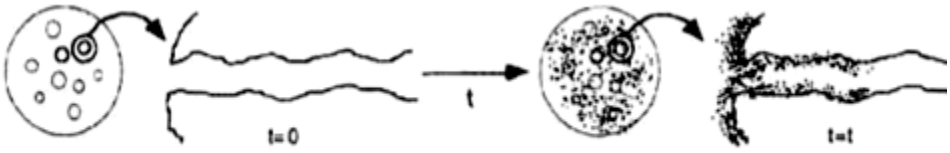

Figure 10-25 Schematic of decay by coking.

Figure 1.11. Schematic of Decay by Coking [14].

Poisoning is similar to coking in the sense that deactivation occurs due to deposition of constituents on the catalyst surface but the mechanism is different. Catalyst poisoning is due to molecules becoming irreversibly "chemisorbed" to the active sites over a period of time, thereby reducing active sites available for reaction. The poison molecules are generally reactants or products involved in the main reaction, or impurities originating from the exhaust stream. These impurities include sulfur and lead. Poisoning can be reversed by exposing the catalyst to high temperatures (~1000 C). However, this also has the potential to permanently damage the catalyst. Sulfur oxides are selective in nature and deposit on only selective sites such as down the axis of the monolith and deep inside the washcoat [9].

Different kinds of driving behaviours lead to different types of deactivation in the catalyst. For example, greater amount of highway driving results in increased thermal deactivation, whereas city driving which includes long idling durations causes deactivation by coking and poisoning since compound accumulation has a greater tendency of occuring and the operating temperatures are also low [28]. We shall now be describing the catalyst in more detail that is most in focus for this project, i.e. the Diesel Oxidation Catalyst (DOC).

1.8 The Diesel Oxidation Catalyst (DOC)

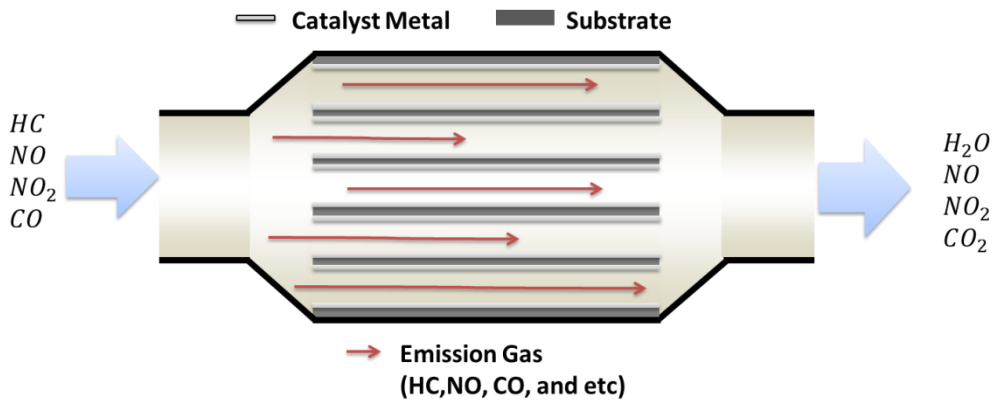

Figure 1.12. DOC Schematic.

A Diesel Oxidation Catalyst has a monolith generally made of ceramics such as 'cordierite' and has a honeycomb-like structure. Figure 1.11 shows a schematic of the same depicting a flow-through structure. As a result of this structure, exhaust gases flow through the rectangular channels without restriction. The surface of these channels is coated with the PGM catalyst metals such as Pt, Pd, or a combination of both which enable the oxidation of the emission gas constituents.

The amount of catalyst metal coated, called 'metal loading', is generally between 50 - 90 g/ft^3. Most of these figures are company trade secrets and it is hard to have an exact amount. Since all or most catalytic reactions occur on the surface of the reactor, a thin layer of catalyst metal coating can be used to achieve the conversion efficiency level desired. Therefore, current research and advancements are being aimed at creating catalysts which will be at a much smaller scale than the current norm (nano scale). This shall help in cost reduction since the PGMs are rare and expensive, and also help in having

a more widespread use of DOCs around the globe[12]. The carrier or washcoat, as mentioned in subsection 1.6.2, is made of oxides of Aluminum (Al_2O_3), cerium (IV) (CeO_2), or zirconium (ZrO_2). It provides a high surface area for the metal catalyst to be deposited on. It has a porous ceramic structure which is stable enough to slow down catalyst sintering. The substrate also has to maintain its form at very high temperatures which occur during Catalyzed Diesel Particulate Filter (CDPF) regeneration.

1.8.1 Functionality

The DOC is supposed to perform four main tasks, namely oxidation of CO and UHCs to CO_2 and H_2O, some reduction in PM content, oxidation of NO to form NO_2, and creating high temperature for DPF (Diesel particulate Filter) regeneration by acting as a catalytic burner [12]. The oxidation of CO and UHCs takes place mainly inside the DOC. The temperature inside the DOC is high enough to achieve up to 90% conversion of the UHCs, and a removal of CO up to 99% in most cases. Among the three exhaust gas constituents required to be converted, CO lights off first followed by the UHCs and then the NO [9]. This light-off temperature depends on the catalyst metal composition, space velocity and exhaust gas composition, and can vary between 160°C and 220°C.

The PM from diesel engines partly contains hydrocarbons and partly carbonaceous particles. With rise in temperature inside the DOC, this HC content desorbs from the particles to some extent. This results in a potential 15-30% removal of this PM by the DOC [12]. The SOF (soluble organic fraction) percentage in the PM limits the conversion of the PM [9].

Oxidation of NO to NO_2 also occurs within the DOC. The ratio of NO2/NOx is an important factor in determining the performance of the catalysts downstream of the DOC i.e. the DPF and more importantly, the SCR catalyst. NO_2 produced by DOC can act as O_2 substitute to carry out DPF regeneration at a considerably lower temperature of around 350°C.

The NO_2 concentration in the exhaust gas entering the SCR system is also important in the reduction of overall NO_x (NO and NO_2) to N_2. The reduction reaction having a stoichiometric NO_2/NO ratio of 1:1 is the fastest and leads to the highest amount of NO_x conversion.

The oxidation reactions of CO and HC are exothermic in nature. This generates heat for DPF regeneration. DPF regeneration requires a high temperature which the engine exhaust gas itself cannot provide without the oxidation reactions within the DOC.

1.8.2 Design and Operation

A very important design criterion in designing a DOC is the capability to perform at low temperatures to minimize cold-start emissions [15]. Since diesel engines are inherently leaner than a gasoline engine, the exhaust temperature is also lower than a gasoline engine. Therefore, the exhaust gas does not have enough enthalpy to warm up the catalyst fast enough to take care of the emissions at engine start.

The reactions in a DOC proceed in the following sequence: first, CO oxidation takes place followed by HC oxidation at a higher light-off temperature than CO, and HC conversion does not usually reach 100%, most probably due to the presence of non-reactive methane in the exhaust [17]. NO oxidation to NO2 is limited kinetically at low

temperatures and thermodynamically at high temperatures. NO conversion to NO_2 increases with temperature before thermodynamic conditions prevent a further increase in conversion rate at temperatures above 350°C[17].

Another phenomenon that occurs within the DOC is that of hydrocarbon storage. This is facilitated by the zeolite material in the washcoat [15,16,18]. At a cold start condition, since the DOC is not warm enough to carry out oxidation of HCs, storage occurs and the HCs desorb and oxidize when the DOC reaches its light off temperature eventually. This phenomenon plays an important role in reducing cold start emissions.

Sulfur poisoning is another criterion that determines the metal catalyst to be used. Since new fuel regulations have reduced the sulfur content in diesel fuel from 500 ppm to 15 ppm, use of less expensive metal catalyst options such as palladium over platinum is being explored [7]. Platinum is highly resistant to sulfur poisoning. Most current catalyst formulations now are alloys of Pt and Pd with a greater proportion of Platinum due to its greater light off activity.

The Pt-Pd catalyst remains thermally stable even at aged conditions [18]. This improves the overall performance of the catalyst. The platinum-only catalyst undergoes significant deterioration after prolonged high-temperature aging in an oxidation atmosphere. On the other hand, the Pt-Pd alloy maintains a significant amount of CO and UHC light off activity even when the catalyst has aged [19,26]. Therefore, palladium brings with it thermal stability to the catalyst and also reduces the price of constructing the DOC. The disadvantage of the Pt-Pd catalyst is that it has a lower activity with respect to NO conversion than the Pt only catalyst. This affects DPF regeneration and SCR NO_x conversion efficiency. If an SCR system becomes less sensitive to the $NO:NO_2$ ratio than

DOCs with 1:2, 2:1 or 1.5:1 Pt-Pd ratio can be incorporated for the same purpose as a Pt only catalyst [18].

1.9 Catalyzed Diesel Particulate Filter (CDPF)

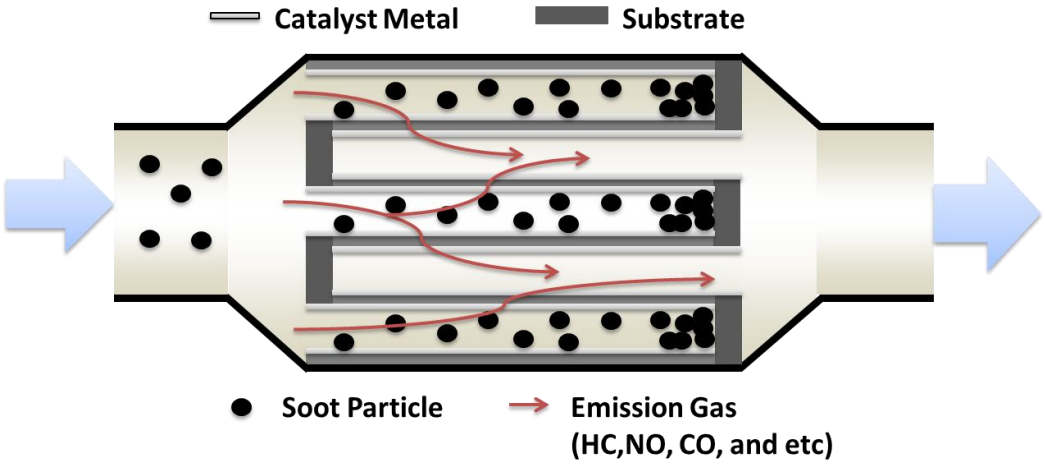

Figure 1.13. Schematic of a CDPF Depicting Gas Flow from the Inlet to the Outlet Channel through Pores in the DPF Substrate, while the Soot Particles are Accumulated in the Inlet Channels.

The CDPF is designed to trap particulate matter (PM) in the exhaust stream, as depicted in the DPF schematic in Figure 1.13. The captured PM is later removed by reacting it with oxygen in a process known as regeneration [19]. The DPF or the CDPF is generally installed downstream of the DOC. The CDPF has a ceramic monolith with a washcoat on which precious metals are coated, which serve as the catalyst. It is also called a wall-flow monolith, which means that there are a number of small parallel plugging channels present inside the catalyst. The exhaust gas is forced through the ceramic walls. The monolith contains a large proportion of cordierite, which helps in preventing thermal

shock cracking that may occur as a result of exposure to high thermal gradients during regeneration [16].

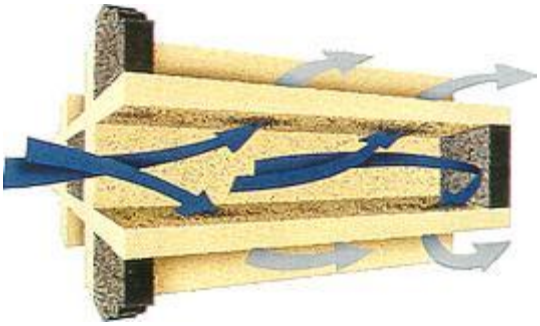

Figure 1.14. Schematic of a Single CDPF Channel Showing the Alternate Open and Closed Pathways.

DPFs are designed to filter as much soot as possible while increasing time between regenerations, thus increasing regeneration efficiency, and minimizing pressure drop across the filter to reduce the engine workload [23, 24, 25]. There are three main designs of DPFs in the automotive market, namely catalyzed, continuously regenerated and additive-based.

Around 85% of the soot particles get electrically charged due to the combustion process inside the diesel engine [19]. This serves as the basis for PM sensors for measuring the PM concentration.

1.10 Selective Catalytic Reduction (SCR) System

Selective Catalytic Reduction system is generally installed downstream of the DOC and the DPF. The purpose of the SCR system is to minimize NOx emissions from diesel engines without necessarily altering the engine operating characteristics.

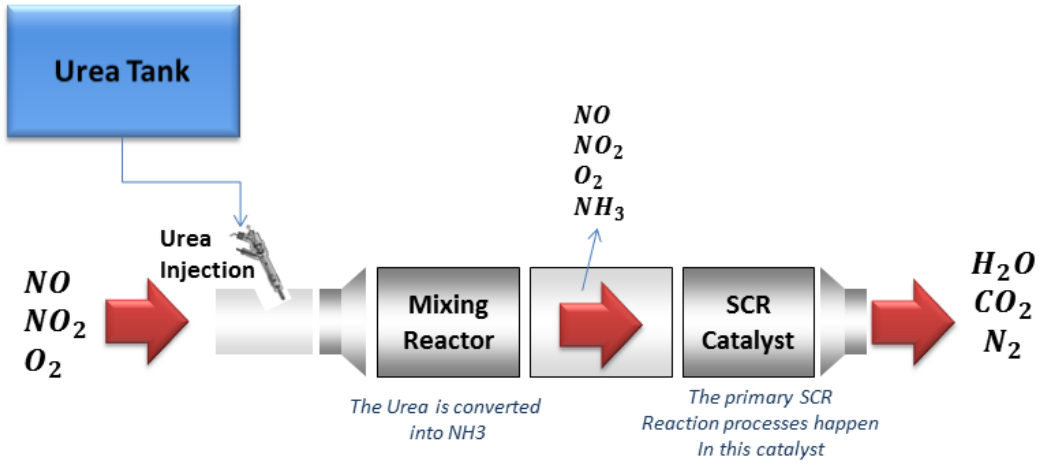

Figure 1.15. Schematic of a Selective Catalytic Reduction System.

There are two main sections of the SCR system: the mixing reactor where the urea injected from the storage tank is converted into NH3 and the main catalyst reactor which converts NO_x into N_2. Figure 1.15 shows a schematic of this system. NOx reduction occurs in the presence of ammonia (NH_3) which selectively reacts with NOx to produce N_2. Selectivity refers to the fact that ammonia has a preference of oxidizing with the oxygen in the NO_x molecules rather than the exhaust stream O_2 [12].

Ammonia is stored in the form of urea in liquid form which is environmentally safe and a good carrier of NH_3. Urea ($chemically, (NH_2)_2CO$) is soluble in water and can be contained as a liquid. The most common brand name for urea used in this application is called 'AdBlue' (composition: 32.5% high purity urea and 67.5% deionized water [26]). The urea needs to be converted into NH3 in order to obtain any useful reduction of the NOx. This is carried out by thermolysis and hydrolysis processes. The thermolysis process follows the following chemical reaction [12]:

$$(NH_2)_2CO \rightarrow NH_3(g) + HNCO(g). \quad (1.6)$$

Where, HNCO is Isocyanic Acid and the isocyanic acid hydrolyses as:

$$HNCO + H_2O \rightarrow NH_3 + CO_2. \quad (1.7)$$

Urea can directly hydrolyse as well following the following chemical reaction [50]:

$$(NH_2)_2CO + H_2O \rightarrow 2NH_3(g) + CO_2(g). \quad (1.8)$$

The obtained ammonia then reacts with NOx present in the exhaust gas stream. The following equations describe the various reactions through which NOx reduction takes place:

$$4\,NO + 4\,NH_3(g) + O_2 \rightarrow 4\,N_2 + 6\,H_2O \quad (1.9)$$

$$NO + NO_2 \rightarrow 2NH_3(g) \rightarrow 2N_2 + 3H_2O \quad (1.10)$$

$$6\,NO_2 + 8\,NH_3(g) \rightarrow 7\,N_2 + 12\,H_2O. \quad (1.11)$$

The second reaction (equ. 1.10) which has a NO_2: NO stoichiometric ratio of 1:1, is the dominant and fastest reaction at low temperatures (<300°C). It is therefore essential to have a NO_2: NO ratio close to 1:1 to facilitate optimal conversion.

Leakage of ammonia is also a very real possibility. Therefore, AdBlue is ideally injected close to the stoichiometric amount, so that there is no excess NH_3 to cause slippage that could lead to potential environment damage, and not too little to diminish the overall NO_x conversion. At a temperature of below 200°C, there is chance of formation of Ammonium Nitrate (NH_4NO_3). With a precise injection of urea as described above and maintaining a temperature of above 200°C, this can be prevented as well. In summary, with an AdBlue quantity equivalent to 5% of diesel fuel quantity, NO_x reduction can reach 90% on average with an ammonia 'slip' of less than 20 ppm [12].

1.11 Problem Definition

1.11.1 NO_x Regulation

NOx emission regulations were first put in place in the year 1974 by the EPA and have been regularly updated since then. In 2007, the NO_x emission limit was reduced to less than a single digit quantity to a value of 0.2 g/bhp-hr for heavy duty trucks. As we know that the California Air Resource Board has separate set of regulations for the state, accordingly, as per section §1971.1(e) 6.2.1 of Title 13, California Code of Regulation, the OBD system is required to detect a catalyst malfunction when its capability decreases to the point where the engine's NOx emissions exceed a value of 0.2 g/bhp-hr. Thus, it is required that NOx emissions are strictly regulated to a value in the range 0.2 - 0.4 g/bhp-hr until the end of useful life of the SCR. In order to ensure that this limit remains maintained, the SCR system operation needs to be monitored constantly.

1.11.2 Purpose of the Project

The final motive of this thesis is to provide insights into different strategies to reduce NOx emissions from a diesel engine after-treatment system. As injection of urea to ultimately form ammonia is directly proportional to the amount and composition of inlet NOx into the SCR system, the factors on which this depends become all the more important. In this spirit, accurate knowledge of the composition of NO and NO_2 at the outlet of the DOC (assuming no oxidation occurs at the DPF) shall allow for an accurate urea injection control algorithm. Since, there is no direct method to measure both NO and NO_2 concentrations in real time, their compositions can be estimated using a NO_x sensor, temperature from inside the DOC and either estimation of or measured value of O_2 at the

outlet of the DOC. This thesis will be focusing more on validating previous work done as a part of this project and will be addressing certain inherent issues.

The other major area of focus in this project is to study the thermal aging of the DOC that would ultimately affect the concentrations of NO and NO_2 at the inlet of the SCR system. This will be carried out using the substrate temperature value from inside the DOC, the gas flow temperature value from thermistors at the DOC inlet and various mass flow rate values. This thesis will carry forward previous work done as a part of this project and will make an attempt to tackle the various issues that have been observed so far.

1.12 Document Organization

In this thesis, chapter 2 has the literature reviews pertaining to the focus area of this thesis. Chapter 3 describes the various experimental setup and procedures used to obtain meaningful data pertaining to our research. Chapter 4 talks about the experimental light off temperature determination strategy for a DOC and indirect HC light off temperature determination. Chapter 5 describes the experimental determination of the DOC out NO and NO_2 concentrations and indirect determination of the same. Chapter 6 is the ultimate chapter in the thesis and it contains the conclusions and future work regarding this research.

1.13 Contributions to the Project

This project was envisioned as a team project and work was carried out by other members as well. Therefore, it becomes imperative that I list out my contributions to this project. The major contributions I had towards this project are:

1.) Designing experiments and carrying out all testing related to the DOC thermal aging aspect of this project as well as for determining the NO and NO_2 concentrations downstream of the DOC which helped in developing the model that estimates the same.

2.) Revisiting the issues raised at the end of the first phase of this project such as the issue of HC adsorption in the DOC as well as the probability of soot loading onto the DOC.

3.) Validating the model developed regarding the shift in light off temperature as a DOC ages for two more aging levels.

4.) Validating the model developed to estimate the concentrations of NO and NO_2 at the outlet of the DOC.

5.) Obtaining NO_x data for the dosed HC experiments and validating the assumption in developing the light off temperature model that dosed HC causes all other reactions to become insignificant in the DOC.

6.) Carrying out data analysis for the NO and NO_2 concentration estimator model using values from an actual oxygen sensor attached downstream of the engine.

CHAPTER 2. LITERATURE REVIEW

This chapter reviews research literature relevant to the scope of this thesis. Section 2.1 discusses the fundamentals regarding the effect of DOC outlet NO and NO_2 concentration on SCR performance. Section 2.2 discusses studies done on the effect of aging on DOC performance with an emphasis on NO oxidation and section 2.3 discusses studies done on light off based strategies for determining aging for a DOC.

2.1 SCR Performance Dependence on NO_x Content

SCR converts around 90% of NO_x emissions in the exhaust to N_2 [9]. The injected urea which converts into ammonia (NH_3), causes reduction of NO_x into N_2 over the SCR catalyst based on the following reactions:

$$4NO + 4NH_3 + O_2 \rightarrow 4N_2 + 6H_2O \text{ (Standard SCR Reaction)} \quad (2.1)$$

$$NO + NO_2 + 2NH_3 \rightarrow 2N_2 + 3H_2O \text{ (Fast SCR Reaction)} \quad (2.2)$$

$$3NO_2 + 4NH_3 \rightarrow 7/2N_2 + 6H_2O \text{ (Slow SCR Reaction)}. \quad (2.3)$$

For optimum conversion, the second reaction should dominate inside the SCR, i.e. the incoming feed gas should have an equimolar mixture of NO and NO_2. This requires precision injection of urea so that ammonia 'slip' can be minimized while maximizing NO_x conversion. In order to achieve these objectives, factors such as catalyst aging, urea injection accuracy and variation in input NO_x content become all the more important [29]. These factors are considered while studying SCR performance and design of a control strategy.

Early SCR control strategies were based on an open-loop methodology and systems [30]. However, an open loop control strategy requires a safety margin for the varying NO_x content to prevent an excessive amount of NH_3 slip [31]. Open loop strategies were good enough to take care of euro 4 emissions but they were not sufficient to meet the requirements of regulations thereafter (Euro 5, US 2007, US 2010) [31]. Therefore, numerous closed loop strategies were developed to address these issues [23,31]. Most closed-loop strategies have the assumption of only NO being the contributor from total NO_x content. This simplifies the model. Factory installed NO_x sensors can read the total NO_x values. However, by taking into account the composition of both NO and NO_2, it is possible to improve the performance of the SCR.

In this regard, the latest control strategies focus on a model based estimator closed loop methodology that analyzes NO and NO_2 content separately instead of treating it as total NO_x. [32]. For example, in one of the studies focusing on this strategy, a NO_x conversion improvement of 36.2% and a reduction by 27% of average NH_3 slip was achieved using this model for a cold FTP test [32]. There is no direct method of measuring the NO: NO_2 ratio. This can only be estimated using physical quantities measured from various sensors attached to the after-treatment system. The model developed in this regard shall be explained more in chapter 5.

In the exhaust stream, NO has the highest concentration followed by NO_2 which is much lesser and N_2O which is almost negligible. A relationship between engine out NO_2/NO_x and total NO_x was observed and evaluated across various engine set points and a correlation was established by Hsieh and Wang [33]. NO_2 concentration can be obtained using this correlation:

$$C_{NO_2,engine} = C_{NO_x} k_1 e^{-k_2 C_{NO_x}} \quad (2.4)$$

where $C_{NO_2,engine}$ is the concentration of engine out NO_2 and C_{NO_x} is the concentration of total NO_x from the engine. The results obtained from the model were compared with the actual data and the same is shown below:

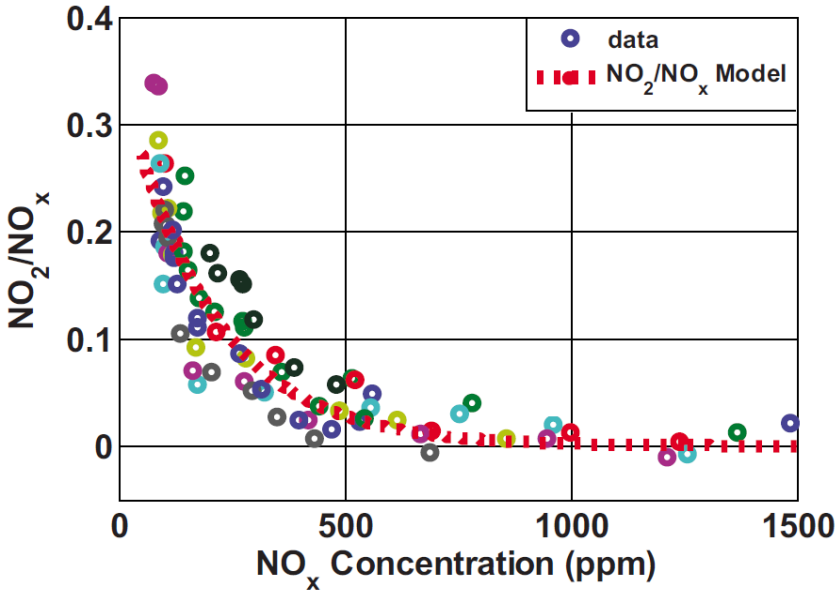

Figure 2.1. Experimental Results of NO_2 /NO_x vs NO_x. The Model Illustrates An Exponential Decay Between NO_2/NO_x and NO_x Concentration [33].

For the model shown above, the DOC was assumed to have a CSTR (Continuous Stirred Tank Reactor) for simplicity. In a CSTR model, the reaction rate is assumed to be uniformly distributed. Also, the reaction is assumed to be in equilibrium at a low temperature.

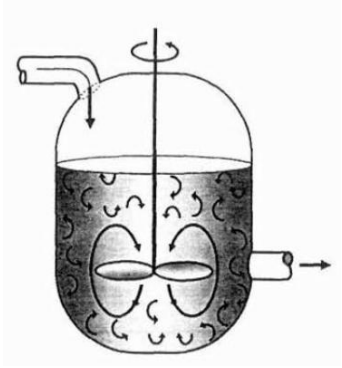

Figure 2.2. Continuous Stirred Tank Reactor (CSTR) Model [34].

Hsieh and Wang [33] have developed an observer based model which can estimate the engine out DOC and DPF NO and NO_2 concentrations as well as predict the NO/NO_2 dynamics for the same. The controller design strategy required for urea dosing in an SCR can benefit from this. However, the effect of aging in the DOC is not taken into account in this estimation.

2.2 Aging Effect on DOC Performance

For a fresh, baseline DOC in a non-extreme driving scenario, ~100% of CO gets oxidized to CO_2 and ~90% of UHCs get oxidized to CO_2 and H_2O. Around 40% of NO gets oxidized to NO_2 before thermodynamic effects limit conversion. This is illustrated in figure 2.4. However, thermal aging as a result of prolonged exposure to high temperatures and chemical poisoning due to elements such as sulfur and phosphorus lead to deactivation of the catalyst. Thus, DOC effectiveness reduces over time.

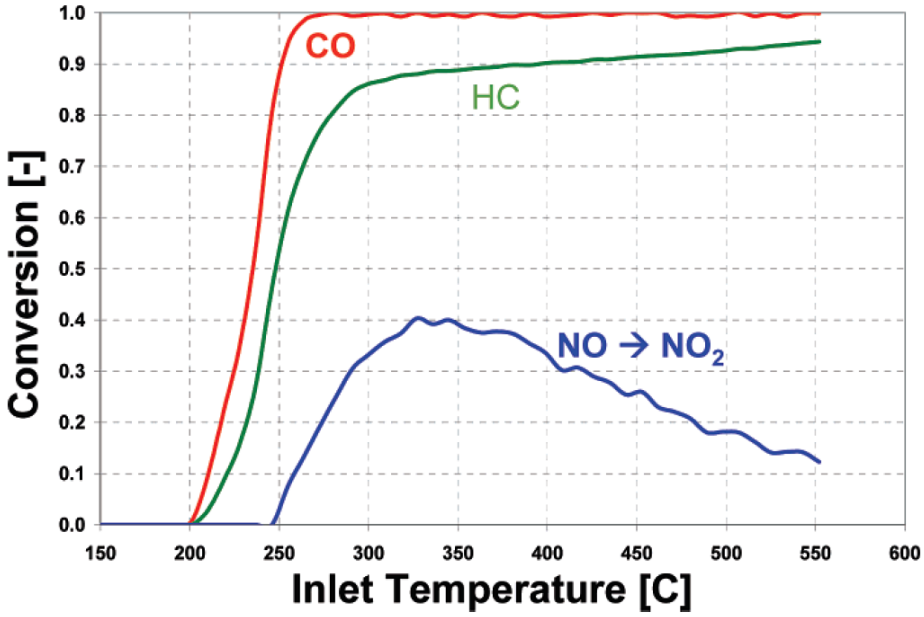

Figure 2.3. Comparison of CO, NO and HC oxidation rates for a typical Diesel Oxidation Catalyst[34].

As we can see from figure 2.4, while a fresh (degreened) DOC can oxidize up to 40% of the NO in the exhaust stream, the aged DOC could become a net consumer of NO_2, which causes decreases NO oxidation activity and causes reduction of NO_2 to NO in the DOC[35]. According to research, this extreme scenario can be caused by soot fouling on the DOC inlet [36]. However, soot fouling is a reversible process. This research also emphasizes hydrothermal sintering as a major cause of catalyst deactivation. The increased size of the Pt-Pd located farthest from the inlet side indicates sintering [36]. This was also confirmed from another study where it was seen that the smallest particle size shifted from ~8nm to ~20nm after the DOC was thermally aged at 850°C for 16 hours [37]. The science behind these phenomena is that high temperatures agglomerate various small particles into a single, large particle. This reduces the surface area containing active sites. This phenomenon occurs more at the rear end of the DOC due to the exothermic

reactions that occur inside the DOC, which raise the temperature and, as a result, the outlet temperature exceeds the inlet temperature.

The case of poisoning is different in the sense that poisoning occurs as soon as the poison compound finds an active catalytic site. This leads to deactivation of the DOC at the front side. Therefore, poisoning is a severe form of catalyst deactivation.

2.2.1 Substantiating DOC Aging Level

A useful terminology that helps to determinie DOC aging is dispersion. Dispersion is defined as the ratio of active to total sites on the catalyst. As the DOC ages, the dispersion number decreases since the total sites remain constant but the number of active sites decreases.

$$D = \frac{n_{active}}{n_{total}}. \tag{2.5}$$

Another parameter for substantiating DOC aging is called specific platinum surface, which is defined as the ratio of active catalytic surface to geometric surface [37]. This number can be used to relate the DOC aging level with the reaction rate of a model DOC, i.e. the model can be a reference to the fresh catalyst and once it is related to the specific platinum surface number, we could better understand the ageing level in a DOC.

$$O_{pt} = D\frac{m_{pt}}{MW_{pt}\varphi_{pt}A_{geo}} \tag{2.6}$$

where D is dispersion, m_{pt} is the total mass of platinum (kg), MW_{pt} is the molecular weight of Pt (g/mol), φ_{pt} is the surface site density in (mol/cm^2), and A_{geo} is the geometric surface area of the monolith (m^2).

2.3 Light Off Based Strategies to Understand DOC Effectiveness Level

Regardless of what aging mechanism is used, it always leads to a reduction in catalyst effectiveness. Relating this extent of aging to the light off temperature is the ultimate goal of this project. During the process of literature review, it was found that a relatively short number of studies related light off temperature to DOC effectiveness level. This project aims to fill this void by correlating the light off temperature to the DOC effectiveness level. This shall further help in relating the effectiveness level to the DOC out NO and NO_2 characteristics.

The light-off temperature approach has been explored previously to determine catalyst aging and corresponding effectiveness level change [36,37]. The light off temperature is found to always increase as the catalyst ages. This theory is never, however, applied to a scenario where laboratory grade HC sensors will not be available, such as onboard a vehicle. In the laboratory scenario, the air flow characteristics are also more or less well defined, unlike in an actual vehicle.

Previous work done regarding on board applications include two projects from Herrick laboratories. Both use a thermal balance approach using temperatures from on board temperature sensors to develop an indirect light off temperature detection model. The second work undertaken by Sutjiono, R. [46] improved upon the weakness inherent in the first work [40], where it was insufficient in predicting the light off temperature in a transient driving environment. Although the second work improved upon it, it was not able to validate the model for light off shifts over multiple aging levels. This forms a core objective of this thesis.

2.4 Impact of Water in a Diesel Oxidation Catalyst Activity

A thorough review was carried out on past literature written regarding impact of water presence in the exhaust stream on the DOC activity. From the paper by Kolli et. al.[51], it was found that water treatment of the DOC had a promoting effect on the oxidation of CO and HCs. In this particular research, different types of commonly used catalysts were treated with water and their activities were measured. The catalysts used were Pd/CeO_2 and $Pd/Zr\text{-}CeO_2$ catalysts which are typically used in diesel oxidation catalysts. For both these types, it was found that the water treated catalysts had a higher activity than the fresh catalyst as well as catalysts which were subjected to SO_2 and $SO_2 + H_2O$ treatment. Figure 2.4 clearly shows this observation.

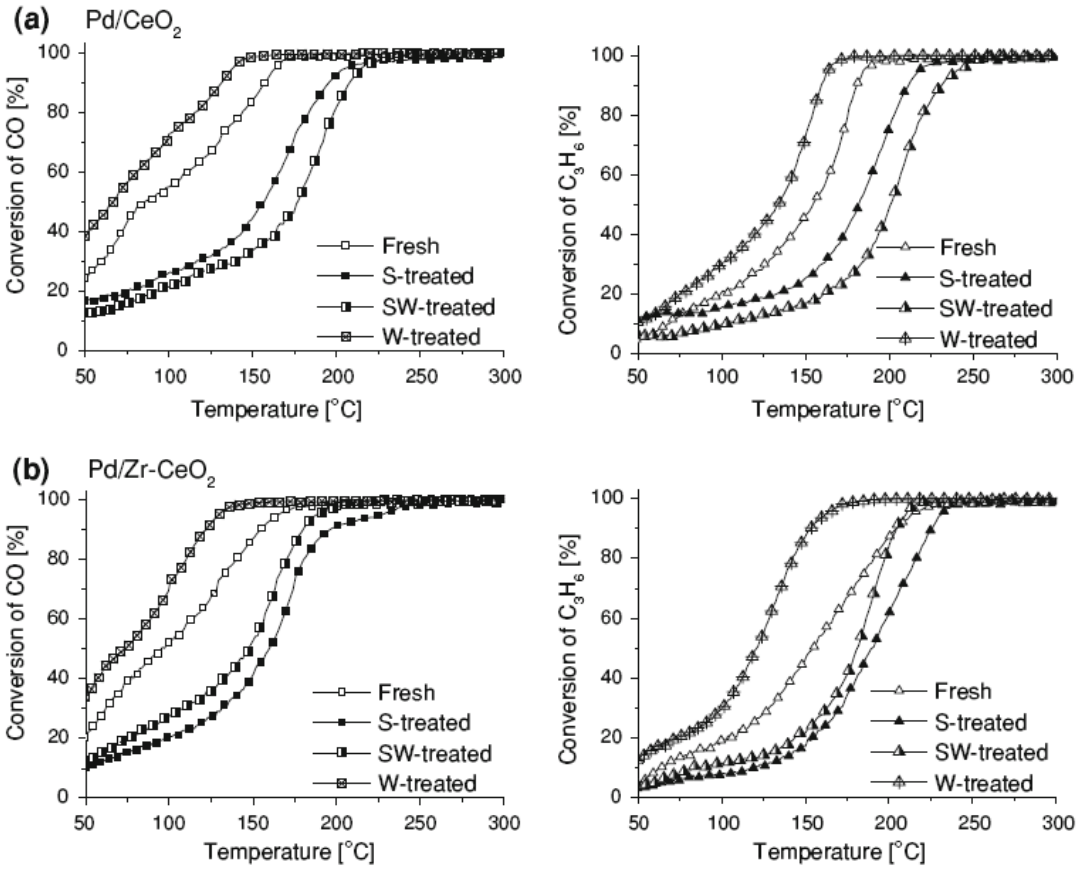

Figure 2.4. Conversion Comparison Between a Fresh Catalyst and a Catalyst Treated Separately with H_2O, SO_2 and H_2O + SO_2 Respectively [51].

CHAPTER 3. EXPERIMENTAL SETUP

The experimental setup used to carry out experiments required to formulate the two different kinds of models has been discussed in this chapter. Largely, the setup consisted of an engine, a dynamometer, various sensors installed on the engine and exhaust stream, exhaust emission analyzers, data acquisition apparatus and lab apparatus pertaining to air and water supply.

3.1 Overview of the Hardware Setup

All the experiments have been carried out on a Cummins 2007 ISB 6.7L diesel engine installed in the engine lab facility at the Ray W. Herrick Laboratories. The engine is a prototype variant and has a VGT (variable geometry turbocharger), EGR (Exhaust Gas Recirculation) system and a custom exhaust piping in order to better suit the needs of exhaust gas measurements. The exhaust gas piping has an outlet to an overhead exhaust fan. The engine is rated at 325 bhp and has a maximum torque output of 650 lb-ft at 1500RPM. The engine is connected to an eddy-current dynamometer via a twin-disk clutch, capable of absorbing 800 lb-ft of torque. Tables 3.1 and 3.2 list out the specifications of the engine and the dyno in more detail. The end of the exhaust pipe is connected up to the roof exhaust fan. Figures 3.1 and 3.2 help in better visualising the hardware:

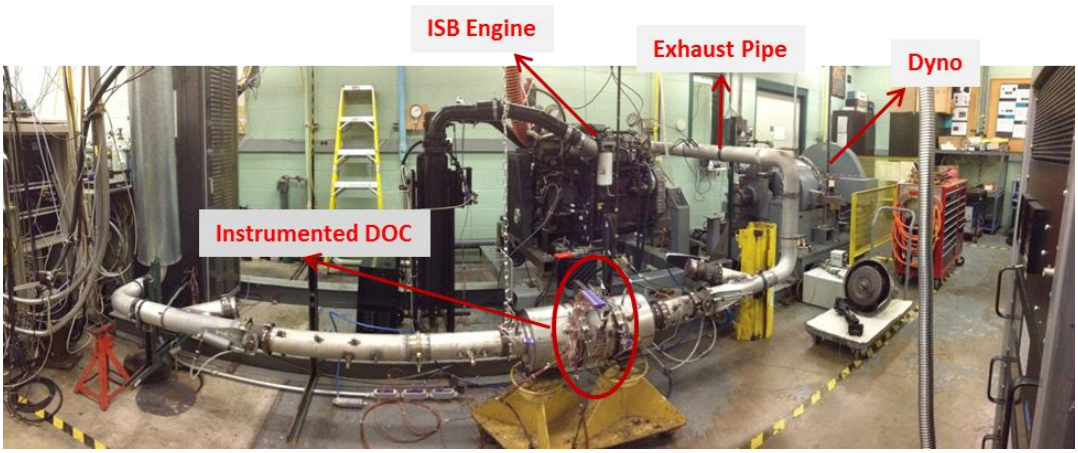

Figure 3.1. Overall Setup of the Engine and the Dyno in the Laboratory.

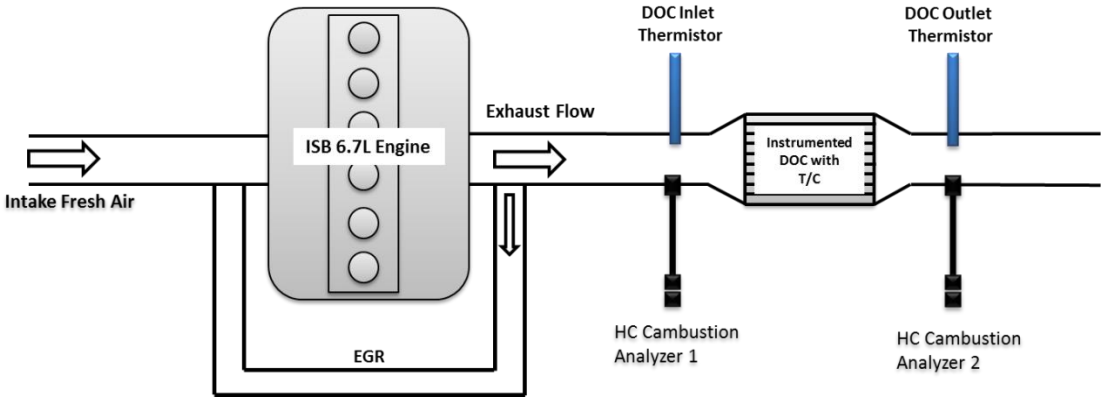

Figure 3.2. Experimental Setup schematic (T/C :Thermocouples).

The engine and dyno are water cooled and employ shop water for this purpose. Shop air is also used for adjusting the EGR intercooler valve. A log book lists out the steps and is used before each experiment involving the engine.

For the purpose of this project, the research focus is on the after-treatment setup and not the engine per say. The engine provides exhaust gas at different temperatures according to the nature of the designed experiments. These exhaust mass flow rate values and temperatures are obtained by running the engine at different speed and torque set points.

Table 3.1. Engine Specifications.

ENGINE	SPECIFICATION
Model	Cummins ISB 6.7L
Configuration	Inline 6 cylinder
Rated Power	325 hp
Peak Torque	650 lb-ft @ 1500 RPM
Charge Induction	Variable Geometry Turbocharger (VGT)
Fuel Injection	Direct Injection high pressure common rail system

Table 3.2. Dynamometer Specifications.

DYNO	SPECIFICATION
Model	GE - 1G473
Excitation volts	60 Volts
Max Power Absorption	800 hp
Controller	DyneSystems Dyn-Loc IV

The instrumented Diesel Oxidation Catalyst (DOC) used in this project is provided by Cummins and the specifications of the same have been listed in Table 3.3. Since all the chemical parameters are not accurately known due to intellectual property rules, some of them were approximated using published literature.

Table 3.3. DOC Properties .

Parameters	Values
Diameter (in)	9.75 inch
Length (in)	4 inch
Configuration	Flow through
Substrate Material	Cordierite
Cell Density	400 cpsi
Catalyst Material	Pt/Pd

From Figure 3.3 , we can see how the instrumented DOC is installed in the exhaust stream. The DOC has 12 thermocouples installed in 3 different axial planes and 4 radial locations per plane to analyze temperature gradients within the DOC. Figure 3.4 illustrates this setup.

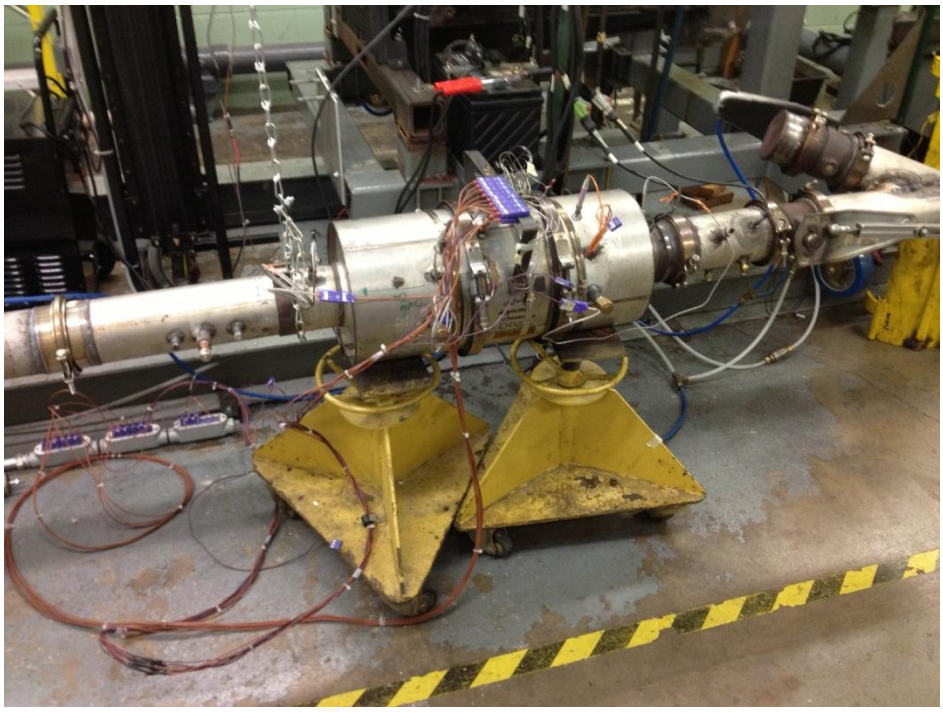

Figure 3.3. Diesel engine aftertreatment Setup with only the DOC installed.

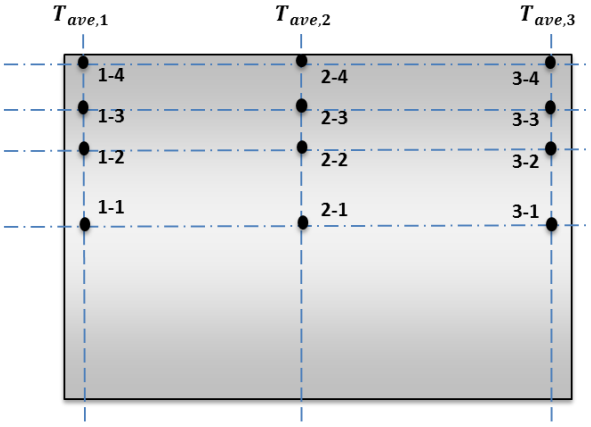

Figure 3.4. DOC Thermocouple Instrumentation Schematic.

Using an actual engine instead of feed gas generator to provide feed gas to the DOC has the advantage that real world conditions are mimicked in terms of exhaust behaviour. However, the dynamic behaviour of the engine in terms of EGR position, VGT position and other parameters has the potential to cause variations in the temperature and exhaust composition that are not desired. Also, accurate concentrations of a particular exhaust gas component cannot be metered into the exhaust stream. These challenges pose a threat as well as an opportunity to develop more robust models. However, factors such as exhaust analyzer calibration, checking for leaks, etc need to be taken into consideration before an experiment is performed.

3.2 Data Measurement and Acquisition

The temperature data forms an essential part of both modeling exercises performed in this project. In order to facilitate this, a combination of thermistors and thermocouples are installed in the engine and exhaust setup. A set of one TC and one thermistor is installed both upstream and downstream of the DOC. As mentioned before, temperature readings are obtained from within the DOC using a set of 12 E-Type TCs. A schematic of the setup is shown in figure 3.5.

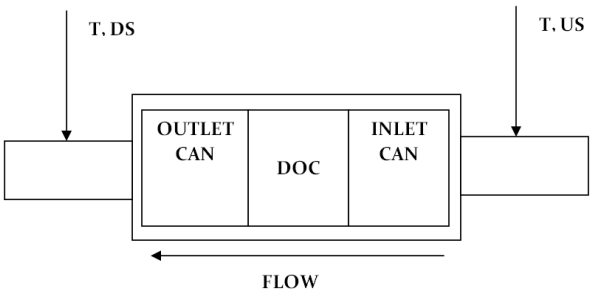

Figure 3.5. Figure showing the position of temperature sensors on the DOC installation.

The thermocouples that are installed within the DOC are connected to signal conditioners for amplification. In order to attenuate undesired high frequency noise, the TCs were made to pass through a low pass analog filter (Krohn-Hite 3364 anti- aliasing filters).

The data acquisition from all the sensors attached to the engine and the after-treatment system, including the emissions analyzers, is carried out using dSpace Controldesk software. The data from the temperature, pressure and mass flow sensors attached to the engine are obtained via the dSpace autobox which is connected to the ECM directly. Other parameters within the ECM are monitored using Cummins proprietary software, Calterm, which interacts with the ECM via the J1939 communications protocol over a Peak systems' RP1210A adapter. Real time data monitoring as well as commanding the engine to different speed and torque points, either manually or via pre-programmed cycles, is carried out using Controldesk, which has a custom made front end visual User Interface (UI) and a back end designed in Simulink. By default, data is acquired at 1 Khz. This is downsampled depending on the length of the experiment by a factor of 30, 40 or 45. Thus, the effective sampling rate becomes 33.33 Hz, 25 Hz and 22.22 Hz, respectively. Controldesk sends signals to the engine either as an analog voltage or digital serial communication. It interacts with the dyno via a 16 pin parallel connection. The block diagram in figure 3.6 gives an overview of the communication structure.

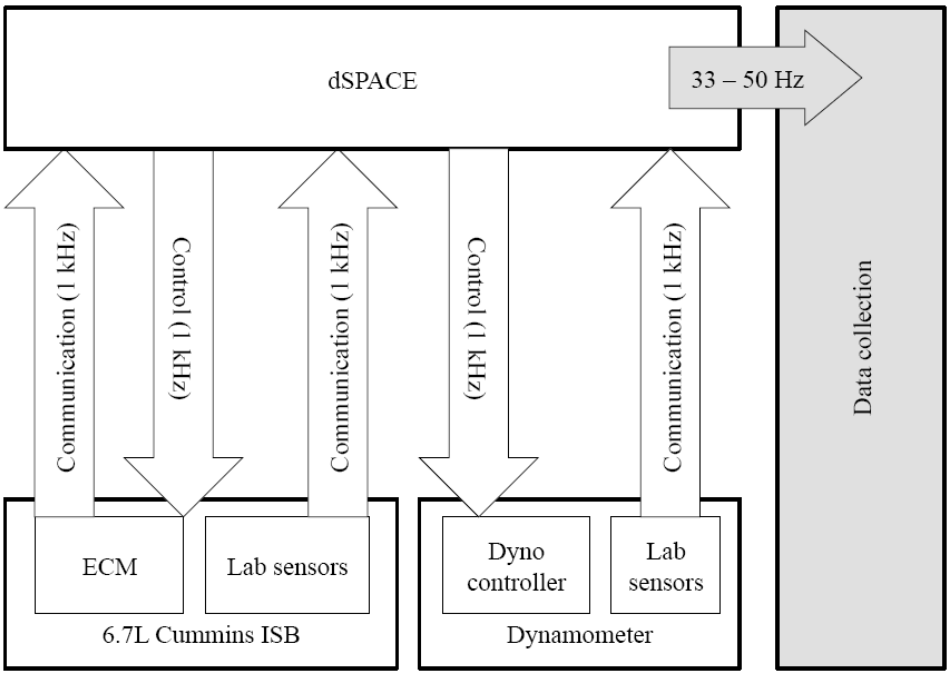

Figure 3.6. Data Acquisition and Hardware Organization Schematic.

3.3 Emissions Analyzers

The modeling work in this project requires measurement of primarily UHCs, NO and NOx in the exhaust stream. In order to fulfill this requirement, two different types of Cambustion exhaust analyzers have been used. These are the Cambustion HFR500, for measuring unburnt hydrocarbons, and the Cambustion fNO$_x$ 400 analyzer for measuring NO$_x$ and NO. Both of these analyzers have 2 channels which facilitate measuring data upstream and downstream of the DOC simultaneously. The HFR500 as well as the fNOx 400 analyzers have very fast response times (< 1 ms) which enables them to record most transient data. These two shall be discussed in brief in the following sub sections.

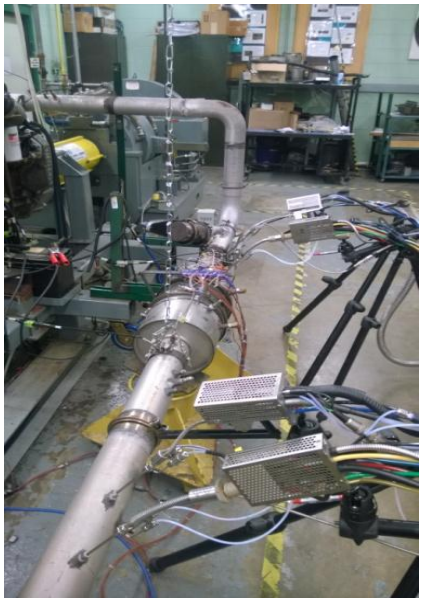

Figure 3.7. Figure Shows a Typical Experiment in Progress Showing 2 Channels of HFR 500 Analyzers and 2 Channels of fNOx 400 Analyzers Connected to the Exhaust Stream.

3.3.1 Cambustion HFR500 HC Analyzer

This analyzer detects a compound as UHCs in the form of 3 carbon atoms (C_3). This means that the concentration value being displayed is one-third of the actual UHC concentration. Figure 3.6 shows a picture of the sampling head of one of the channels. The exhaust gas is sampled here and the signals are sent to the main unit to process and display the HC content on a user computer. Table 3.4 lists the details of this analyzer.

Table 3.4. Cambustion HFR500 Specifications.

Detector	FID
Ranges	0-2000 ppm C to 0-1000000 ppm C
Response Time	< 0.9 ms
Repeatability	1% Full-Scale
Linearity	1% Full-Scale

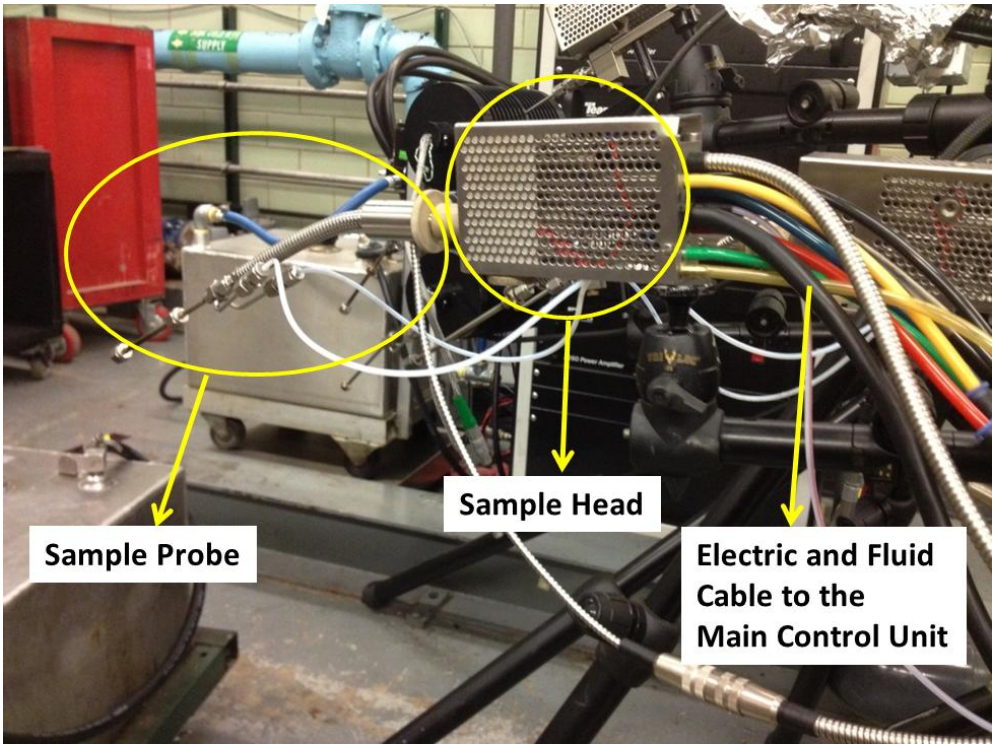

Figure 3.8. Picture of the Sample Head of One of the Two Cambustion HFR500 Channels.

3.3.2 fNO$_X$ 400 NO$_x$ Measurement System

This system measures NO and total NO$_x$ depending on what sampling head is connected to the main unit. Both heads have different operating requirements in terms of probes and operating temperatures. The NO$_x$ measurement sampling head has a NO$_x$ convertor unit which basically converts all non-NO components (NO_2 and N_2O) into NO since it operates at a temperature of 840°C. The probe for measuring only NO operates at a temperature of 150°C. The output is obtained as a voltage in the range of 0-10V and after applying an appropriate slope and intercept value, data is acquired in ppm. The drawback

of using this system is that it consists of a number of components that can frequently break down, hence rendering the equipment not useful. Therefore, careful practices need to be adopted while using this piece of equipment in order to obtain useful data that can be used towards the project objective. Figure 3.7 shows the fNO_x 400 exhaust sampling system and Figure 3.8 shows the NOx sampling head with the NOX convertor head.

Figure 3.9. fNOx400 exhaust analyzer.

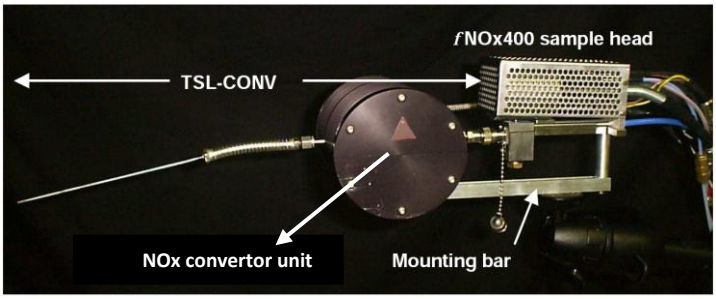

Figure 3.10. NO_x measuring head.

3.4 DOC Aging Procedure

The Diesel Oxidation Catalyst used was thermally aged to simulate deactivation that would have been caused if the DOC was used on an on board system for a certain number of miles. The DOC was aged at Alcoa's facility in Lafayette, IN. A total of 3 such aging routines were carried out according to the procedure listed in Table 3.5. Figure 3.11 shows a visual comparison between the state of the DOC prior to and after an aging routine.

Table 3.5. DOC Aging Procedure.

Temperature (°C)	**Duration (Hours)**	**Process**
25-650	2	Initial warm-up phase
650	20	Main aging phase
650-25	15	Oven cool-down phase

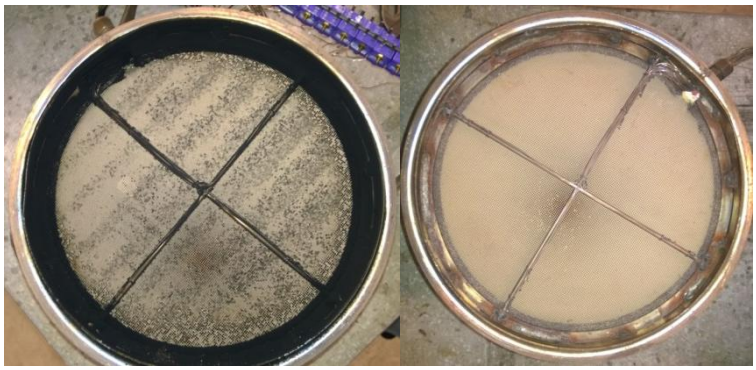

Figure 3.11. Comparison between the Physical Condition of the DOC Pre (left) and Post (right) a Thermal Aging Routine.

CHAPTER 4. DIRECT AND INDIRECT HYDROCARBON LIGHT OFF TEMPERATURE DETERMINATION FOR A DOC AND EFFECT OF AGING ON LIGHT OFF

This chapter discusses the techniques used to determine the direct HC light off temperature for a diesel oxidation catalyst as well as the mathematical model (indirect method) developed to determine the same. It also discusses the effect that thermal aging has on the light off temperature for a DOC.

4.1 Experimental Method to Determine HC Light Off for a DOC

4.1.1 Introduction

We know that the light off temperature ultimately determines the catalyst effectiveness level. In order to determine the light off temperature on board a vehicle, a mathematical model/virtual sensor will have to be developed which can mimic the trends shown by an actual HC analyzer, based on certain inputs. The mathematical model development work has been carried out already in a previous phase of this project. In order to validate the models, experimental methods play a vital role. This section explains more about how the experiment was designed and the procedures that were carried out to determine the light off temperature experimentally.

As mentioned in the introduction, we know that in a DOC, out of all the exhaust emissions, CO lights off first, followed by the HCs and finally, NO lights off. From separate experiments done at Herrick labs as a part of this project, it was determined that CO concentration was very low in the exhaust stream. Also, in order to nullify NO oxidation,

the HC concentration in the exhaust stream was amplified by carrying post fuel injection in the exhaust stroke of the engine.

In order to determine the light off temperature for a DOC, previous work entails a steady state procedure. However, it is not entirely effective in developing a model that is to be used in a real world on-board setup. Therefore, a different experiment that can determine the light off temperature in transient aftertreatment conditions will be discussed now.

4.1.2 Procedure

For this particular experiment, the exhaust stream only encounters an instrumented DOC and not the complete after-treatment configuration for a diesel engine. This DOC contains 12 thermocouples installed at 4 radial positions at 3 locations along the axis of the DOC. Two on board thermistors are used to measure the temperature upstream and downstream of the DOC. During analysis, the four temperature readings at the 3 axial locations are averaged.

The design of experiments (DOE) plays a crucial role in determining the exhaust temperature characteristics and emission characteristics. A very fast exhaust temperature ramp is not desired since the light off temperature of the catalyst (~200°C) may be exceeded in a very short time, rendering the data unusable. Therefore, an experimental plan where the engine would go from idle to subsequent speed and torque points one after the other in steps is selected. At idle, the DOC inlet temperature was found to be ~60°C which is much lower than the DOC light off temperature. This is a suitable set point from which to begin the test. Table 4.1 lists the engine set points selected to carry out this experiment. We can see that there are 4 speed and 2 torque points, and neither of the

torque points is below 100 lb-ft. This is such because the eddy current dynamometer installed in the facility is not capable of sustaining constant torque points below 100 lb-ft. The speed points increase from 1200 RPM to 1800 RPM since this helps in providing a wide range of exhaust mass flow rates to analyze.

Table 4.1. Engine Operating Points for DOC Light-off Temperature Experiments.

Engine Speed (RPM)	**Engine Torque (lb-ft)**	**Fuel Dosing (g/s)**
1200	150	0.3
1200	300	0.3
1400	150	0.3
1400	300	0.3
1600	150	0.3
1600	300	0.3
1800	150	0.3
1800	300	0.3

The 'Fuel Dosing' term is the quantity of diesel fuel injected during the exhaust stroke of the engine to intentionally increase the HC content. This injection is carried out using Cummins Calterm. For example, during normal operation, HC content is generally below 100 ppm concentration. However, for the fuel dosing value selected, the concentration goes up to a value around 1000 ppm. The EGR valve is closed during the duration of the dosing to prevent plugging of the EGR intercooler. The HC concentration values as detected by the analyzer are monitored and acquired using the Controldesk software.

4.1.3 Results and Analysis

The experiments as listed above were carried out on the current DOC in its degreened state and another set was carried out after thermally aging it according to the procedure

mentioned earlier. The entire cycle of set points was organized into an automated time based cycle with time gaps during which the engine was kept at idle. This time gap allowed the DOC to cool below 100°C and also, to carry out calibration of the HC, NO and NOx analyzers as per the design of the experiment.

The previous phase of this project had essentially completed testing for two phases in the life of the DOC. At the end of the second set of tests, it was thermally aged again. Therefore, for this project, the experiments were carried out for the third aged level followed by another thermal aging event and consequently, for a fourth aged level. Unlike the previous project phase, NOx and NO analyzers were also used along with the HC analyzers. Description of the same has been given in chapter 3.

Figure 4.1 shows the upstream and downstream measurements of hydrocarbons as measured by the HC analyzer, for the DOC in aged level 3.

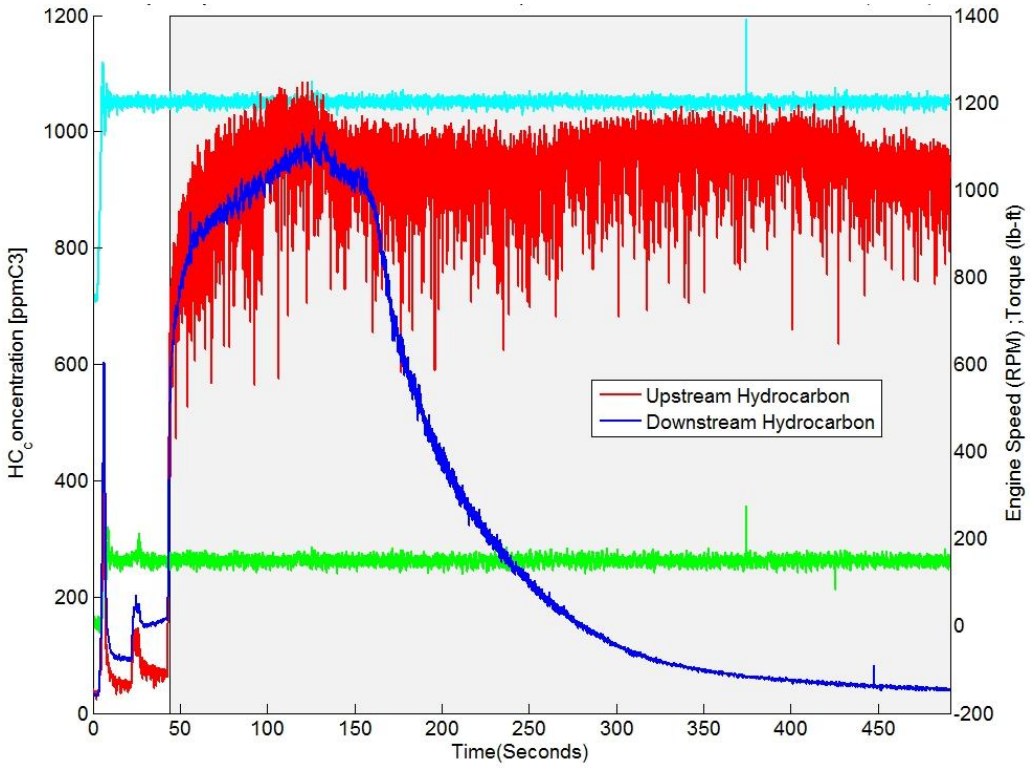

Figure 4.1. Figure showing the upstream and downstream HC concentration as the reaction proceeds for Aged level 3, 1200 RPM-150 lb-ft.

The shaded region in the above figure denotes the region of post fuel injection. We can clearly see the downstream HC concentration reducing with time. The corresponding temperature characteristics are shown in Figure 4.2.

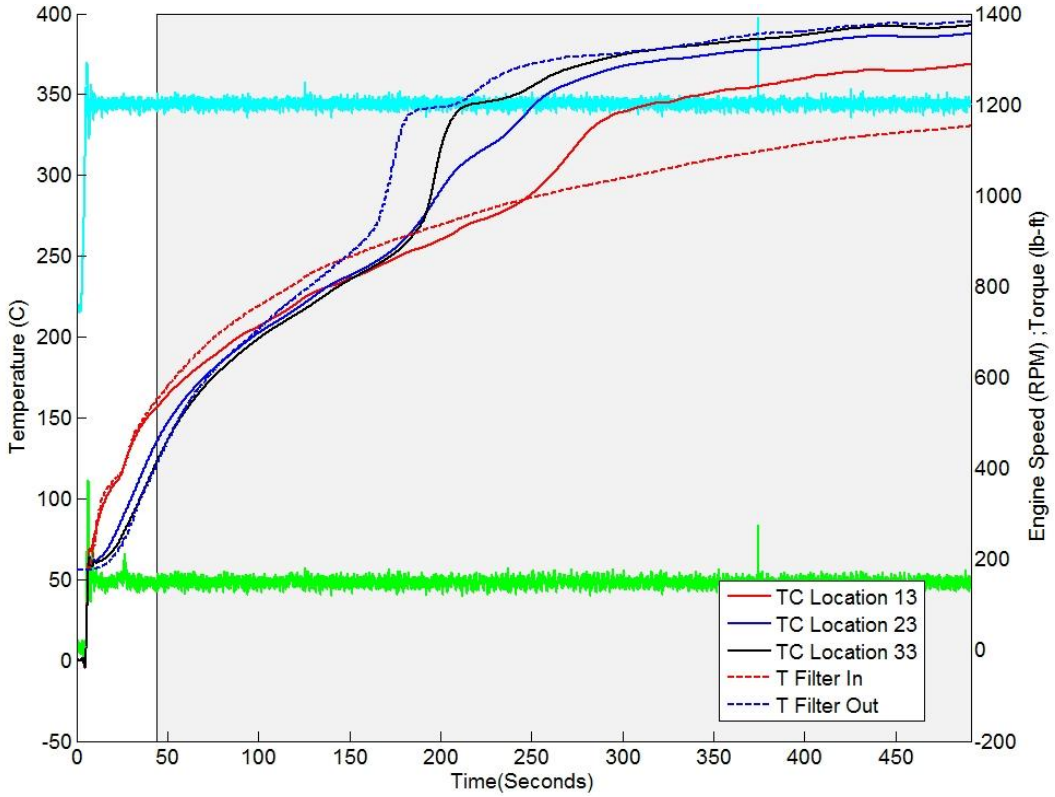

Figure 4.2. Figure showing the temperature values at inlet and outlet of the DOC as well as averaged temperature at the three axial locations as the reaction proceeds for Aged level 3, 1200 RPM-150 lb-ft.

From Figure 4.2, we can clearly see that light off is achieved at the point where the temperature values for all but the inlet temperature suddenly increase. The outlet temperature also increases since the conversion reactions in the DOC are exothermic in nature.

The direct HC conversion is calculated using the following simple relation:

$$Direct\ Conversion\ Efficiency\ (\%) = \frac{(HC\ conc)_{Upstream} - (HC\ conc)_{Downstream}}{(HC\ conc)_{Upstream}} * 100. \quad (4.1)$$

Figure 4.3 depicts the direct conversion efficiency for the 1200 rpm-150 lbft case.

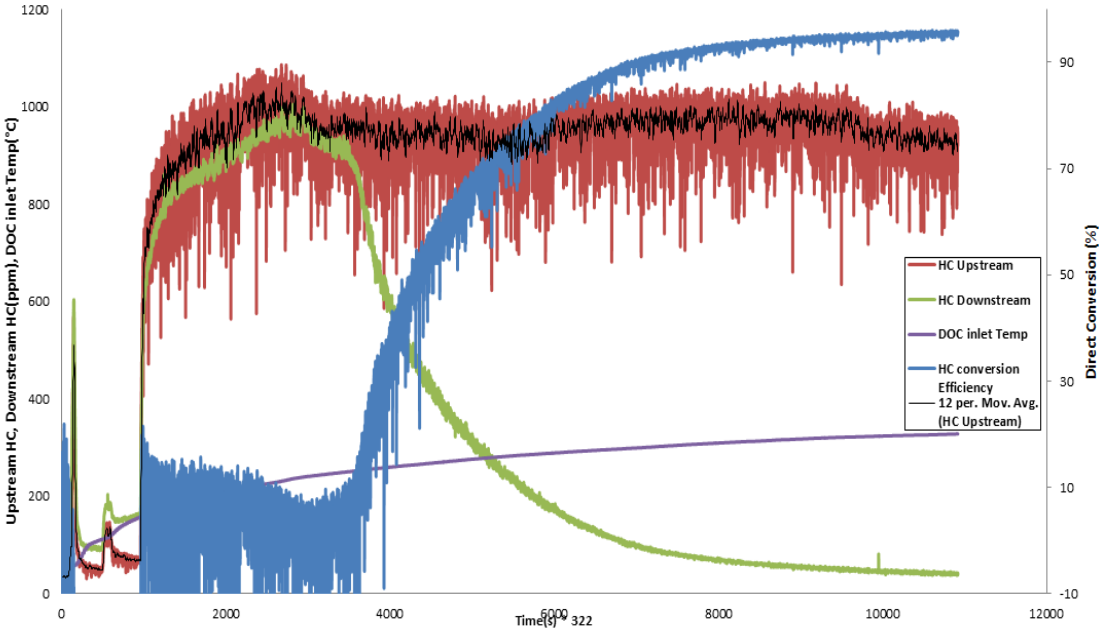

Figure 4.3. Figure showing the Direct conversion efficiency trend for the DOC at Aged level 3, 1200 RPM-150 lb-ft. Notice the negative value of conversion at start of fuel injection.

We can clearly see that HC conversion shows an upward trend as the DOC inlet temperature increases and peaks at around 95% conversion efficiency.

4.2 Indirect Method to Determine Light Off Temperature for a DOC

4.2.1 Introduction

The indirect method to determine the HC light off temperature has been developed using thermal balance equations. In other words, this method uses temperature measurements inside the DOC to determine the light off temperature. The aim of this

modeling exercise was to improve upon a previously developed indirect light off detection equation by Cummins. This old equation was given by:

$$X_{indirect} = \frac{[\dot{m}_{exh} + \dot{m}_{dose}]\ [C_{out}T_{out} - C_{in}T_{in}]}{\dot{m}_{dose}\ LHV} * 100\% \qquad (4.2)$$

where $\dot{m}_{exh}$ and $\dot{m}_{dose}$ stand for the mass flow rate of the exhaust and dosed fuel respectively, C_{out} and C_{in} denote the inlet and outlet HC concentrations and T_{out} and T_{in} denote the DOC inlet and outlet temperatures. *LHV* stands for the lower heating value of diesel fuel. In this kind of experiment, the exhaust temperatures were raised very slowly, which meant that the thermal dynamics inside the reactor could be essentially ignored.

However, for a real world application, changing the engine operating conditions in steps, such as going from idle to 1600 RPM in a short duration, is considered more realistic. Taking these factors into consideration, the indirect equation so developed has terms that capture the dynamic behavior of the engine during transient thermal conditions.

4.2.2 Development of the Model

The model was developed by Sutjiono, R. [46] treating the reactor as a one dimensional control volume. The differential equations used determined the HC conversion using the temperature field measurement. These measurements were used to develop a heat distribution profile for each control volume into which the reactor was divided, which was obtained in the form of differential thermal equations.

The model was derived using the differential thermal balance of the exhaust flow and the catalyst solid. The obtained model was then discretized to implement the test data into the model. For developing the differential equations, a 1D model was preferred over a 2D model due to ease and computation speed as well as for the fact that the light off temperature difference between the two was found to be less than 2°C [41]. The axial coordinate system was chosen for describing the 1D model. The assumption of perfect insulation was made for the outer surface, since the tests were carried out on a stationary engine bench. Non-isothermal assumption was applied. Most of the heat transfer occurs between the exhaust gas and the monolith. The model equation has two main parts, i.e. the solid heat storage term and the gaseous heat storage term.

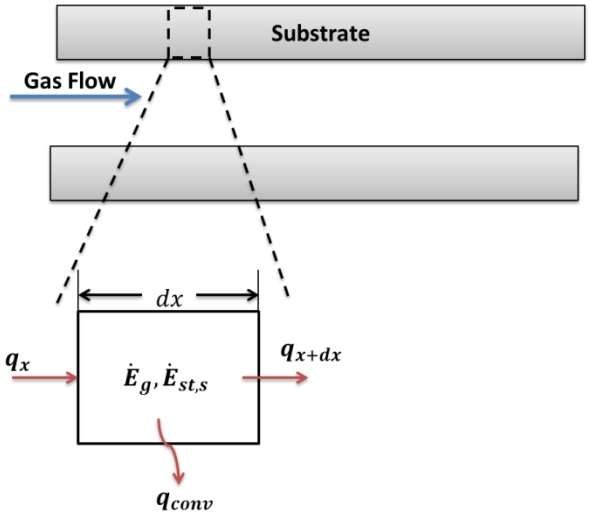

Figure 4.4. 1D Differential Control Volume for the solid [46].

For the solid heat storage equation, a rate based energy balance was carried out according to the Cartesian system as shown in Figure 4.4:

$$\dot{E}_{st} = \dot{E}_{in} - \dot{E}_{out} + \dot{E}_{gen}. \tag{4.3}$$

From the 1D control volume, we can see that conduction occurs in the axial direction and can be written as:

$$q_{x+dx} = q_x + \frac{\partial q_x}{\partial x}\, dx \tag{4.4}$$

where, using Fourier's Law [42]:

$$q_x = -k\frac{\partial T}{\partial x}\, dydz\,. \tag{4.5}$$

Here dydz is the differential cross sectional area of the control volume.

Convective heat transfer occurs in the y direction and is given as:

$$q_{conv} = \mathrm{h}_{conv}\left(T_s - T_g\right)dxdz \tag{4.6}$$

where h_{conv} is the convective heat transfer coefficient, T_g is the gas temperature and T_s is the solid temperature.

Solid heat storage ($\dot{E}_{st}$) is given as:

$$\dot{E}_{st} = \rho_s\, c_{p,s}\frac{DT_s}{Dt}\, dx\, dy\, dz \tag{4.7}$$

where the non-steady state 1D flow for temperature is given by:

$$\frac{DT}{Dt} = \frac{\partial T}{\partial x}\frac{dx}{dt} + \frac{\partial T}{\partial t}. \tag{4.8}$$

Thus, equation 4.7 becomes:

$$\dot{E}_{st} = \rho_s\, c_{p,s}\left[u_s\frac{\partial T_s}{\partial x} + \frac{\partial T_s}{\partial t}\right]dx\, dy\, dz\,. \tag{4.9}$$

Here, the u_s term is zero since the catalyst is stationary. This gives:

$$\dot{E}_{st} = \rho_s\, c_{p,s}\left[\frac{\partial T_s}{\partial t}\right]dx\, dy\, dz\,. \tag{4.10}$$

Chemisorption in the catalyst is exothermic, and this is considered as heat generation. This is given as:

$$\dot{E}_g = R_{DF}\,\Delta H^o_{DF}\,dx\,dy\,dz \tag{4.11}$$

where R_{DF} is the chemisorption reaction rate in $\left[\frac{mol}{m^3 s}\right]$ and ΔH^o_{DF} is the energy content of diesel fuel in $\left[\frac{J}{mol}\right]$.

Combining all terms gives:

$$\rho_s\,c_{p,s}\frac{\partial T_s}{\partial t} = k\frac{\partial^2 T_s}{\partial x^2} + h_{conv}(T_s - T_g)\frac{\Delta A_{conv}}{\Delta V} + R_{DF}\,\Delta H^o_{DF} \tag{4.12}$$

where ΔA_{conv} is the differential surface area of the channel.

The general form of 1D thermal balance for a solid control volume is thus obtained. The conduction term is generally neglected owing to it being negligible.

The next step was to derive the gas thermal balance equation [46].

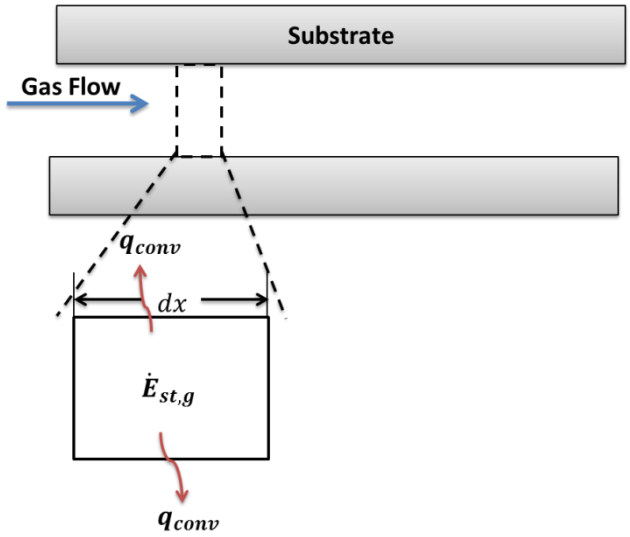

Figure 4.5. 1D Differential Control Volume for Exhaust Gas Flow [46].

A thermal balance similar to the one carried out for the solid heat storage term was carried out. The various terms were obtained as follows:

Energy storage of the gas:

$$\dot{E}_{st,g} = \rho_g c_{p,g} \frac{DT_g}{Dt}\, dx\, dy\, dz \tag{4.13}$$

which can be modified as:

$$\dot{E}_{st,g} = \rho_g c_{p,g} \left[u_g \frac{\partial T_g}{\partial x} + \frac{\partial T_g}{\partial t} \right] dx\, dy\, dz. \tag{4.14}$$

The convective heat transfer for the exhaust:

$$q_{conv} = h_{conv}(T_g - T_s) dx dz \tag{4.15}$$

The combined energy conservation equation for the control volume of the exhaust gas was obtained as:

$$\rho_g c_{p,g} \left[u_g \frac{\partial T_g}{\partial x} + \frac{\partial T_g}{\partial t} \right] dx\, dy\, dz = -h_{conv}(T_g - T_s) dx dz. \tag{4.16}$$

Since, $\frac{\partial T_g}{\partial t}$ = o, $u_g\, dy\, dz = \Delta \dot{V}$ and $\Delta \dot{V} \rho_g = \dot{m}_g$, we get:

$$\dot{m}_g c_{p,g} \left[\frac{\partial T_g}{\partial x} \right] dx = -h_{conv}(T_g - T_s) \Delta A_{conv}. \tag{4.17}$$

A species balance was then carried out [46]. A plug flow reactor (PFR) model was assumed for the DOC. According to this model, reaction rates continuously vary over the length of the catalyst and there is no distinction between reactions that occur in solid and gas as in thermal balance. Figure 4.6 shows flow schematic in a PFR model.

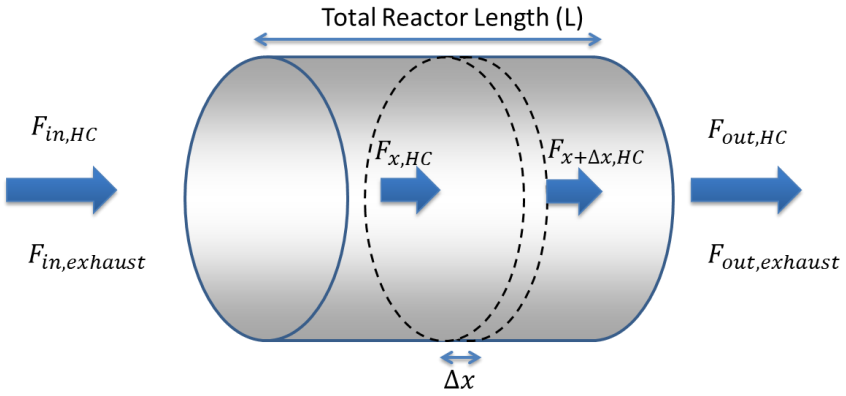

Figure 4.6. Plug Flow Reactor (PFR) Model.

The general species balance is defined as [14]:

$$F_{in} - F_{out} + F_{gen} = \frac{dN}{dt} \tag{4.18}$$

where F (concentration flow rate) is given as $F = C\dot{V}$, F_{in} and F_{out} represent the rate of flow of HC into and out of the system, F_{gen} is called the rate of generation of HC, and dM/dt represent the rate of accumulation of HC species in the system.

For our purpose, a differential control volume analysis gives:

$$F_x - F_{x+dx} + \int_0^V R\, dV = 0. \tag{4.19}$$

This integral is discretized into:

$$\frac{F_{x+dx} - F_x}{\Delta V} = R. \tag{4.20}$$

As ΔV tends to zero, R becomes:

$$R = \lim_{\Delta V \to 0} \frac{F_{x+dx} - F_x}{\Delta V} = \frac{dF_x}{dV}. \tag{4.21}$$

The conversion of HC can be given in the following relation:

$$F_{HC,0} - F_{HC,0}X = F_{HC} \tag{4.22}$$

where $F_{HC,0}$ is the initial HC flow rate at the inlet, F_{HC} is the HC flow rate evaluated along the reactor length and X is the conversion term. By combining Eq 4.21 and Eq 4.22, we get a differential HC conversion balance term:

$$-F_{HC,0}\,\frac{dX}{dV} = R \text{ or } \frac{dX}{dV} = -\frac{R}{F_{HC,0}} \tag{4.23}$$

which is rearranged to:

$$R = \frac{F_{HC,0}}{\Delta A_c}\,\frac{dX}{dx} \tag{4.24}$$

where ΔA_c is the change in cross sectional area.

Combining Eq. 4.12, 4.17, and 4.24 gives:

$$\rho_s\, c_{p,s}\frac{\partial T_s}{\partial t}\Delta V = \dot{m}_g c_{p,g}\left[\frac{\partial T_g}{\partial x}\right] dxdydz + \frac{F_{HC,0}}{\Delta A_c}\,\frac{dX}{dx}\,\Delta H_{DF}^{o}\Delta V \tag{4.25}$$

where $F_{HC,0} = \frac{\dot{m}_{HC,0}}{M_{HC}}$ and $\Delta H_{DF}^{o} = M_{HC}\,\Delta H_{DF}$. $\dot{m}_{HC,0}$ is the inlet mass flow rate of HC, M_{HC} is the hydrocarbon molar mass, ΔH_{DF}^{o} is the diesel molar enthalpy and ΔH_{DF} is the diesel mass enthalpy. Eq. 4.25 is modified to give:

$$\rho_s c_{p,s} A_{c,s}\frac{dT_s}{dt} = \dot{m}_g c_{p,g}\frac{dT_g}{dx} + \dot{m}_{HC}\frac{dX}{dx}\,\Delta H_{DF}. \tag{4.26}$$

In equation 4.26, the first term is the solid heat storage term, the second term is the gas heat storage term and the last term is the heat generated by oxidation of HC. The DOC effectiveness level is indicated by the light off temperature which changes as the DOC ages. This is determined by the temperature of the substrate corresponding to the 50% conversion rate as obtained from the indirect equation.

In order to simplify the calculation of the space-time derivative terms in the model equation, discretization using finite difference methods was carried out. This allows better calculation of the conversion term with a computer code.

Equation 4.26 was first multiplied by Δx. This gives:

$$\dot{m}_g c_{p,g} \frac{dT_g}{dx} \Delta x + \dot{m}_{HC} \frac{dX}{dx} \Delta H_{DF} \Delta x = \rho_s c_{p,s} A_{c,s} \frac{dT_s}{dt} \Delta x. \tag{4.27}$$

Then, $\frac{dT_g}{dx}$ was written as:

$$\frac{dT_g}{dx} = \frac{\left(T_g(t_p, x_{n+1}) - T_g(t_p, x_n)\right)}{\Delta x}. \tag{4.28}$$

Similarly, $\frac{dX}{dx}$ became:

$$\frac{dX}{dx} = \frac{\left(X(t_p, x_{n+1}) - X(t_p, x_n)\right)}{\Delta x}. \tag{4.29}$$

And finally, $\frac{dT_s}{dt}$ became:

$$\frac{dT_s}{dt} = \frac{\left(T_s(t_{p+1}, x_n) - T_s(t_p, x_n)\right)}{\Delta t}. \tag{4.30}$$

Combining Eq 4.27, 4.28, 4.29, and 4.30 and modifying, we get the discretized equation to calculate the overall HC conversion as:

$$X(t_p, x_N) = \frac{1}{\dot{m}_{HC} \Delta H_{DF}} \left[\sum_{n=1}^{N} m_s c_{p,s} \frac{\left(T_s(t_{p+1}, x_n) - T_s(t_p, x_n)\right)}{\Delta t} \right]$$

$$+ \frac{1}{\dot{m}_{HC} \Delta H_{DF}} \left[\dot{m}_g c_{p,g} \left(T_g(t_p, x_N) - T_g(t_p, x_1)\right) \right]. \tag{4.31}$$

Here, N represents the number of subdivisions within the reactor. The solid and gaseous heat storage terms are separately analyzed as well using the following equations:

$$X_{SolidHeatStorage} = \frac{1}{\dot{m}_{HC} \Delta H_{DF}} \left[\sum_{n=1}^{N} m_s c_{p,s} \frac{\left(T_s(t_{p+1}, x_n) - T_s(t_p, x_n)\right)}{\Delta t} \right] \tag{4.32}$$

$$X_{GasHeatStorage} = \frac{1}{\dot{m}_{HC} \Delta H_{DF}} \left[\dot{m}_g c_{p,g} \left(T_g(t_p, x_N) - T_g(t_p, x_1)\right) \right]. \tag{4.33}$$

These equations are used to determine how conversion is affected by these two phases separately. From these equations, we can see that the sensor values used here are from the DOC substrate temperature sensors (T_s), gas flow temperature sensor(T_g), gas mass flow rate and the substrate mass.

The model equation was used on the Aged level 3 and 4 measurements to determine the conversion efficiency and light off temperature. Figures 4.7 and 4.8 show the conversion efficiency for two such cases:

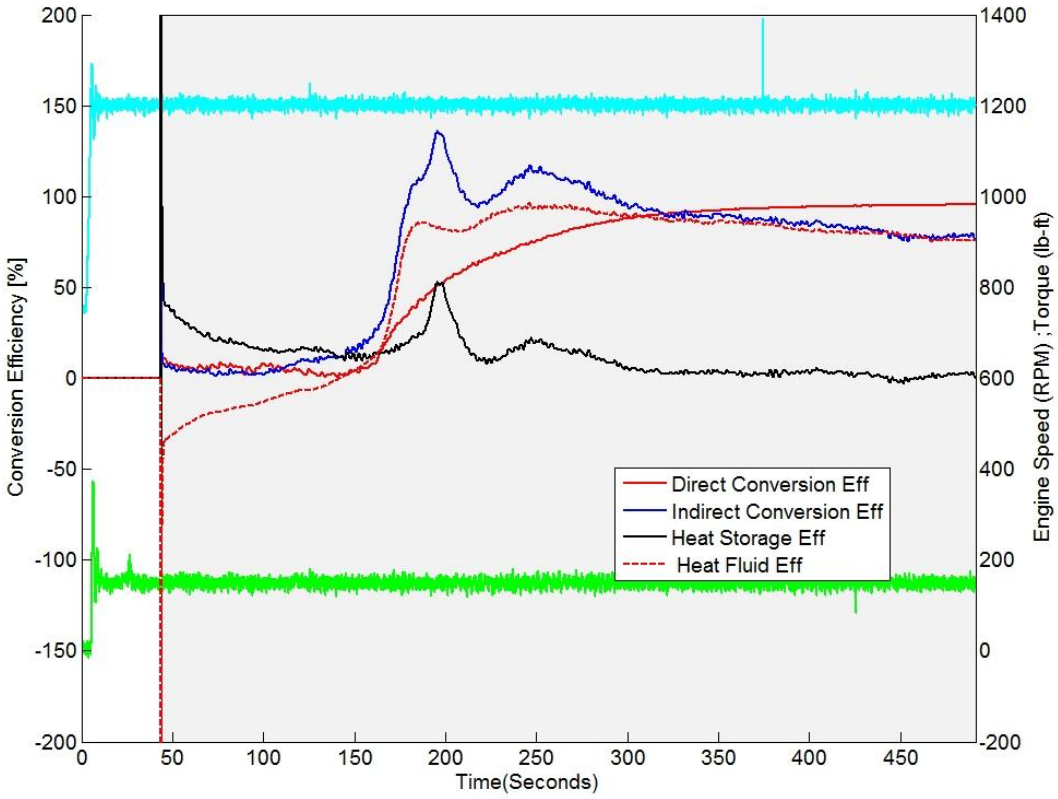

Figure 4.7. Figure showing the direct and indirect conversion efficiencies for the DOC at Aged level 3, 1200 RPM-150 lb-ft.

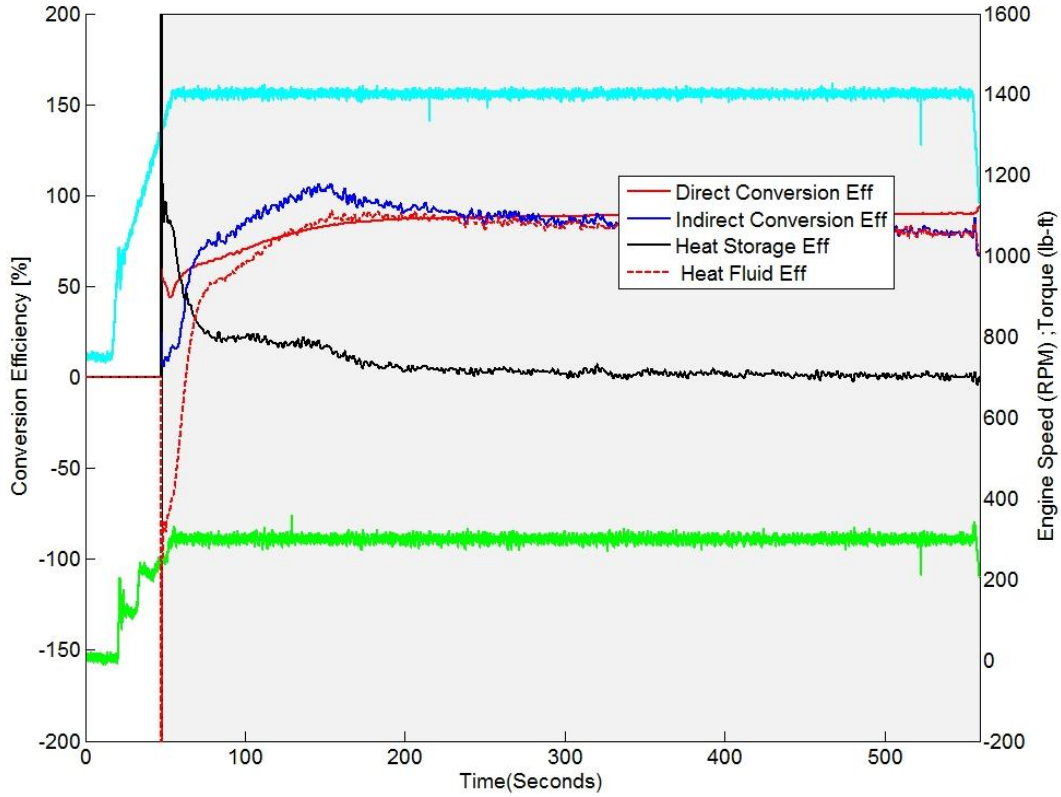

Figure 4.8. Figure showing the direct and indirect conversion efficiencies for the DOC at Aged level 3, 1400 RPM-300 lb-ft.

We can see that in both these cases, the conversion efficiency obtained from the model follows the direct conversion efficiency very closely. The indirect conversion equation was applied to the data obtained from the aged level 3 and aged level 4 tests, hence displaying the applicability of the model over multiple aging cycles of the DOC. 'Heat Storage Eff' stands for the solid heat storage term and 'Heat Fluid Eff' stands for the gaseous heat storage term. We can clearly see that the solid heat storage term has significant contribution to the overall efficiency term only at the start of an engine set point. After that, it is the gaseous heat storage term that keeps increasing or maintains a high level of conversion and consequently, the solid heat storage term keeps decreasing or

levels off at a low value. This is evident from the heat rate plots as well as shown in Figure 4.9.

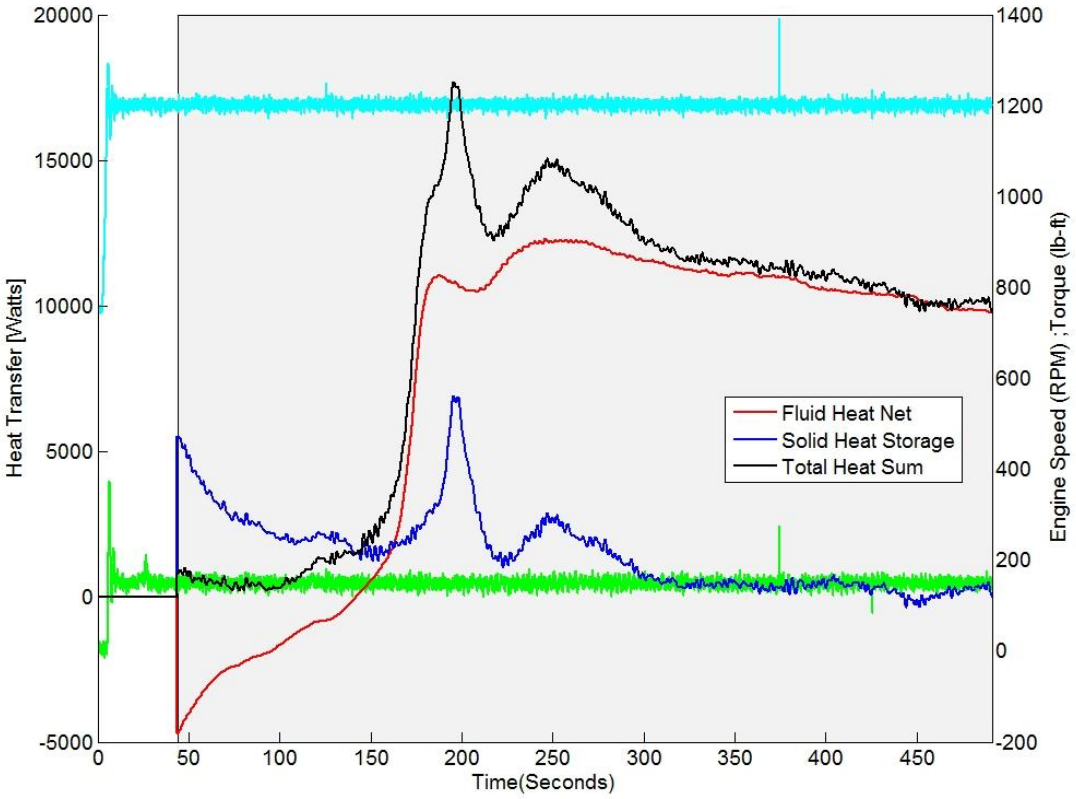

Figure 4.9. Figure showing the heat rate comparison for the DOC at Aged level 3, 1200 RPM-150 lb-ft.

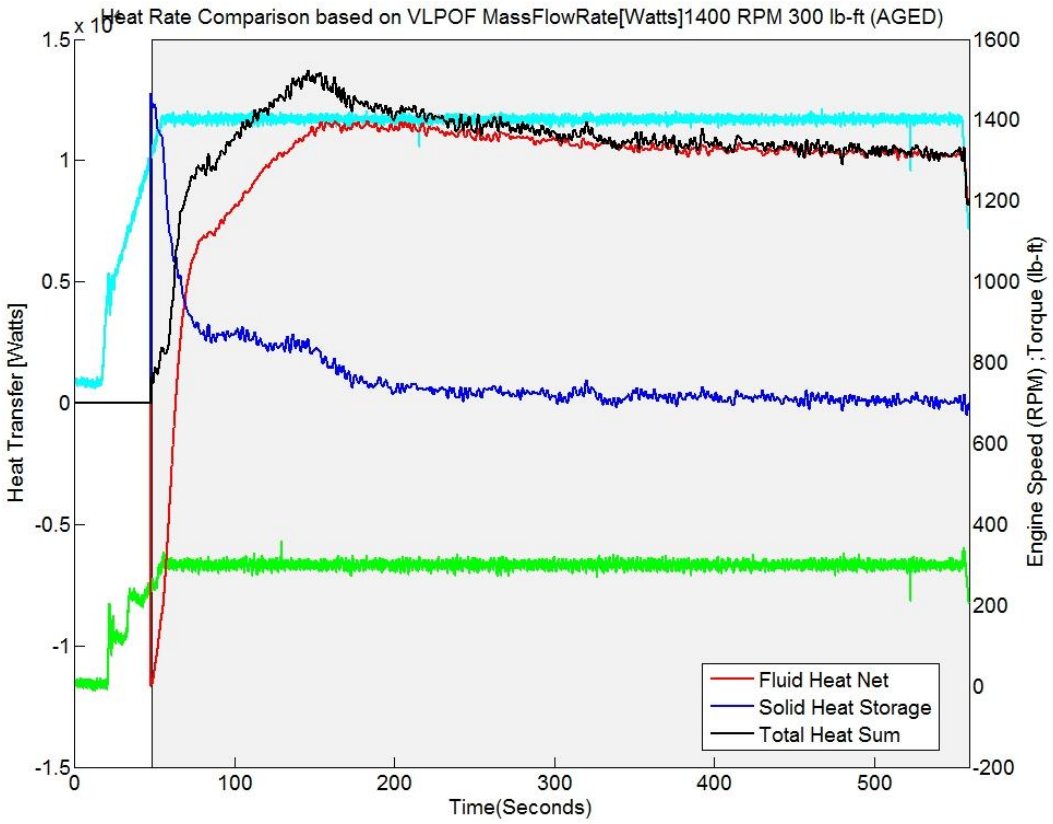

Figure 4.10. Figure showing the heat rate comparison for the DOC at Aged level 3, 1400 RPM-300 lb-ft.

4.2.3 Reducing Input Parameters for Practicality

The initial analysis regarding the indirect conversion efficiency required the use of 12 thermocouples to obtain the temperature data from within the DOC. This however, was impractical for an on board application in terms of increased effort and resources required to do so. Therefore, an exercise involving the same analysis with successively reducing thermocouples was carried out to determine the minimum number of thermocouples that could effectively determine the light off temperature and subsequently, the conversion efficiency [46]. In this process, the four readings at each axial location were averaged and

compared against each individual thermocouple at this location to determine which one was the closest. Figure 4.11 depicts one such analysis.

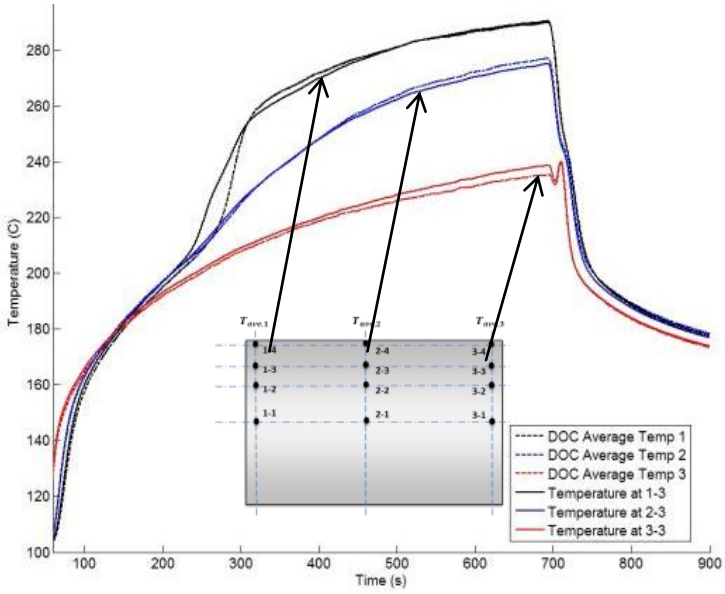

Figure 4.11. Figure showing the axial locations of the thermocouples.

This analysis determined that 3 thermocouples could be used instead of 12. However, further reduction of input data was sought. For this purpose, the indirect conversion efficiency trends were observed with temperature from 12 TCs, 3 TCs and a single TC located at the 2-3 position. Figure 4.12 shows the obtained result.

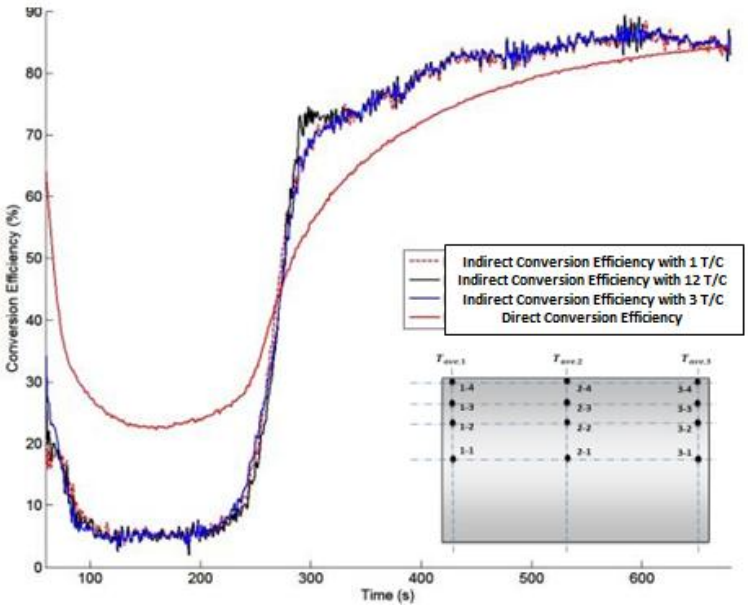

Figure 4.12. Indirect Conversion Efficiency Calculated Using Reduced Number of TCs.

We can see that the indirect conversion efficiency values from all the 3 cases follow each other closely and also, the direct conversion efficiency plot. Hence, the TC at the 2-3 position was proposed as the position to install the single thermocouple if the model was to be implemented [46].

4.3 Effect of Thermal Aging on Light Off Temperature and Conversion

The first phase of this project involved one thermal aging cycle as described in a previous section. For this project, thermal aging was carried out two more times and similar experiments were carried out. This section presents the trend in conversion rates from one aging level to another and also, a broad comparison across four different levels in the operating life of the Diesel Oxidation Catalyst.

4.3.1 Aging Level 2 vs. Aging Level 3

We have established from theory and past experiments and analyses that thermal aging causes a shift in the light off temperature of the DOC. In a similar light, Figure 4.13 shows a clear shift in light off temperature for the 1200 rpm 300 lb-ft case.

This trend is observed for all the other setpoints. The light off shift varies from case to case but a shift is visible. Let us take another set point as an example. Figure 4.14 shows the comparison for the 1400 rpm 300 lb-ft case. A clear shift in light off temperature is visible. Table 4.2 lists the light off temperatures as measured and obtained from the direct and indirect methods, respectively, for all the cases.

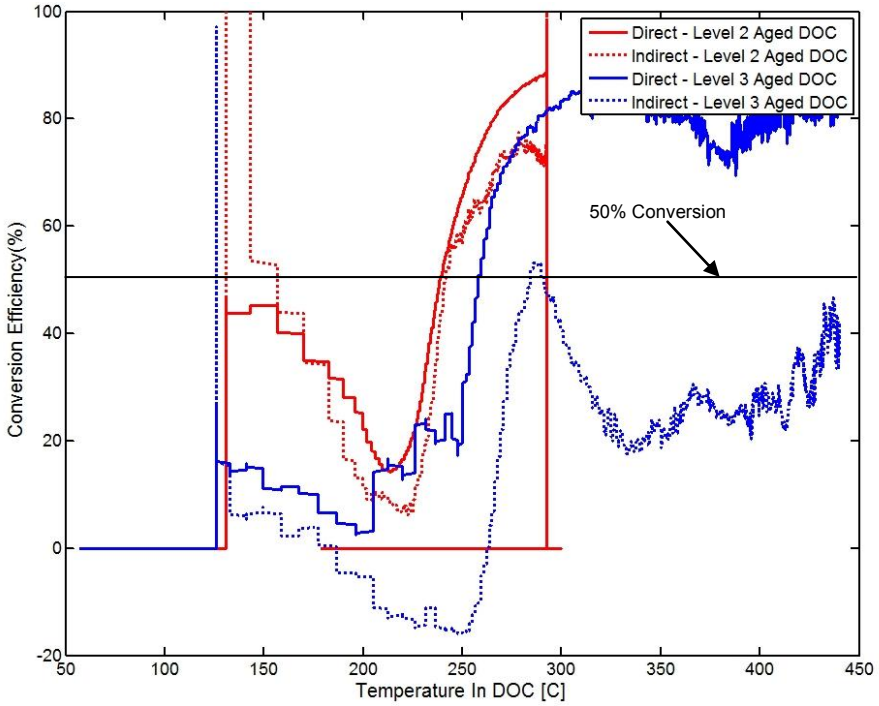

Figure 4.13. Figure showing the conversion efficiency comparison between the DOC at aged level 2 and aged level 3 for the 1200 rpm 300 lb-ft case.

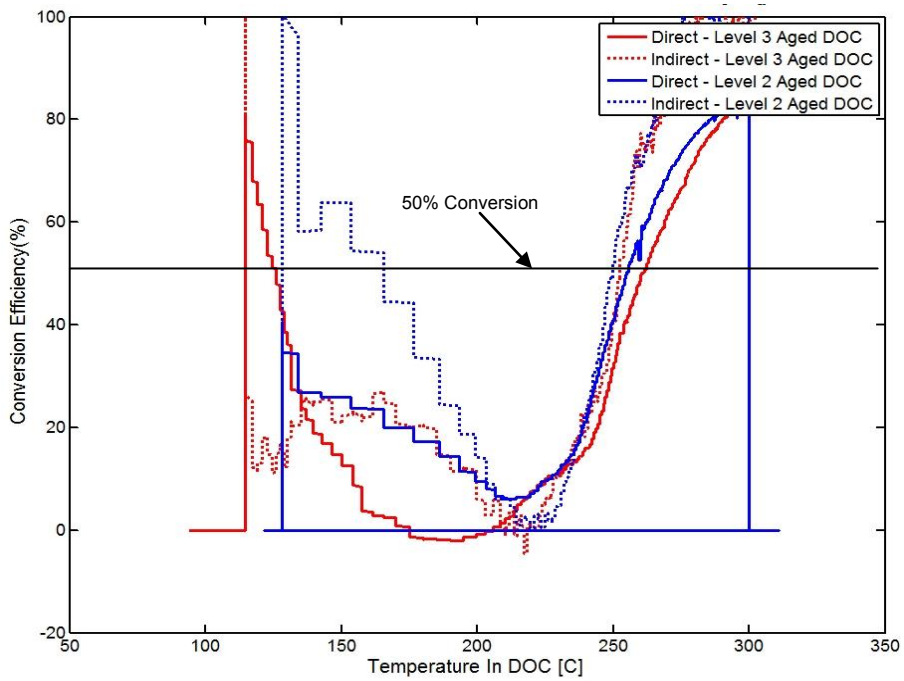

Figure 4.14. Figure showing the conversion efficiency comparison between the DOC at aged level 2 and aged level 3 for the 1400 rpm 300 lb-ft case.

Table 4.2. Direct and Indirect Light Off Temperature Comparison between Aging Levels 2 and 3.

Set point	**Aging Level 2 (deg C)**		**Aging Level 3 (deg C)**	
	Direct Method	**Indirect Method**	**Direct Method**	**Indirect Method**
1200-300	235	236	263	280
1400-150	210	212	223	214
1400-300	260	246	265	249
1600-150	226	215	234	225
1600-300	250	230	262	238
1800-150	230	220	243	221
1800-300	250	231	263	239

4.3.2 Aging Level 2 vs. Aging Level 4

Light off shifts are visible clearly when comparing aging level 2 trends with aging level 4 trends. Figure 4.15 shows one such plot.

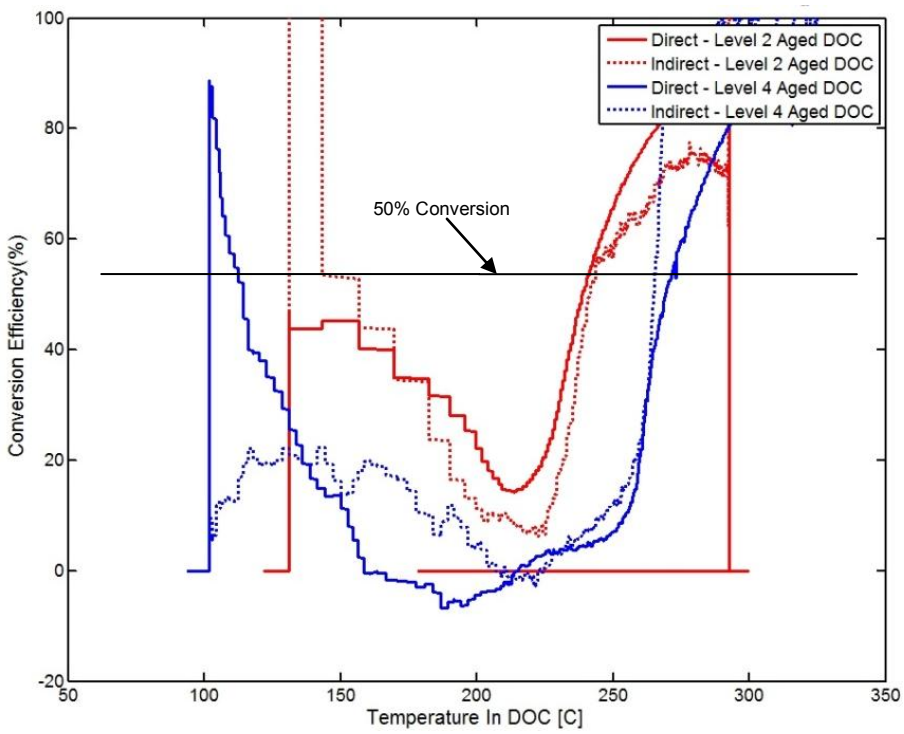

Figure 4.15. Figure showing the conversion efficiency comparison between the DOC at aged level 2 and aged level 4 for the 1200 rpm 300 lb-ft case.

These shifts were visible for all the cases. Table 4.3 lists out the direct and indirect Light off temperatures for the two aging levels.

Table 4.3. Direct and Indirect Light Off Temperature Comparison between Aging Levels 2 and 4.

Set point	Aging Level 2 (deg C)		Aging Level 4 (deg C)	
	Direct Method	Indirect Method	Direct Method	Indirect Method
1200-300	235	236	271	267
1400-150	210	212	230	220
1400-300	260	246	270	262
1600-150	226	215	238	225
1600-300	250	230	262	243
1800-150	230	221	243	228
1800-300	250	231	263	250

4.3.3 Aging level 3 vs. Aging level 4

Major light off temperature shifts were not detected between aging levels 3 and 4, although the conversion efficiency peaked to around 90%. The set point which showed the maximum amount of shift was the 1400 rpm and 300 lb-ft case. However, even for this case, the shift is very minor. Figure 4.17 shows this case. From Figure 4.16, we can see the trends for the 1200 rpm, 300 lb-ft case. Even for this case, the shift in light off is very less.

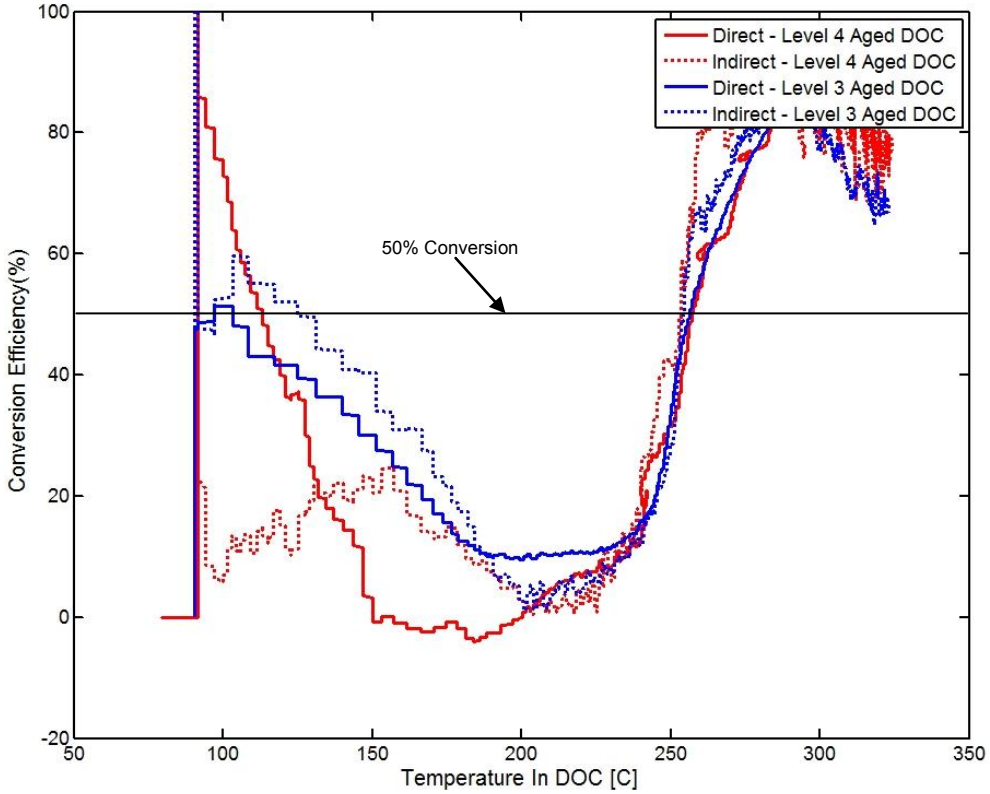

Figure 4.16. Figure showing the conversion efficiency comparison between the DOC at aged level 3 and aged level 4 for the 1200 rpm 300 lb-ft case.

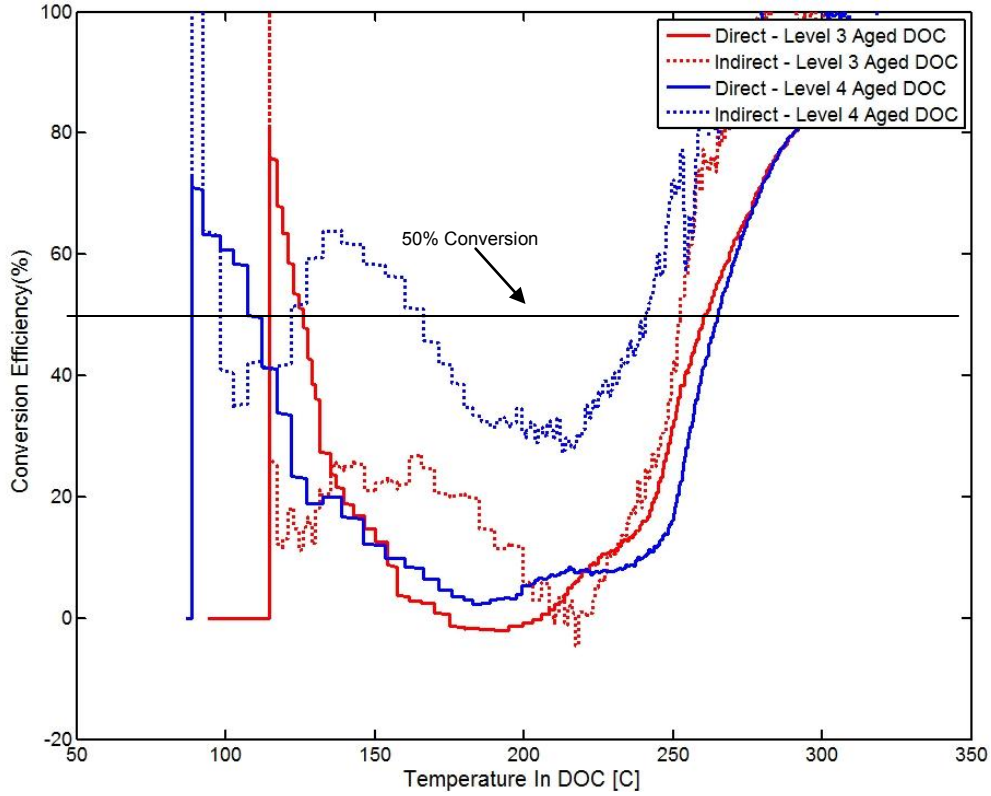

Figure 4.17. Figure showing the conversion efficiency comparison between the DOC at aged level 3 and aged level 4 for the 1400 rpm 300 lb-ft case.

Let us take the case of the 1800 rpm 300 lb-ft set point which is a high rpm and high torque case. In this case, we do not see any significant shift in light off temperature. This might indicate that the DOC is nearing its end of useful life since 3 thermal aging cycles have been completed on the same. Figure 4.17 shows this case.

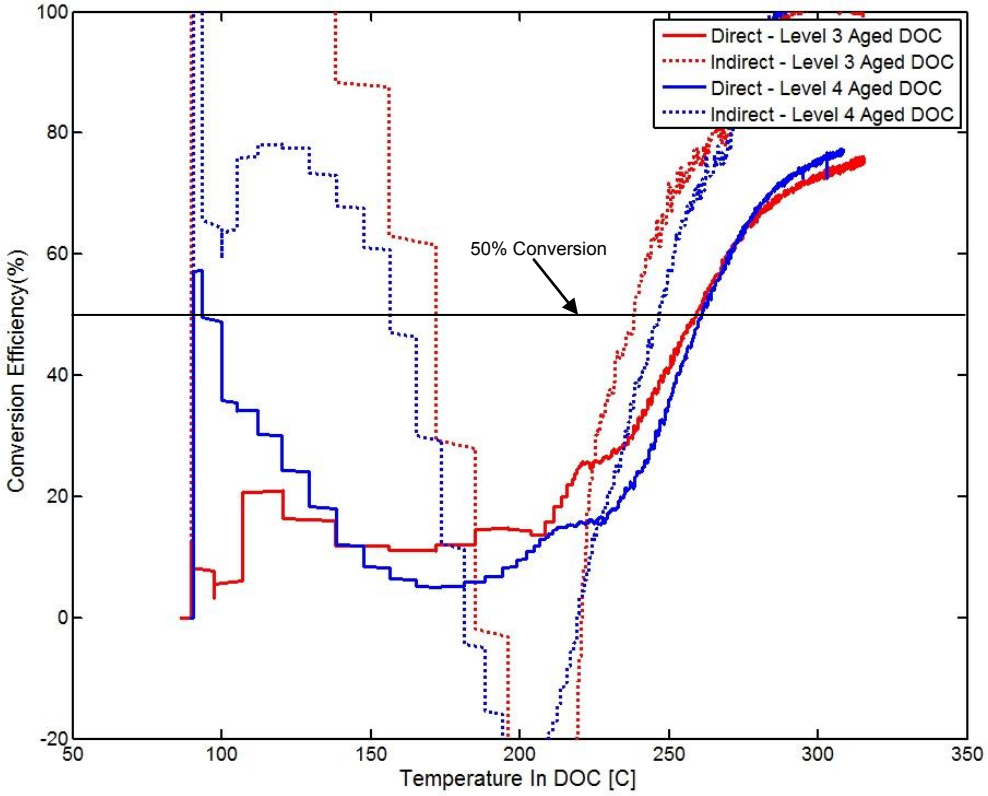

Figure 4.18. Figure showing the conversion efficiency comparison between the DOC at aged level 3 and aged level 4 for the 1800 rpm 300 lb-ft case.

Similar trends are seen in other cases as well and all the light-off temperatures have been listed in table 4.4.

Table 4.4. Direct and Indirect Light Off Temperature Comparison between Aging Levels 3 and 4.

Set point	Aging Level 3 (deg C)		Aging Level 4 (deg C)	
	Direct Method	Indirect Method	Direct Method	Indirect Method
1200-300	263	252	263	252
1400-150	223	214	230	212
1400-300	265	249	270	240
1600-150	234	225	235	225
1600-300	262	246	262	243
1800-150	243	226	243	228
1800-300	263	239	263	250

The shift in direct light off temperature from the degreened DOC to aging level 4 can be better visualized in figure 4.18. Figure 4.19 exhibits the shift across the aging levels in the indirect light off temperature.

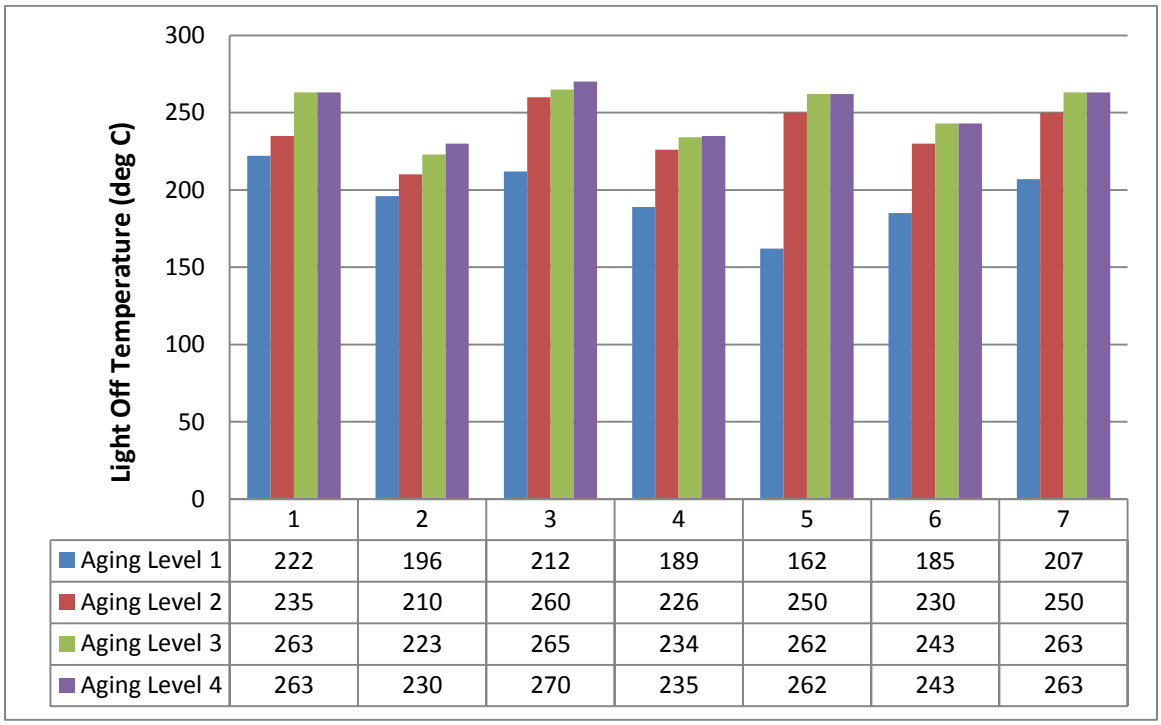

	1	2	3	4	5	6	7
Aging Level 1	222	196	212	189	162	185	207
Aging Level 2	235	210	260	226	250	230	250
Aging Level 3	263	223	265	234	262	243	263
Aging Level 4	263	230	270	235	262	243	263

Figure 4.19. Figure showing the comparison between the Direct light off temperatures from the degreened DOC to aging level 4. Numbers 1-7 denote engine set points according to Table 4.4.

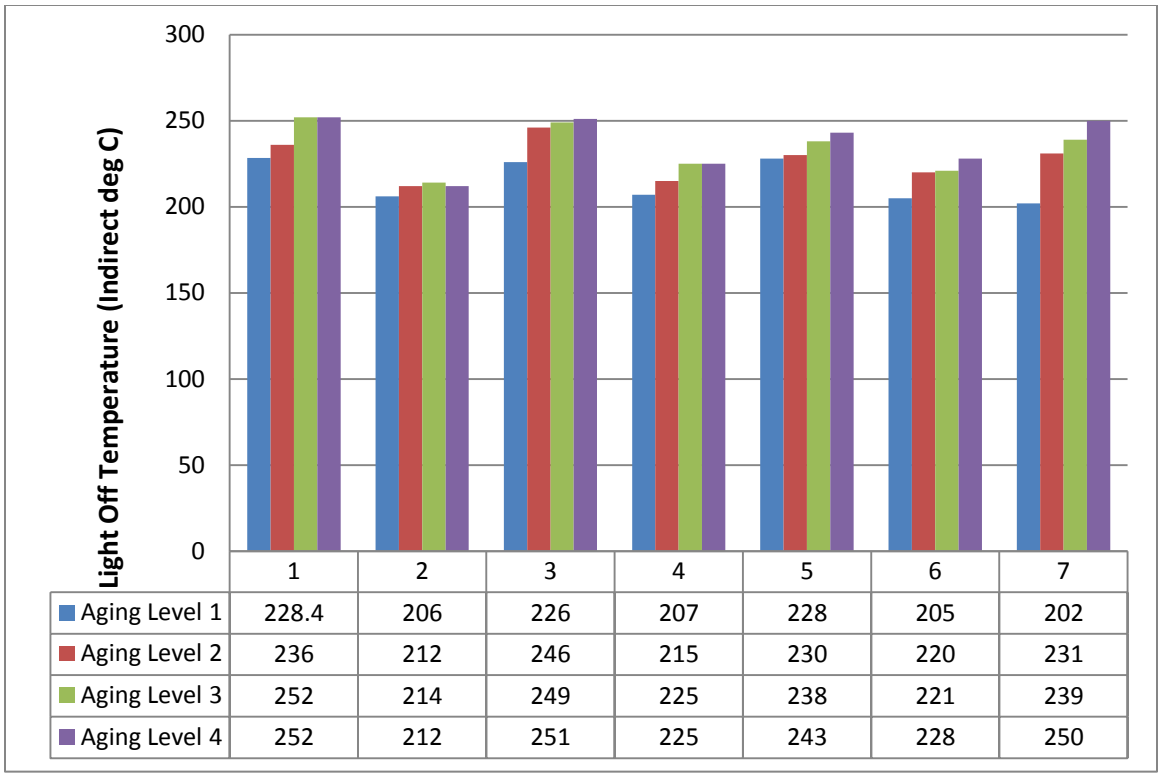

	1	2	3	4	5	6	7
Aging Level 1	228.4	206	226	207	228	205	202
Aging Level 2	236	212	246	215	230	220	231
Aging Level 3	252	214	249	225	238	221	239
Aging Level 4	252	212	251	225	243	228	250

Figure 4.20. Figure showing the comparison between the Indirect light off temperatures from the degreened DOC to aging level 4. Numbers 1-7 denote engine set points according to Table 4.4.

4.4 Consistency of Data

From Figures 4.19-4.21, we can see that the indirect light off temperature data is consistent within 10% error bounds for all the aging levels that have been mentioned here i.e. Aging Levels 2, 3 and4.

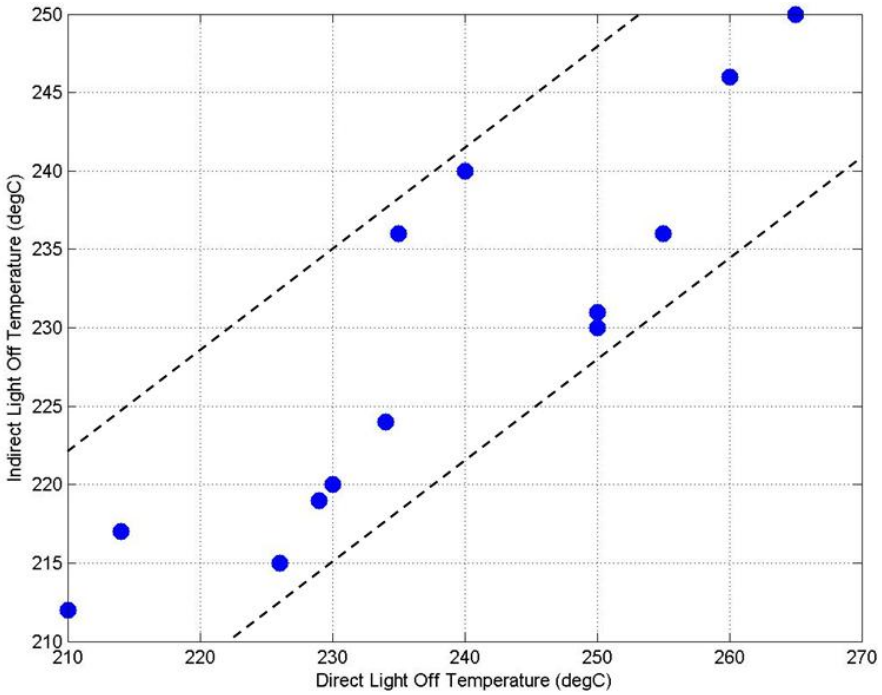

Figure 4.21. Indirect Light Off Temperature vs. Direct Light Off Temperature Error plot for the Aging Level 2 DOC.

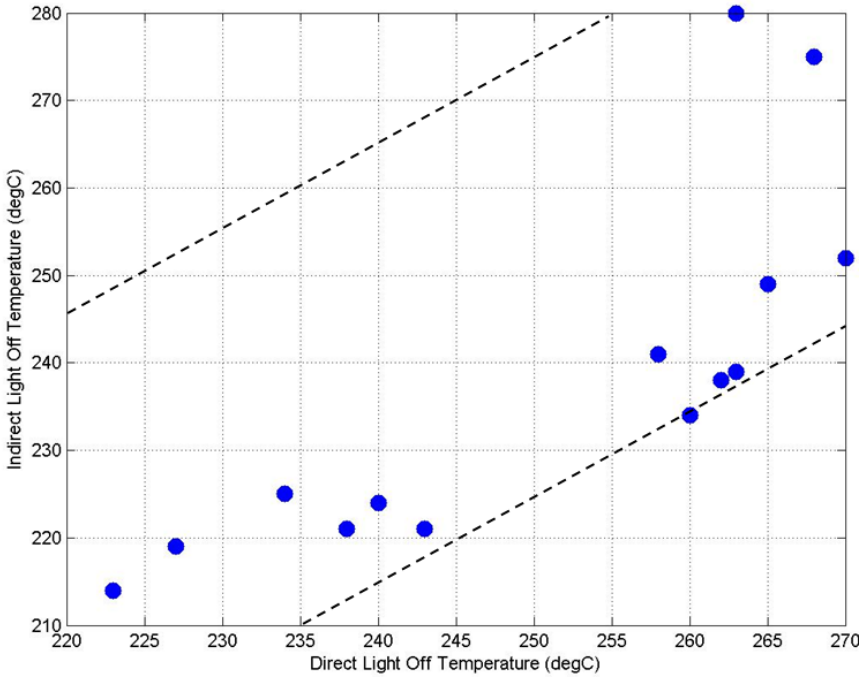

Figure 4.22Indirect Light Off Temperature vs. Direct Light Off Temperature Error plot for the Aging Level 3 DOC.

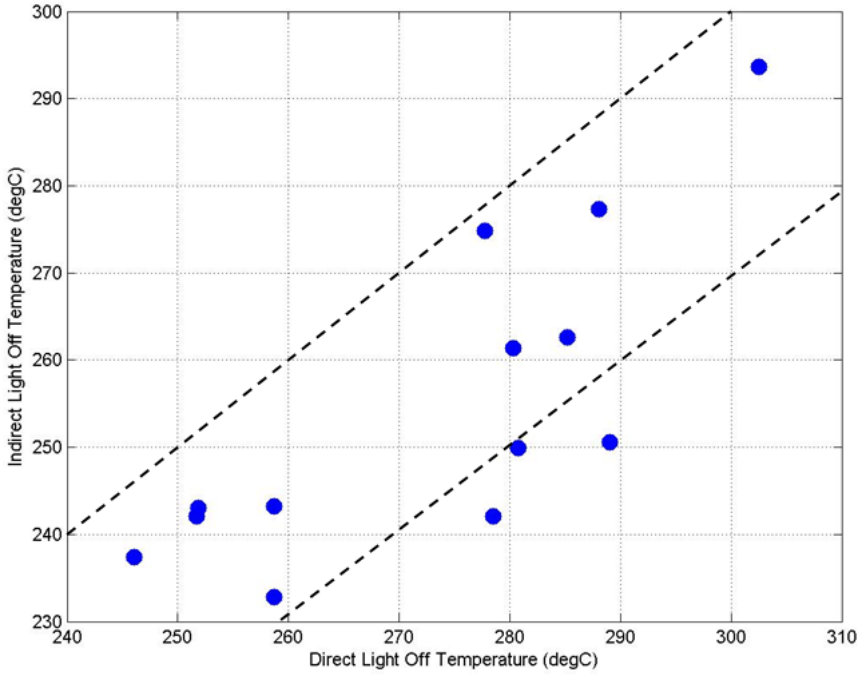

Figure 4.233. Indirect Light Off Temperature vs. Direct Light Off Temperature Error plot for the Aging Level 4 DOC.

4.5 Validation of Assumptions

This sections aims at validating a crucial assumption made for the light off experiments which played an important role in the design of experiments. It also makes an attempt at addressing a potential question about the viability of the model developed for the light off temperature detection part of the project.

4.5.1 Assumption of NO conversion being minimal for the light off Experiments

The light off experiments were so designed that a fixed amount of diesel fuel was injected in the exhaust stroke of the engine so that HC conversion would dominate the reactions and NO conversion would be restricted to a minimum. This assumption was not

validated previously since NO and NO_x measurements had not been taken up till the second aging level. In order to validate this assumption, for the third and fourth aging levels, NO and NO_x measurements were taken upstream and downstream of the DOC and the trends were observed. Figure 4.19 presents the results.

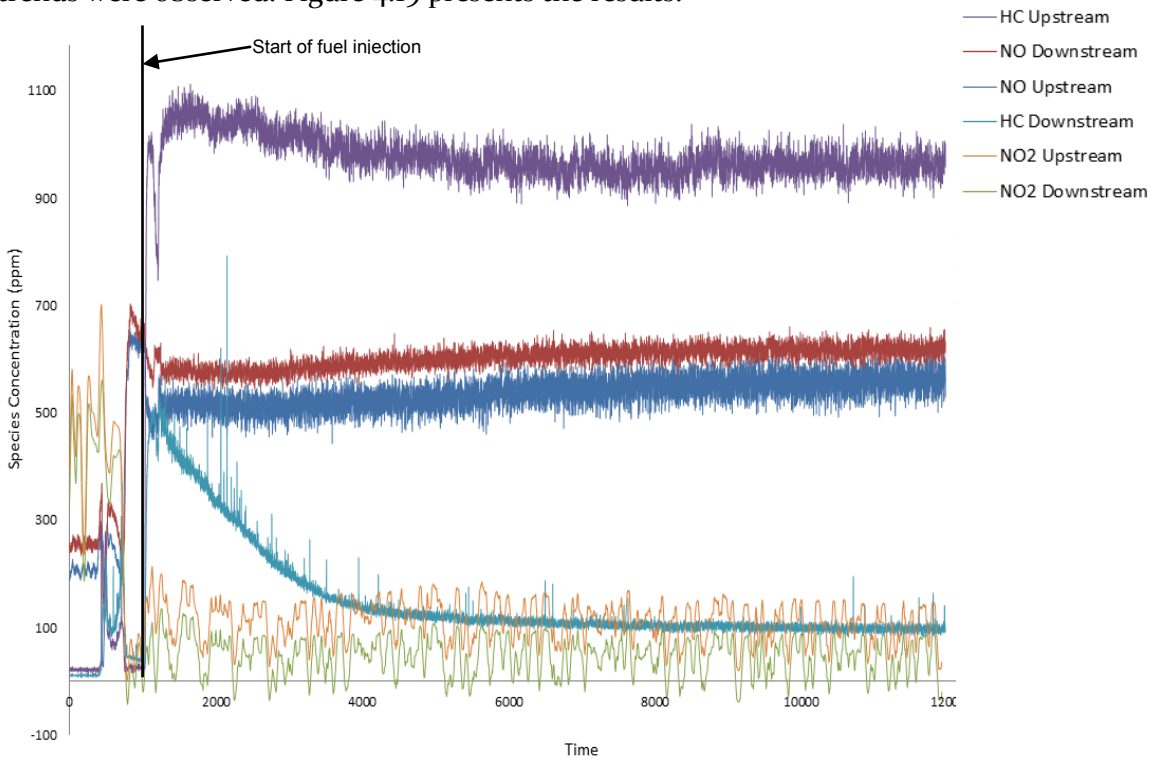

Figure 4.24. Figure shows the concentrations of various species for the 1400 rpm-300lb-ft aging level 4.

We can clearly see from Figure 4.19 that at start of fuel injection and afterwards, the NO concentration downstream of the DOC becomes greater than the Upstream NO concentration. As explained in a later section (sec 5.2.2), this is not the case for NO reaction when HC dosing is not taking place. This increase in NO concentration was found to be almost the same amount as the decrease in NO2 content from upstream of the DOC to downstream of the DOC. This is visible in Figure 4.19 as well. The orange line denotes Upstream NO2 and the green line denotes downstream NO2. We can clearly see

that the level difference between the green and the orange lines is approximately equal to that between the red and the blue lines which denote the downstream and upstream NO concentrations respectively. This indicates a reduction of upstream NO_2 to NO which validates the initial assumption made.

The other major conclusion that can be made from these trends is that during the light off tests in which diesel fuel dosing takes place, NO oxidation is not occurring as a result of the HC particles dominating the reaction dynamics inside the DOC.

4.5.2 HC Adsorption in the DOC at Cold Start of the Engine

According to the work by Katare [47], the DOC might adsorb HC particles during the initial warm up period of the DOC. Figure 4.20 shows that at a DOC inlet temperature of around 115°C, conversion rate becomes negative and keeps dropping until the temperature reaches 160°C. This indicates desorption as marked on the plot. Desorption indicates adsorption that would have taken place at an earlier time when the DOC was not sufficiently warmed up. As a result of that, the greater outlet HC concentration than inlet concentration led to desorption. This concern was raised for the degreened as well as the second level aged DOC. Figure 4.21 shows various quantities from one such case for the second aging level DOC.

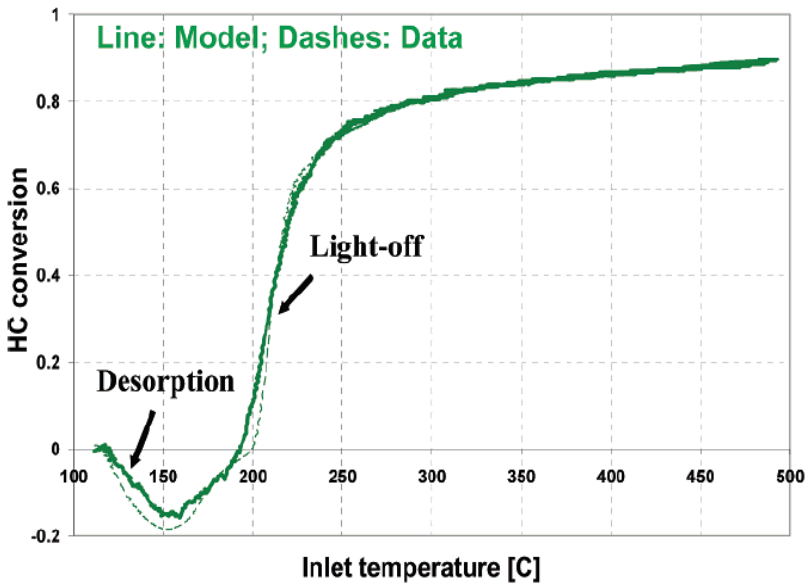

Figure 4.25. Figure indicates adsorption and desorption of HC for a DOC [47].

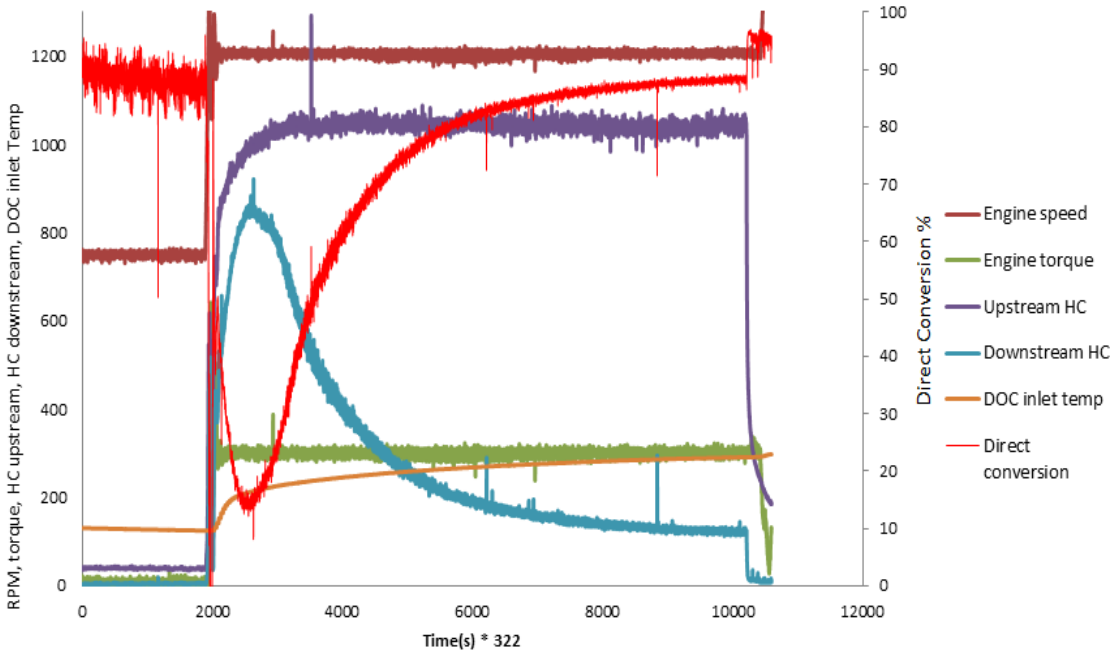

Figure 4.26. Figure shows the trend for HC conversion for the 1200 rpm 150 lb-ft case.

From Figure 4.21, we can clearly see that since start of fuel dosing occurs at a DOC inlet temperature much above 100°C, which is shown to be the temperature at which

desorption is occurring in Figure 4.20, it is difficult to say if adsorption ever occurred. Also, for the degreened and the second level aging DOC, in most of the experiments, fuel dosing was started at a temperature above 100°C which negated the chances of observing a negative conversion efficiency trend. To tackle this issue, all future tests were conducted in such a manner that fuel dosing was started below 100°C. This procedure was followed in the aging level 4 DOC as well. Also, in Figure 4.21 though we do see the conversion plot (red plot) dip in value initially and then rise, we can account this to the slow ramp up in DOC temperature (orange plot) instead of the HC adsorption. Figure 4.22 shows a plot from the aging level 4 DOC where we do see negative conversion for a short duration at the start of fuel dosing. During this period, the DOC temperature is also largely at a low value. These two evidences point at a possibility of HC adsorption.

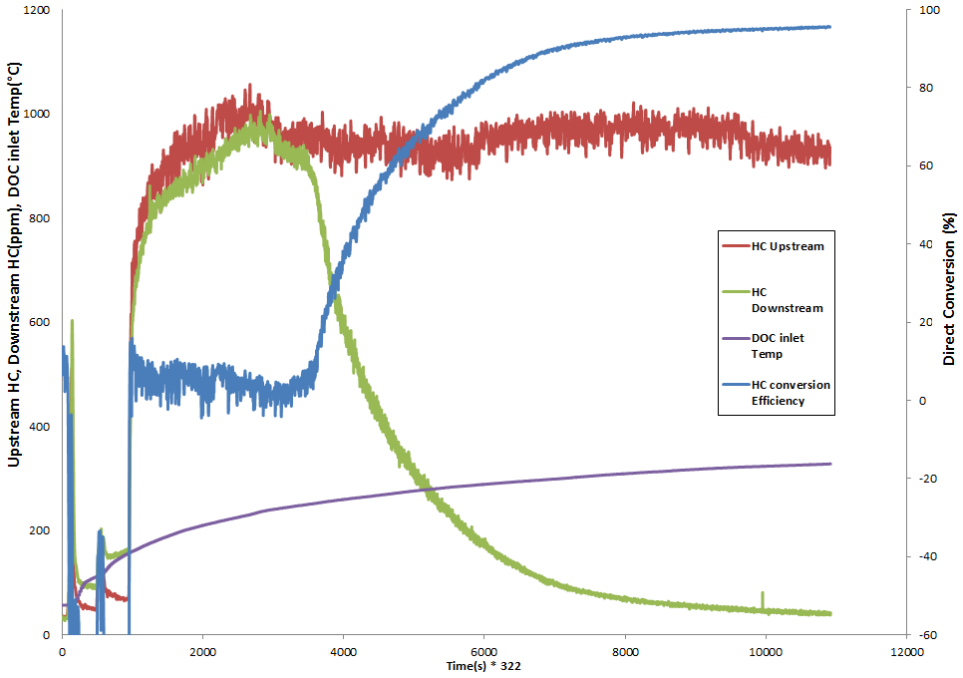

Figure 4.27. Figure shows the 1200rpm 150 lb-ft case for the aging level 4 DOC. We clearly witness a negative HC conversion rate potentially hinting at HC adsorption.

CHAPTER 5. DOC OUTLET NO AND NO_2 CHARACTERISTICS AND THE EFFECT OF THERMAL AGING ON CONCENTRATION

This chapter discusses the modeling techniques developed as a separate part of this project to determine the DOC outlet NO and NO_2 concentration based on DOC temperature input and NO_x concentration. Also, the model shall be validated for the last aged level of the DOC, i.e. level 4.

5.1 Experimental Method to Determine NO and NO_2 Concentration

5.1.1 Introduction

The exhaust stream was analyzed for NO and NO_2 content upstream and downstream of the Diesel Oxidation Catalyst. The cambustion fNO_X 400 exhaust analyzers were used for this purpose. Since these measuring units have only 2 channels and we were measuring both upstream and downstream information, the technique followed to determine both NO and NO_2 was that NO was measured first, upstream and downstream of the DOC, followed by total NO_x upstream and downstream. The concentration was obtained in ppm. Once this information was obtained, NO2 was calculated by subtracting the NO concentration from the total NO_x content. The modeling work during the previous project phase was carried out on the second level aged DOC and was validated on the third level aged DOC [48]. During the second aged level tests, after multiple experiments, when it was found that there was little or no variation in the NOx content, during the third aged level tests, the experimenting time was reduced by placing both the analyzer probes

downstream of the DOC where one measured NO concentration and the other measured total NO_x content. This information along with the DOC temperature was enough to validate the model developed during the previous aged level of the DOC.

The results from the aging levels 2 and 3 have been described in the thesis by Zhou [48]. As a part of this project, experiments were carried out for the aging level 4 and these were similar to the experiments conducted during aged level 3, i.e. the NO_x and NO probes were placed downstream of the DOC.

5.1.2 Design of Experiments

The NO_x content in a diesel engine exhaust increases with the torque applied since fuelling is a function of the torque. Also, since it has been shown that HC oxidation dominates for the fuel dosing cases, these tests did not involve any post fuel injection and reflected normal engine operation.` A total of five speed points were selected, i.e. 1200 rpm, 1350 rpm, 1500 rom, 1650 rpm and 1800 rpm. These points covered a large swath of the engine operating regime. At each of these speed points, the engine was made to operate at four torque points, i.e. 100 lb-ft, 200 lb-ft, 300 lb-ft and 350 lb-ft. The last torque point had to be restricted to 350 lf-ft since the dyno connected to the engine was not capable of sustaining a higher torque at most points and also, since a higher torque would have meant operating the turbocharger at a turbine exit temperature greater than 550°C, which was not recommended. Each speed and torque combination was written into an automated cycle just like the one used for the HC tests and the engine operated at each setpoint (except 1200 rpm) for ~500 seconds. A time of 500 seconds allowed the DOC temperature to saturate and this meant that most of the NO conversion had taken place.

The results obtained in these exercises will be presented along with the results from the model analysis for aging level 4.

5.2 Development of Model to Determine DOC Out NO and NO_2 Concentration

Majority of the work in developing the mathematical model which determines the NO and NO2 concentration downstream of the DOC was developed by Zhou, K. as a separate part of this project. This chapter will briefly go over the modeling basics used and will also present the use of those techniques to obtain model parameters for the aging level 4 DOC and the subsequent results.

5.2.1 Modeling Procedure

The dominant chemical reaction involved in the oxidation of NO to NO2 is given as follows:

$$NO + \frac{1}{2}O_2 \leftrightarrow NO_2. \tag{5.1}$$

The double headed arrow denotes that this reaction is reversible and the reaction rate is given as:

$$r_{NO} = k_{NO}\left(C_{NO}{C_{O_2}}^{0.5} - \frac{C_{NO_2}}{K_{NO}}\right) \tag{5.2}$$

.

In this equation, k_{NO} is the Arrhenius reaction rate constant given as:

$$k_{NO} = A_{NO}e^{-(\frac{Ei}{RT})} \tag{5.3}$$

where A_{NO} is the pre-exponential factor, E_i is the activation energy, R is the universal gas constant and T is the catalyst reactor temperature. Therefore, from this equation, we learn

that, kinetically, the higher the temperature, the higher will be the value of k_{NO} and thus, the faster will be the reaction rate. However, since this reaction is reversible, thermodynamics play an important role at high temperatures and this restricts the maximum conversion rate of NO. For this reversible reaction, an equilibrium constant K_p can be defined as:

$$K_P = \frac{C_{NO_2,DOC\ outlet}}{C_{NO,DOC\ outlet}\ C_{O_2,DOC\ outlet}^{0.5}}. \tag{5.4}$$

K_P is a function of only temperature. Also, the expected trend of this quantity as the DOC will age will be to reduce since the NO_2 concentration will reduce as a result of aging. The concentration from the obtained data was converted from ppm into mol/m³ to simplify calculations.

The mathematical model developed has been depicted in Figure 5.1.

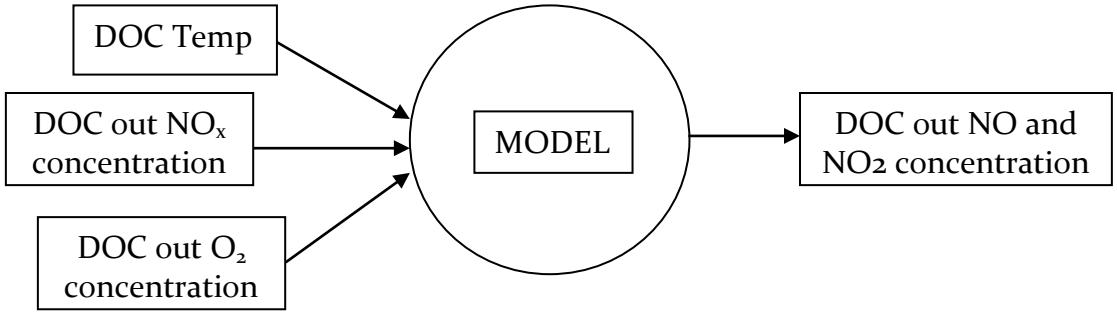

Figure 5.1. Figure Showing the Overall Functionality of the Mathematical Model.

The NO_2 and NO concentrations were used from the measured values. However, in the absence of an oxygen sensor downstream of the DOC, the oxygen concentration was assumed fixed at 13% [48]. Once the K_p values are obtained using the measured concentration values and DOC temperature, it is made to fit a Gaussian distribution to

obtain the nonlinear model. The Gaussian distribution was selected after a comprehensive application of different nonlinear curve fits such the polynomial distribution and the Weibull Distribution. The major advantage of this modeling technique is that a few K_p value from the entire data set is sufficient to provide parameters for the nonlinear model that allows the model to fit the real data within acceptable limits. Table 5.1 and Figure 5.2 depict this modeling exercise for the second level aged DOC.

Table 5.1. Table showing the data points used to develop the model for the second aging level DOC .

Setpoint	DOC out NO (ppm)	DOC out NO_x (ppm)	DOC temp (K)	Kp calculated
1200 rpm, 100 lb-ft	377.9679392	403.0617215	442.3058802	0.028659
1200 rpm, 200 lb-ft	446.6166986	677.1599095	521.4343662	0.244167
1200 rpm, 300 lb-ft	406.3057485	844.3112744	604.672512	0.551642
1200 rpm, 350 lb-ft	471.6758831	914.1176647	642.903933	0.494663
1350 rpm, 100 lb-ft	370.9920058	453.1869812	439.9253295	0.044337
1350 rpm, 200 lb-ft	525.4912178	616.5488649	543.2687275	0.350878
1350 rpm, 300 lb-ft	651.7339045	737.3488049	635.7176977	0.519366
1350 rpm, 350 lb-ft	752.6582358	849.7889484	668.9572504	0.422033
1800 rpm, 100 lb-ft	278.5212126	317.879229	476.5046087	0.064111
1800 rpm, 200 lb-ft	164.9451623	306.8262456	577.3027144	0.429544
1800 rpm, 300 lb-ft	310.4967245	361.834455	744.2351162	0.093747
1800 rpm, 350 lb-ft	347.7269991	369.6170516	800.9734234	0.037029

We can clearly see from Figure 5.2 that the Gaussian distribution fits the data points reasonably well. The Model equation obtained from the Gaussian distribution is given as:

$$K_P = y_0 + \frac{A}{w(\sqrt{\frac{\pi}{2}})}\left[e^{\left(\frac{-2(T_{DOC}-x_C)}{w}\right)^2}\right]. \quad (5.5)$$

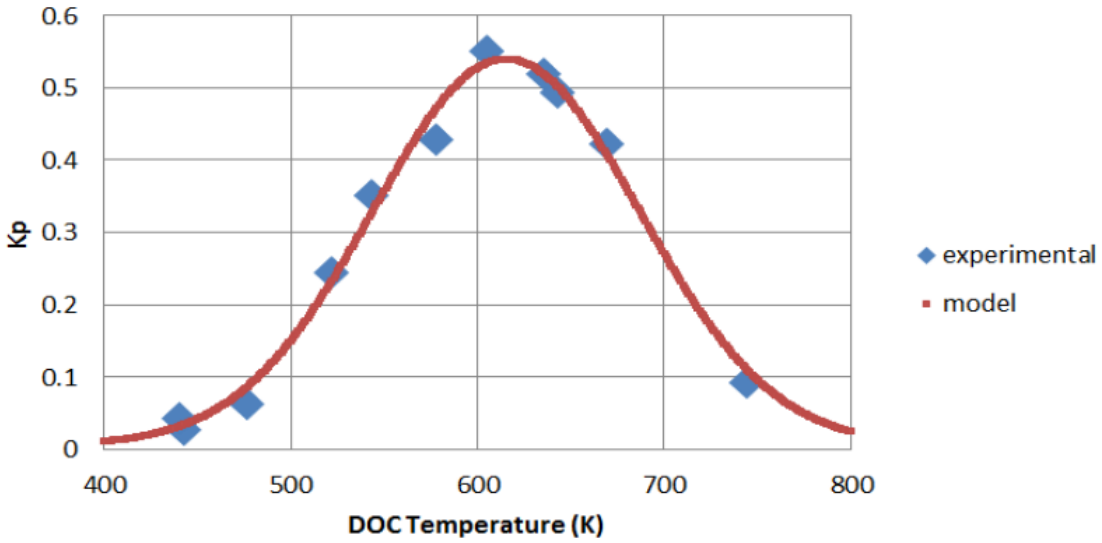

Figure 5.2. Figure Showing Gaussian Distribution Fitting the Measured Data.

The parameters (y_o,A,w and x_C) obtained from this exercise were obtained as shown in Table 5.2. These were used in the model equation to obtain Kp values that were further used to obtain the model concentration values for NO and NO2 downstream of the DOC.

Table 5.2. Parameters Obtained for the Second Aging Level Model.

	Parameter value
y_0	0.005998593
x_c	615.3603029
w	142.8901865
A	95.65060446

The model DOC out NO and NO_2 concentrations were obtained using the following equations:

$$C_{NO_2} = \frac{\sqrt{C_{O_2}}(K_P)}{\sqrt{C_{O_2}}(K_P) + 1}(C_{NO_x}) \tag{5.6}$$

$$C_{NO} = \frac{1}{\sqrt{C_{O_2}}(K_P) + 1}(C_{NO_x}). \tag{5.7}$$

Here, NO_x concentration is obtained from the sensor and the value of *Kp* is obtained from the model.

5.2.2 Modeling Applied to Aging Level 4

This procedure was applied to the data obtained from the aged level 4 of the DOC from similar experiments. The first stage as described in the previous section was to choose data points from the entire data set to fit to the Gaussian distribution. Table 5.3 lists out these points.

Table 5.3. Data Points used to develop the model for the fourth aging level DOC.

Setpoint	DOC Temp(K)	Kp calculated
1200 rpm, 100 lb-ft	434.96893	0.02213
1200 rpm, 200 lb-ft	534.87183	0.18603
1200 rpm, 300 lb-ft	613.80104	0.51361
1200 rpm, 350 lb-ft	652.21573	0.52465
1350 rpm, 100 lb-ft	437.68637	0.03272
1350 rpm, 200 lb-ft	547.42145	0.43767
1350 rpm, 300 lb-ft	620.81697	0.43307
1350 rpm, 350 lb-ft	668.84151	0.68111
1500 rpm, 100 lb-ft	452.95343	0.0424
1500 rpm, 200 lb-ft	564.66483	0.41609
1500 rpm, 300 lb-ft	629.7104	0.27574
1500 rpm, 350 lb-ft	699.54855	0.19603
1650 rpm, 100 lb-ft	458.9812	0.05748
1650 rpm, 200 lb-ft	511.55127	0.13144
1650 rpm, 300 lb-ft	671.46013	0.4426
1650 rpm, 350 lb-ft	725.41362	0.11679
1800 rpm, 100 lb-ft	476.05165	0.03769
1800 rpm, 200 lb-ft	581.36472	0.33378
1800 rpm, 300 lb-ft	670.62019	0.39145
1800 rpm, 350 lb-ft	707.08327	0.2226

These calculated K_p values were made to fit a Gaussian distribution using the Origin 8 software as specified by Zhou, K. The curve obtained is shown in Figure 5.3.

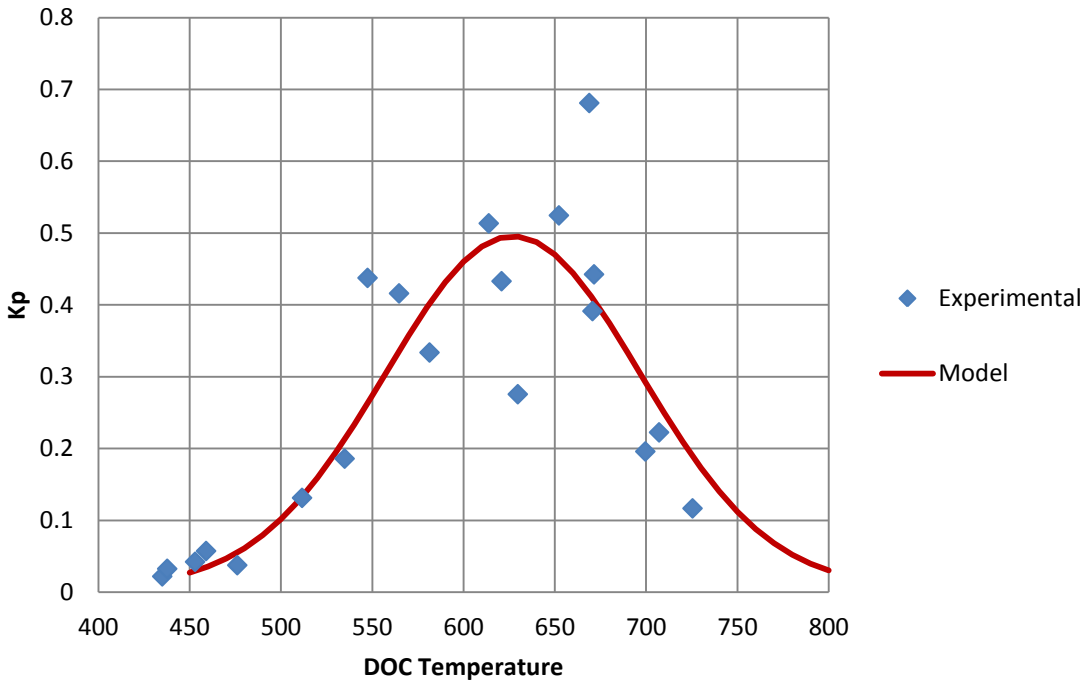

Figure 5.3. Figure Showing Gaussian Distribution Fitting the Measured Data for Aging Level 4.

The parameters obtained are given in Table 5.4.

Table 5.4. Parameters Obtained for the Fourth Aging Level Model.

Parameter	Parameter value
yo	0.00722
xc	627.04564
w	140.1178
A	85.74315

These parameters were used in equation 5.5 to obtain the model value of *Kp* which was further used to obtain the model DOC out NO and NO_2 concentrations. These were validated by plotting the values alongside the measured NO and NO_2 data. Figures 5.4 to 5.13 illustrate this. Figure 5.4 shows the measured value of NO at the DOC outlet in blue and the model NO value in black. We can see that the model fits the real values quite accurately. The error plots depicted by Figures 5.5 and 5.7 depict this as well.

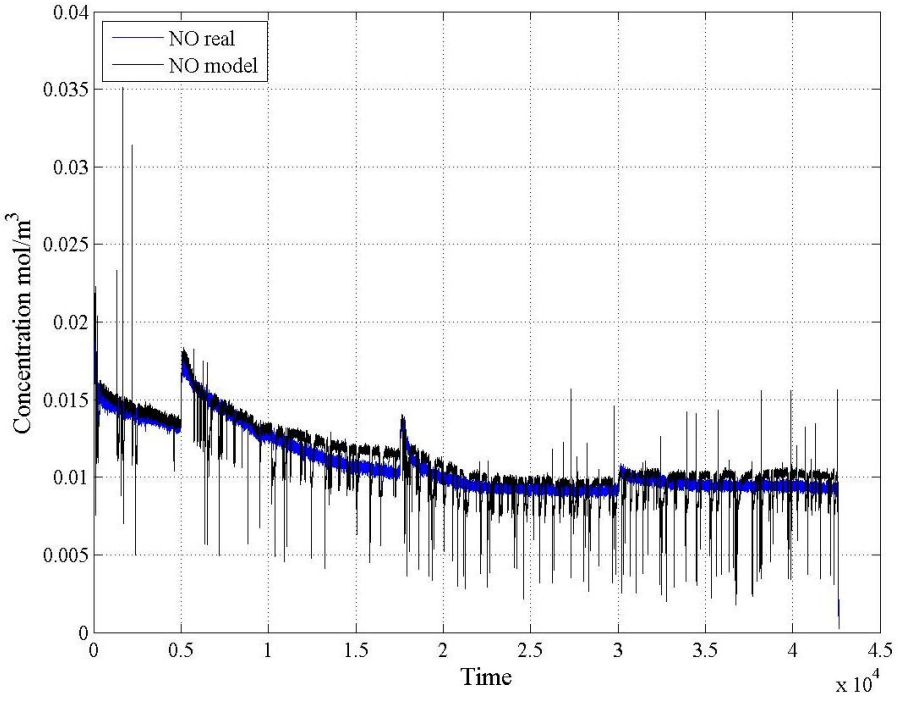

Figure 5.4. NO real vs. NO model for the DOC at aging level 4, 1200 rpm case.

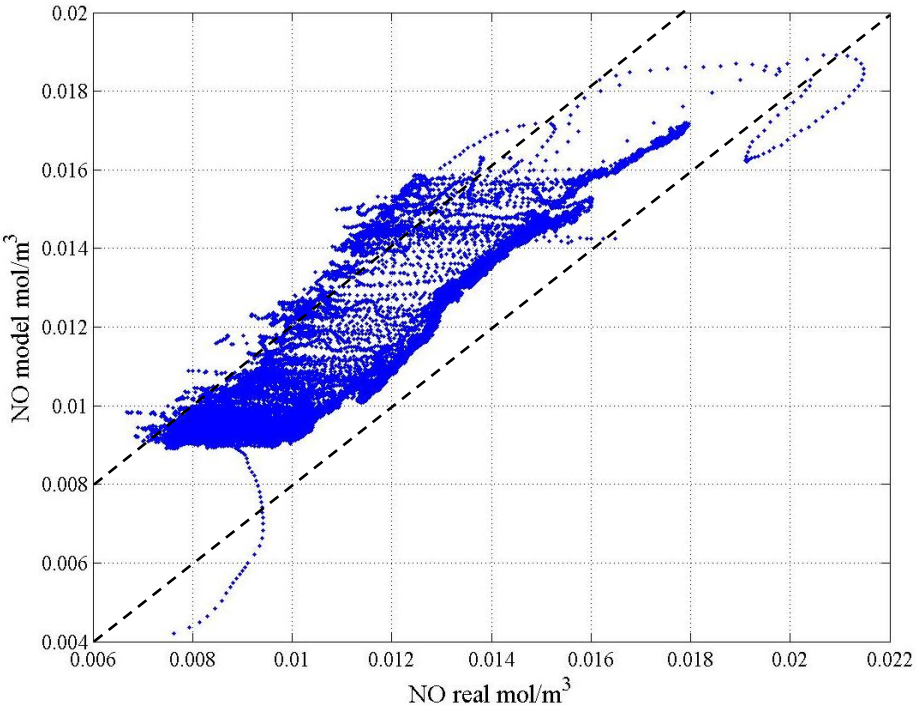

Figure 5.5. NO model vs. NO real at Aging Level 4, 1200 rpm, error plot.

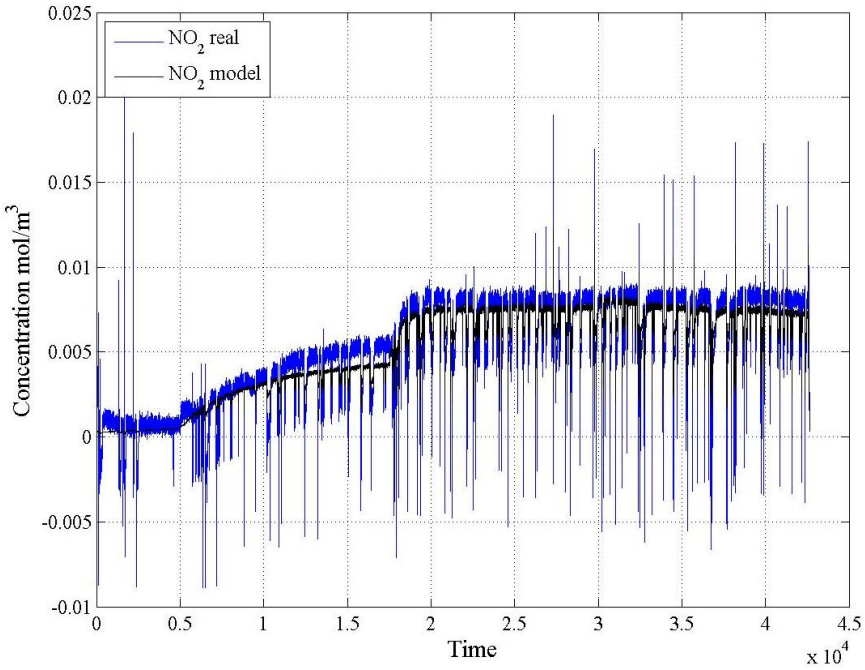

Figure 5.6. NO2 real vs. NO_2 model for the DOC at aging level 4, 1200 rpm case.

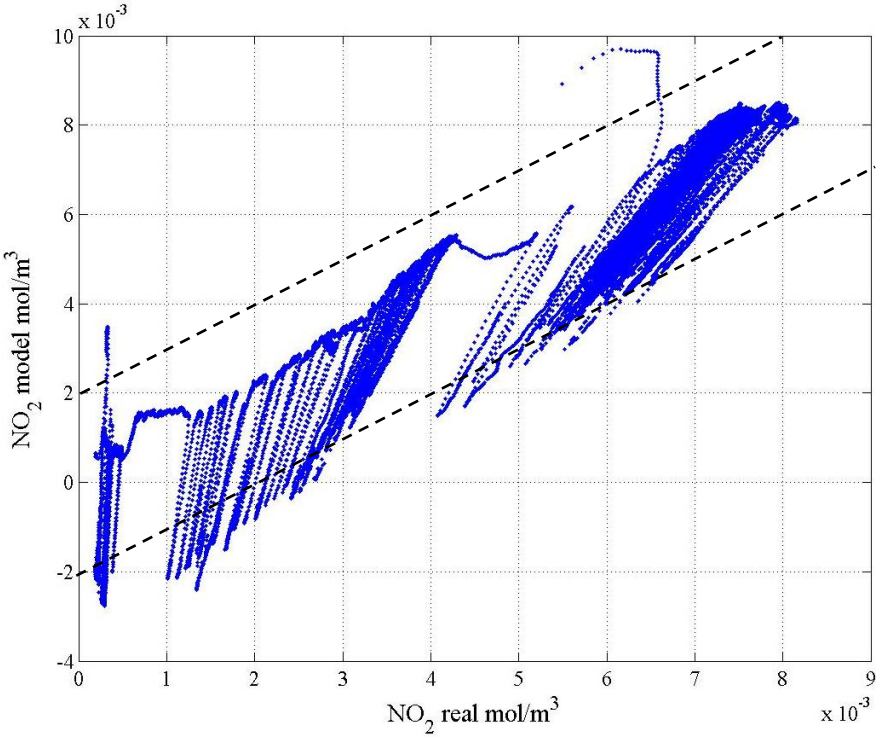

Figure 5.7. NO_2 model vs. NO_2 real at Aging Level 4, 1200 rpm, error plot.

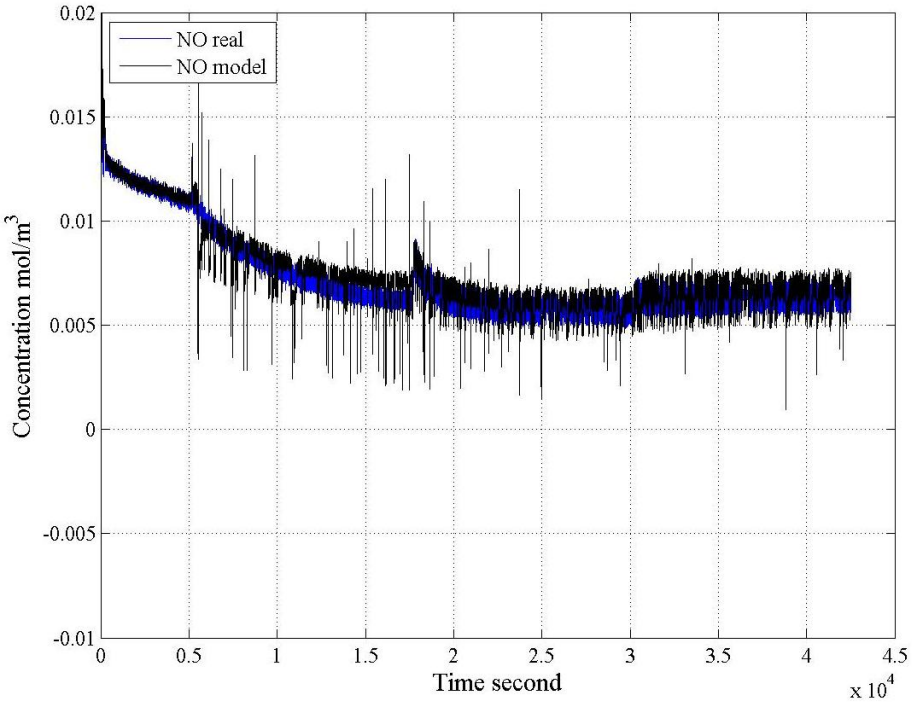

Figure 5.8. NO real vs. NO model for the DOC at aging level 4, 1350 rpm case.

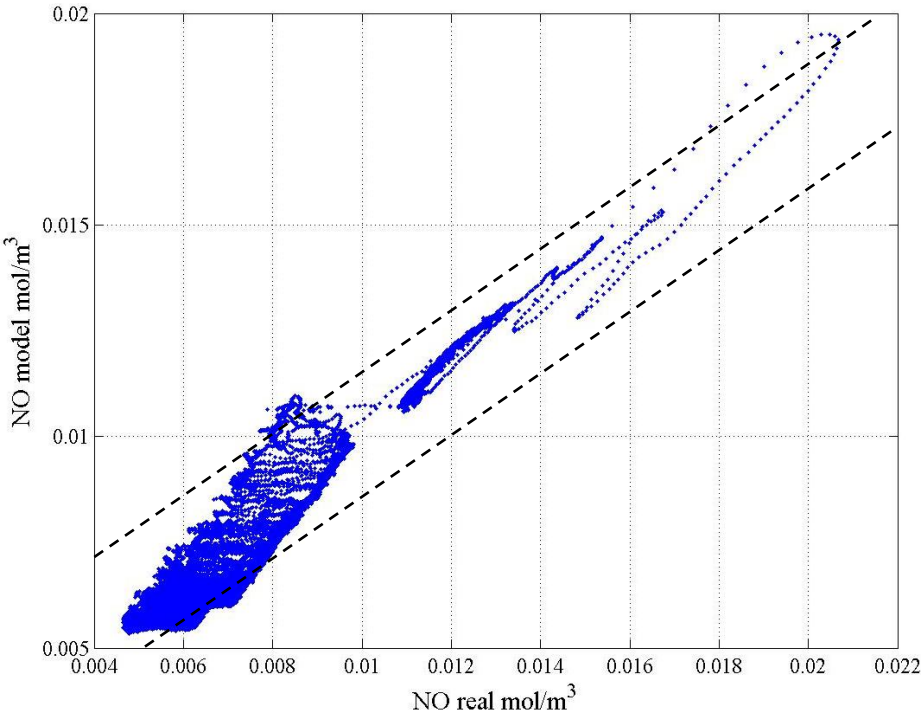

Figure 5.9. NO model vs. NO real at Aging Level 4, 1350 rpm, error plot.

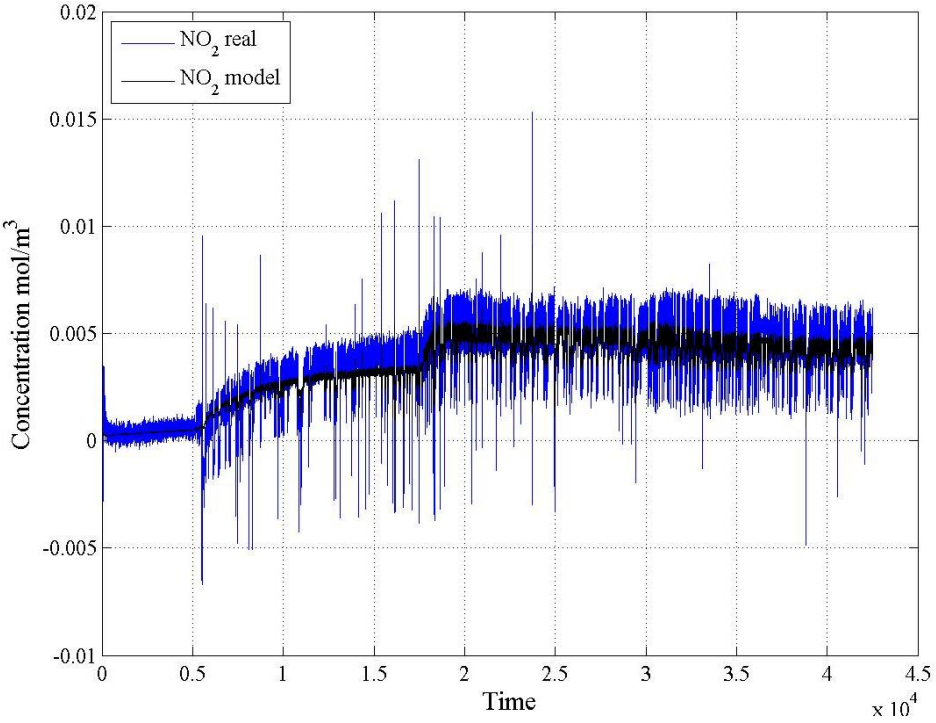

Figure 5.10. NO_2 real vs. NO_2 model for the DOC at aging level 4, 1350 rpm case.

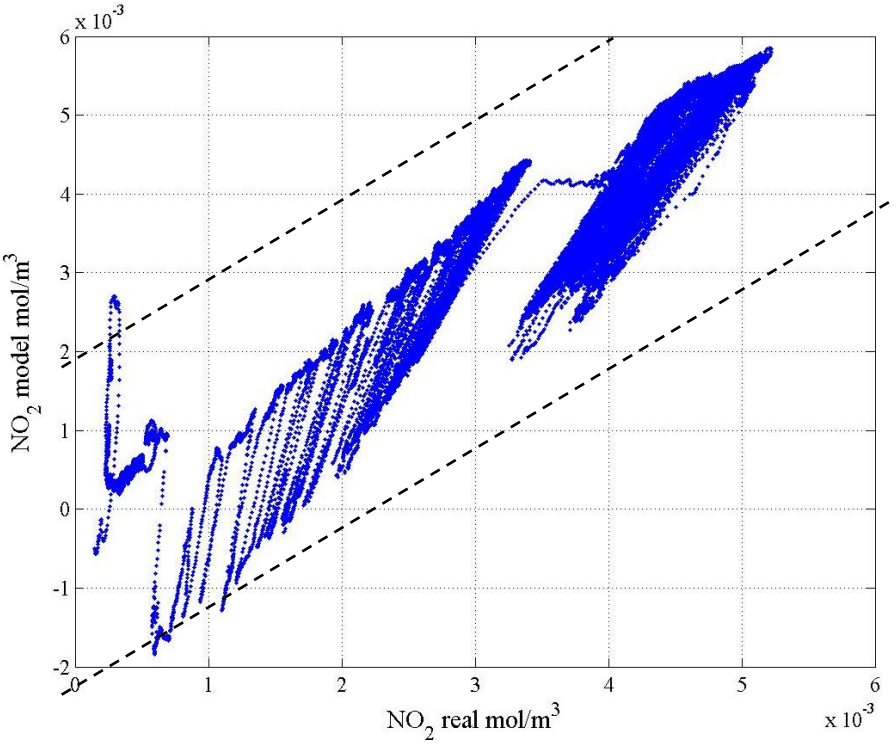

Figure 5.11. NO_2 model vs. NO_2 real at Aging Level 4, 1350 rpm, error plot.

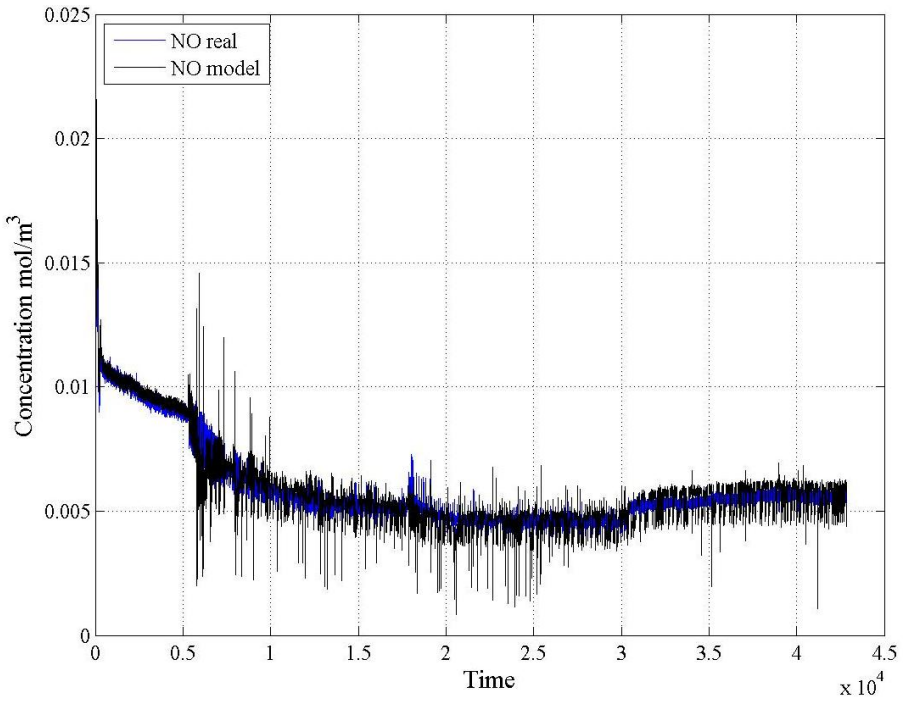

Figure 5.12. NO real vs. NO model for the DOC at aging level 4, 1500 rpm case.

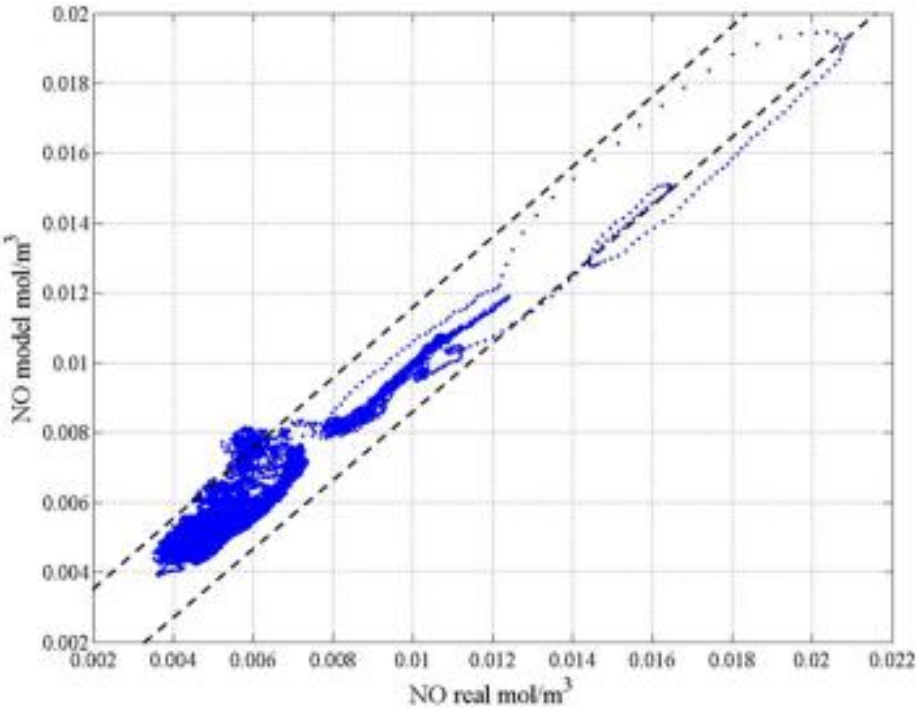

Figure 5.13. NO real vs. NO model for the DOC at aging level 4, 1500 rpm case, error plot.

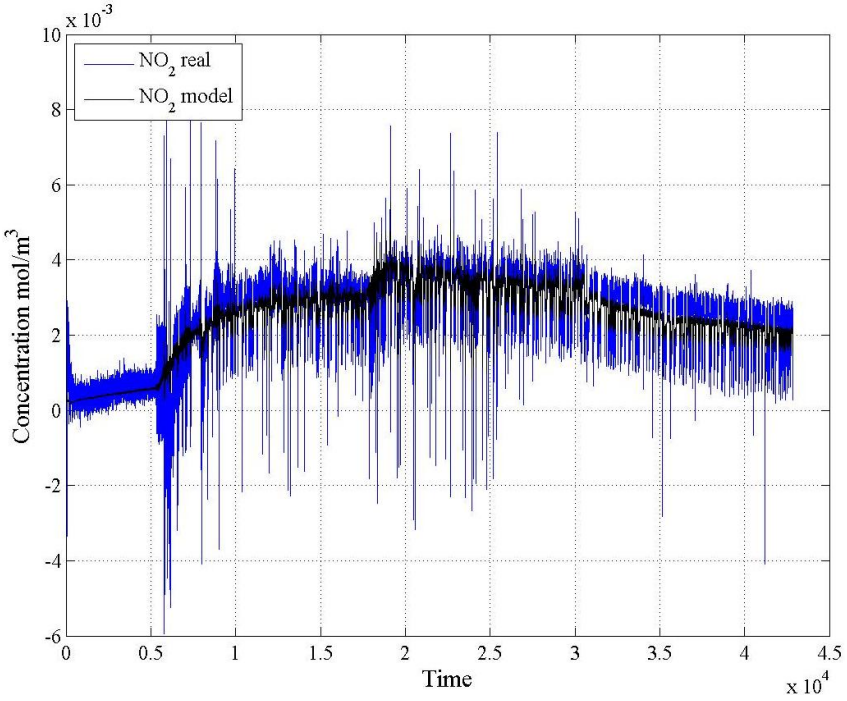

Figure 5.14. NO_2 real vs. NO_2 model for the DOC at aging level 4, 1500 rpm case.

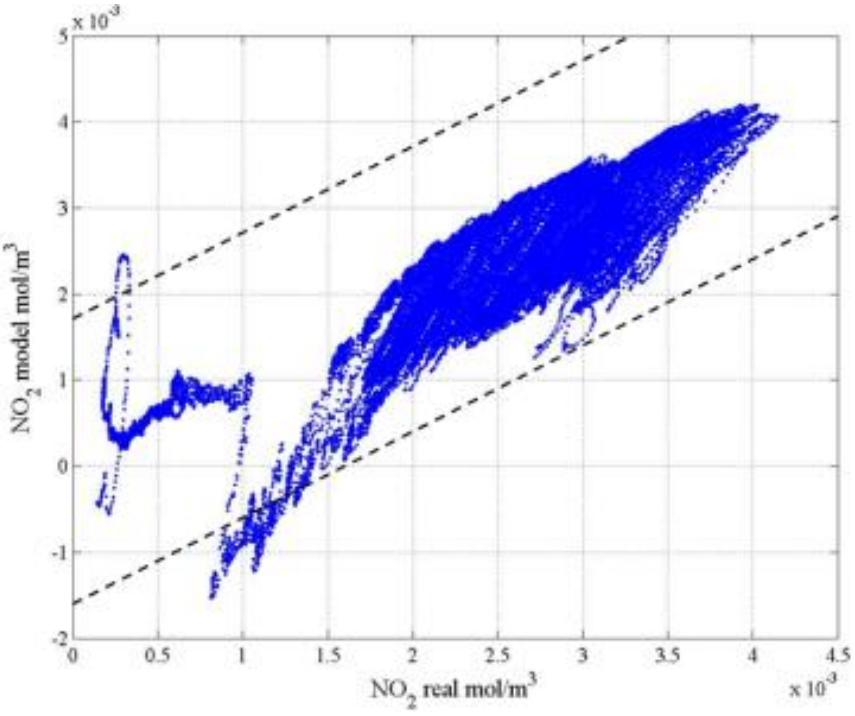

Figure 5.15. NO_2 real vs. NO_2 model for the DOC at aging level 4, 1500 rpm case, error plot.

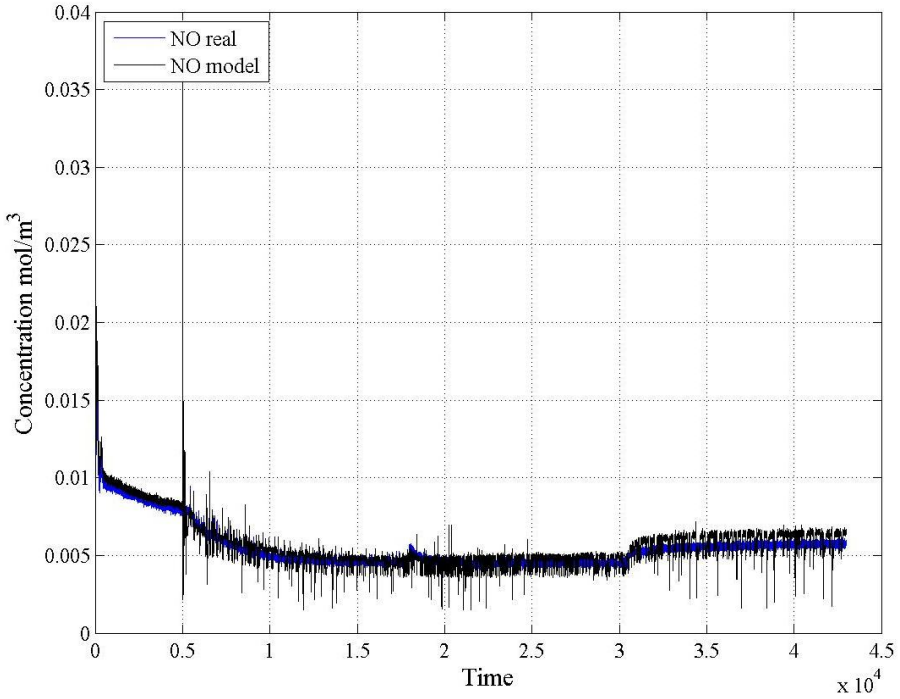

Figure 5.16. NO real vs. NO model for the DOC at aging level 4, 1650 rpm case.

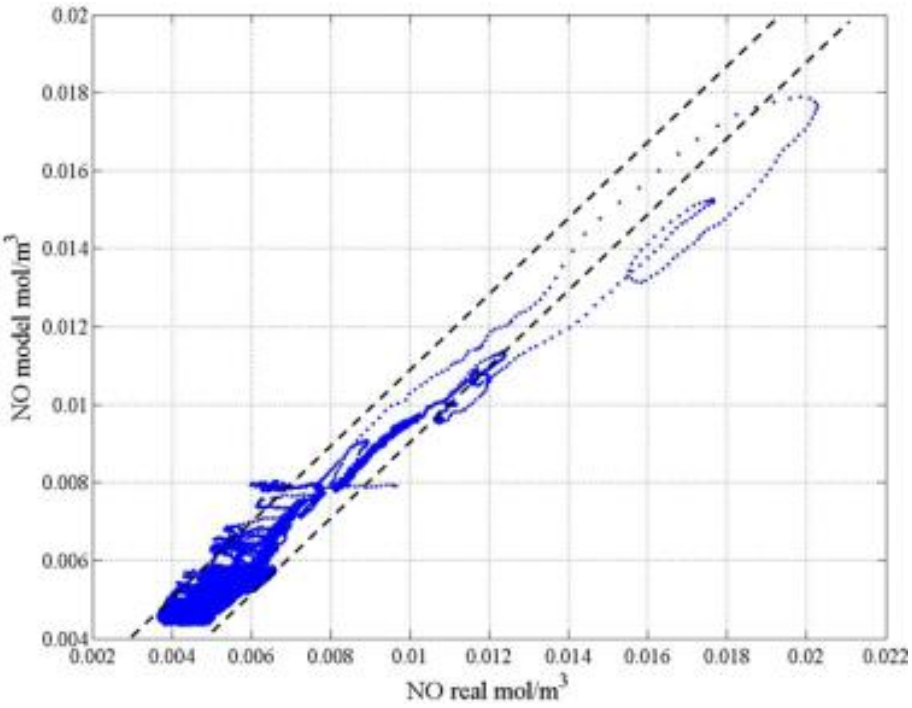

Figure 5.17. NO real vs. NO model for the DOC at aging level 4, 1650 rpm case, error plot.

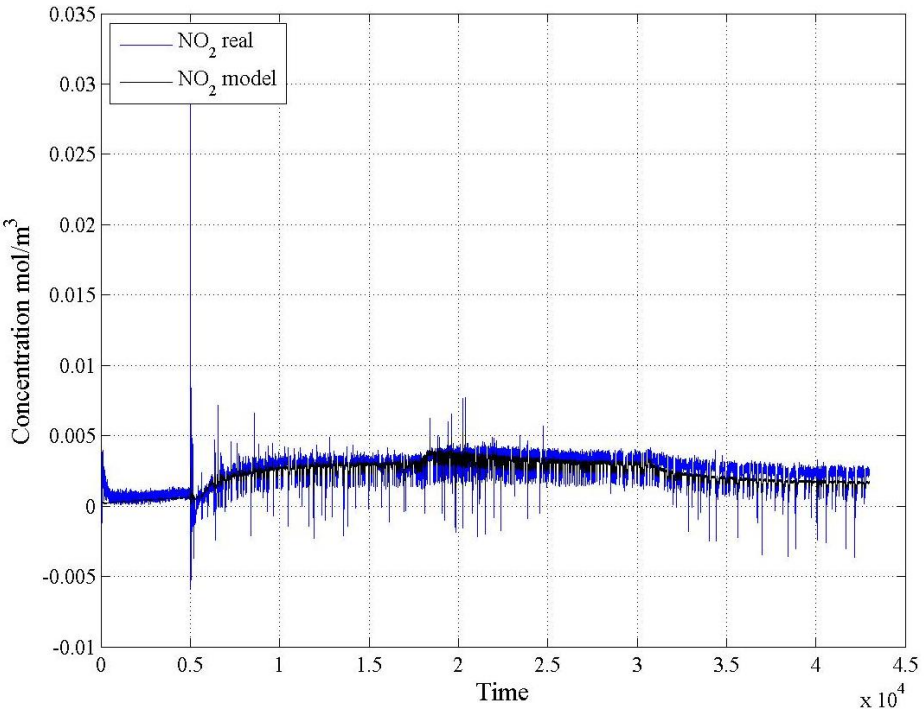

Figure 5.18. NO_2 real vs. NO_2 model for the DOC at aging level 4, 1650 rpm case.

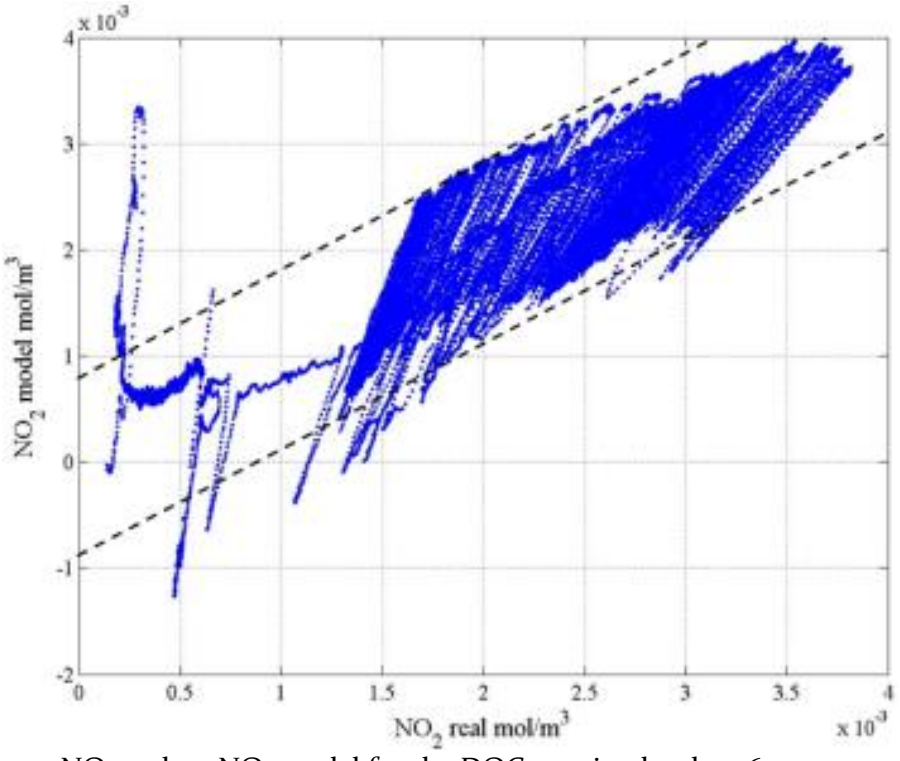

Figure 5.19. NO_2 real vs. NO_2 model for the DOC at aging level 4, 1650 rpm case, error plot.

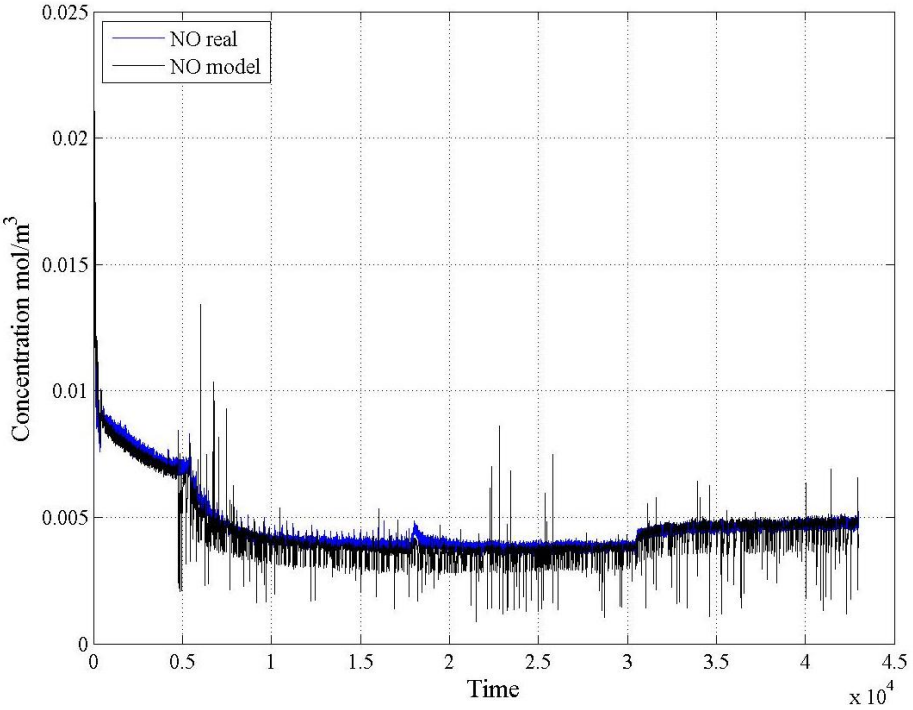

Figure 5.20. NO real vs. NO model for the DOC at aging level 4, 1800 rpm case.

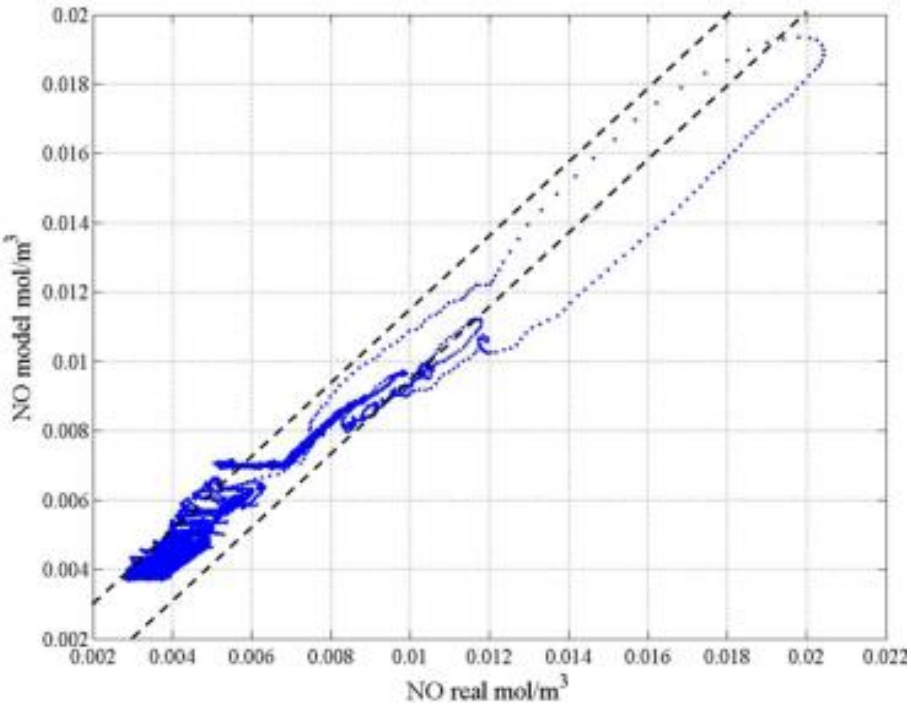

Figure 5.21. NO real vs. NO model for the DOC at aging level 4, 1800 rpm case, error plot.

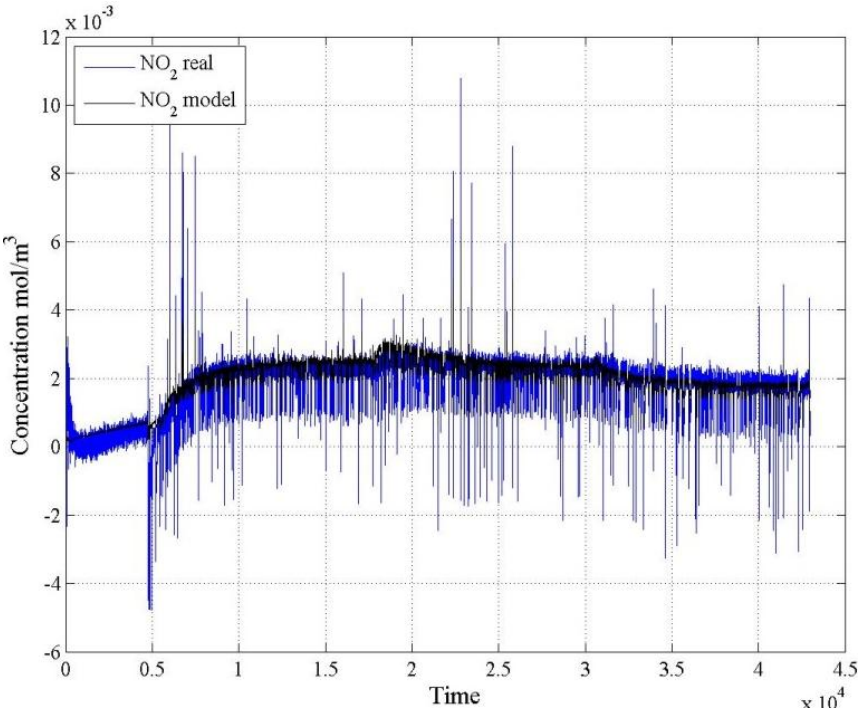

Figure 5.22. NO_2 real vs. NO_2 model for the DOC at aging level 4, 1800 rpm case.

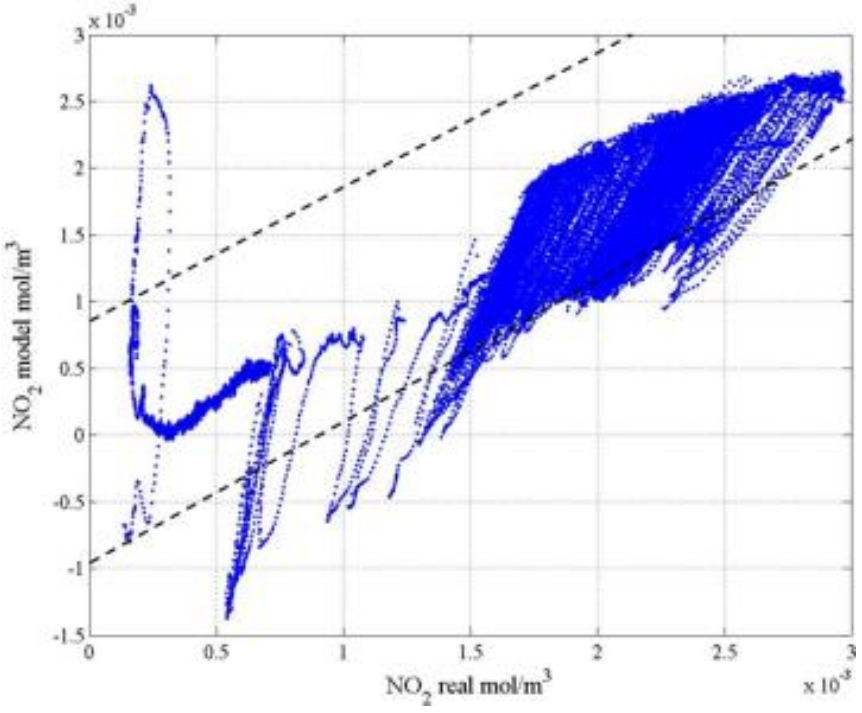

Figure 5.23. NO_2 real vs. NO_2 model for the DOC at aging level 4, 1800 rpm case, error plot.

5.2.3 Effect of Aging on K_P

As previously discussed, the value of *Kp* is a measure of the amount of NO conversion into NO2. In light of this, the value of *Kp* for aging level 4 was plotted against level 2 and level 3 *Kp* values against DOC temperature. Figure 5.14 shows the trend.

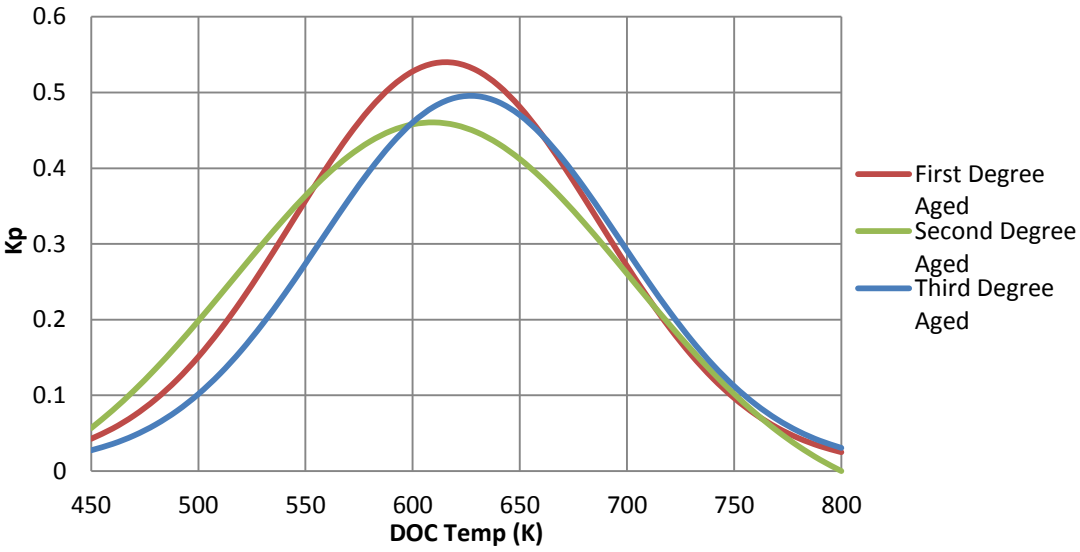

Figure 5.24. Comparison of K_P Values between the Three Aging Levels of the DOC.

From Figure 5.14, we can see that the value of model K_P is the least for the third degree aged (or aging level 4) from a DOC temperature of 450K to around 600K. This indicates that conversion was least for the third degree aged DOC among the 3 aging levels so discussed.

5.2.4 Effect of Using Engine Out Oxygen Sensor for Calculations

As discussed in a previous section, since there was not an oxygen sensor attached at the outlet of the DOC, the oxygen concentration was assumed to be constant at 13% for

calculating the *Kp* value. However, for the aging level 4 DOC, calculations were made using an oxygen sensor attached downstream of the DOC. K_P values were obtained and a model was generated which was used to obtain DOC out NO and NO_2 concentrations.

From Figure 5.19, we can clearly see that the model on the left, where oxygen concentration was assumed, fits the measured data better than the model obtained from using the values from the oxygen sensor. This shows that only a sensor attached downstream of the DOC can provide accurate measurements to use in the modeling procedure. The same trends are also visible for NO2 concentrations and over multiple engine setpoints.

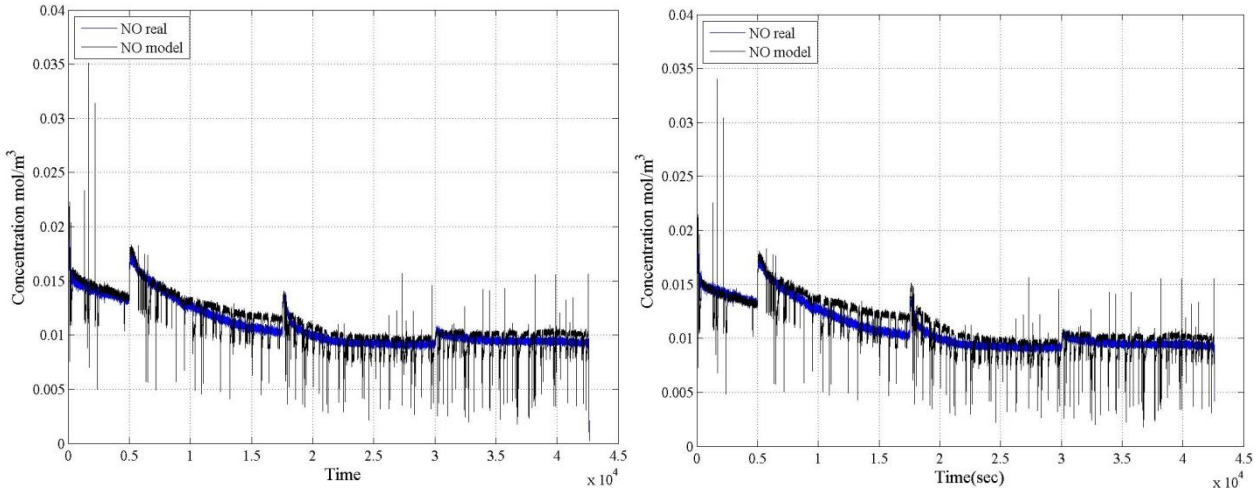

Figure 5.25. Comparison between the NO concentration results obtained by assuming constant O_2 concentration (Left) and by using the O_2 sensor values (Right) for the 1200 rpm set point.

5.2.5 Techniques to Optimize Data Point Selection for Gaussian Curve Fitting

From Section 5.2.1, we have learnt that in order to obtain a non-linear model, values of K_P were calculated for the entire range of DOC temperatures and based on a few points covering the entire data set, parameters were obtained for the non-linear equation corresponding to the Gaussian curve fitting the selected points. This strategy, however, was found not to give the most optimum results in all the cases. For example, from Figure 5.3, we can see that not all the points accurately follow the Gaussian curve. Especially at a temperature of around 625°C, we can see that there are three K_P values for nearly the same temperature. Also, there was an anomaly in the selection of points which was not necessarily ensuring an accurate depiction of the entire range of the DOC temperatures.

In order to resolve this issue, an effort has been made to determine a method to choose points from the data set that would better reflect the entire temperature range of the DOC and would ultimately lead to a better NO and NO_2 concentration model.

Figure 5.26 shows the result after an improved point selection strategy. For this particular case, points were selected in such a manner as to ensure that the DOC temperature range across the entire experiment was being considered. For a particular temperature point, an averaging was done for K_P values at other instances of that temperature for a particular speed and torque point and then the averaged value was plotted. The outliers were manually eliminated. These values were then made to undergo a non-linear curve fitting exercise, basically, the Gaussian fitting. It was found the error between the experimental and the model values was much lesser than what was prevalent in the previous strategy.

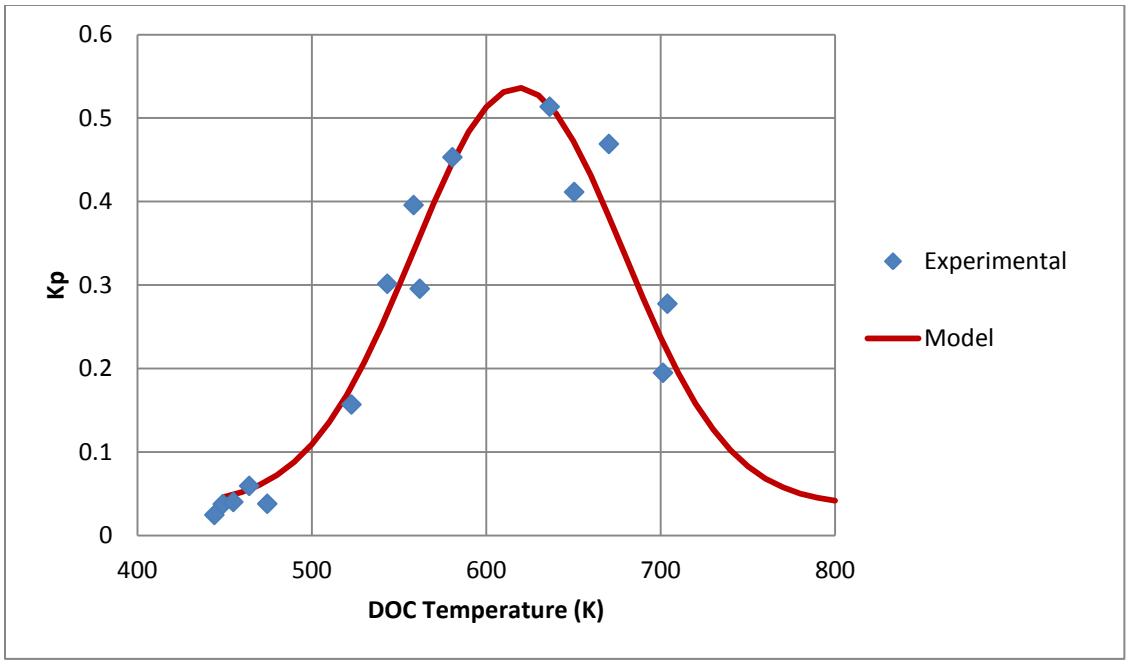

Figure 5.26. Gaussian Fitting on Experimental K_P Values After Using Improved Point Selection Strategy.

5.3 Integrating the Light-Off Temperature Model and the K_P Model

As per the current strategies, the light off temperature model is first used to determine the degree of aging in the DOC which also gives an idea of the effectiveness level of the DOC. This is then followed by conducting a different set of experiments to determine the NO and NO_2 concentrations which are further used to generate the K_P model. Framing the K_P model currently involves 2 steps, i.e. first, calculating the K_P values from the experimental data, and then fitting it to the Gaussian distribution curve to obtain model parameters. This 2-step process would ideally like to be in a single step. Also, there is not currently a clear mathematical correlation between the light-off temperature model and the K_p model. Such a correlation shall enable us to obtain the model NO and NO_2

concentrations by just knowing the extent of the DOC aging based on the light off temperature.

Therefore, a mathematical correlation wherein once the light off temperature is known, and one comes to know about the corresponding K_P value could be one such method. Since, we know that as light off temperature shifts, the K_P trend also shifts, this could save the effort of carrying out multiple calculations. In order to obtain such a model, we need to identify a physical quantity that can link these two models together. Temperature value cannot be used since the light off temperature is different for the two different kinds of experiments used as discussed earlier in chapters 4 and 5. Total mass flow rate cannot also be used since it is different in the light off experiments as a result of post fuel dosing, which is absent in the K_P experiments.

Therefore, as a part of future effort in this project, determining a physical quantity that would have the same values for both kinds of experiments will be of prime importance. This quantity will have to be from the sensors which have been used with the current DOC. Only on a fresh DOC shall it be beneficial to install different kinds of sensors that shall output a different physical quantity than the current ones viz. temperature, mass flow rate, O_2 concentration, NO and NO_x concentration and HC concentration.

CHAPTER 6. CONCLUSIONS AND FUTURE WORK

6.1 Conclusions

1. The testing procedure recommended for DOC light off testing involved running the engine at four speed points and 2 torque points per speed point. Post fuel dosing of a constant amount was introduced at each of these set points once the engine was below 100°C. These tests were performed on the DOC for two aged levels which were the states of the DOC after the second and third aging exercises. Testing was automated using a time based cycle which had alternating cooling cycles at the idle point of the engine.
2. The thermal balance based model obtained from these experiments was validated on aging levels 3 and 4 of the DOC and it was found to give reasonably accurate results.
3. The light off temperature shift was observed over four states of the DOC, i.e. degreened, aging level 2, aging level 3 and aging level 4. A clear shift was observed between levels 1, 2 and 3 but between levels 3 and 4, light off temperature did not shift a lot, indicating possible nearing to end of useful life of the DOC.
4. It was confirmed that light off temperatures increase on increasing the torque given the engine speed is a constant. This occurs as a result of an increased mass flow rate that takes place due to an increased amount of fuelling to maintain the engine speed at a higher torque point. This was concluded at the end of the thesis work by Sutjiono [46] and validation over two more aging levels confirmed the trend.

5. The possibility of HC adsorption was explored and it was found that HC adsorption can occur at low temperatures (~90-100°C), especially if fuel dosing has begun. The assumption that post fuel dosing of diesel fuel renders the oxidation of all other species negligible was confirmed by measuring and calculating the DOC upstream and Downstream NO and NO_2 concentrations.
6. Transient state experiments were carried out on the engine over 3 aging levels to determine the DOC out NO and NO_2 characteristics.
7. These transient state experiments carried out using multiple analyzers and using an automated cycle were used to develop a mathematical model based on the Kp value, by Zhou [48] that predicts the DOC out NO and NO2 concentration values by using total NO_x concentration, temperature from inside the DOC and the oxygen concentration.
8. This mathematical model was validated over a third DOC state (aging level 4) with successful results.
9. The K_P shift observed from one aged state to a higher aged state was confirmed when the same was observed between aging levels 3 and 4.
10. It was shown that the possibility of using engine out O_2 sensors for use in this mathematical model would not yield good results and that DOC out O_2 sensors would be required to use measured O_2 concentration values.

6.2 Future Work

1. Developing a more robust model to determine light off temperature.

2. Carrying out thermal aging on the DOC for a few more times and repeating the experiments performed to further validate the model.
3. Installing an oxygen sensor downstream of the DOC to obtain more accurate values of K_P which shall further help in developing a more accurate predictor model for determining the DOC out NO and NO_2 concentration.
4. Determining a physical quantity that can help in obtaining a mathematical correlation between the light off model and the K_P model.

LIST OF REFERENCES

LIST OF REFERENCES

[1] Heywood, John B. *Internal Combustion Engine Fundamentals*. McGraw-Hill, 1988.

[2] Jonietz, Erika "New Diesel Engine Emits Cleaner Fumes." *Technology Review*. December 2009

[3] Pyper, Julia "Diesel Cars Make a Comeback in the U.S.: Scientific American." *Scientific American,* April 2012.

[4] Ury, Allen B. "8 Advantages of Diesel Engines." *WyoTech*, March 2012

[5] Johnson, Timothy V. "Vehicular Emissions in Review." *SAE Paper 2012-01-0368,* 2012

[6] Eastwood, Peter. *Critical Topics in Exhaust Gas Aftertreatment*, 2001.

[7] Twigg, Martyn V. "Catalytic Control of Emissions from Cars." *Catalysis Today* 163.1 (2011): 33-41.

[8] "Dangerous to Breathe: Why EPA needs to protect us from Coarse Particles." *American Lung Association, (Anonymous,* 2011)

[9] Heck, Ronald M. Catalytic Air Pollution Control Commercial Technology Book. Wiley, 2009

[10] US EPA, "Health Assessment Document for Diesel Engine Exhaust." 2002.

[11] Tankersley, Jim "U.S. to limit greenhouse gas emissions from autos" Los Angeles Times, May 2009

[12] Bosch GmbH, Robert. *Diesel-engine Management*. Robert Bosch GmbH, 2005. "Heavy-Duty Highway Compression-Ignition Engines And Urban Buses -- Exhaust Emission Standards." *EPA*. Environmental Protection Agency, 17 Oct. 2012.

[13] Fogler, H. Scott. *Elements of Chemical Reaction Engineering*.: Prentice Hall PTR, 2006.

[14] Katare, Sathoji R. "A hybrid framework for modeling aftertreatment systems: A Diesel Oxidation Catalytst Application." *SAE Paper 2006-01-0689*, 2006

[15] Farrauto, Robert J. “Catalytic Converters: State of the art and perspectives.” Catalysis Today 51 (1999): 351-360

[16] Katare, Sathoji R. “Aged DOC is a net consumer of NO2: analyses of vehicle, engine-dynamometer and reactor data.” *SAE Paper 2007-01-3684*, 2007

[17] Kim, Chang H. & Schmid, Michelle. “The effect of Pt-Pd Ratio on Oxidation Catalysts Under Simulated Diesel Exhaust.” *SAE Paper 2011-01-1134*, 2011

[18] Johnson, Jon E. & Kittelson, David B. “Physical factors affecting hydrocarbon oxidation in a diesel oxidation catalyst.” *SAE Paper 941771*, 1994.

[19] Tamaru, Kenzi & Mills, G. Alexander. “Chapter 8: Catalysts for control of exhaust emissions.” *Catalysis Today*, 22 (1994): 349-360.

[20] Clerc, James C. “Catalytic diesel exhaust aftertreatment.” *Aplied Catalysis B: Environmental*, 10 (1996): 99-115.

[21] “Fine particulate air pollution responsible for 9,000 premature deaths in California each year.” California Air Resources Board (CARB), August 2010

[22] Yamaguchi, S., Fujii, S., Kai, R., Miyazaki, M. et al., "Design Optimization of Wall Flow Type Catalyzed Cordierite Particulate Filter for Heavy Duty Diesel," *SAE Paper 2005-01-0666*, 2005.

[23] Mayer, A., Ulrich, A., Heeb, N., Czerwinski, J. et al., "Particle Filter Properties after 2000 hrs Real World Operation," *SAE Paper 2008-01-0332*, 2008.

[24] Lee, J., Kwon, C., Kim, S., & Yeo, G., "Control of Diesel Catalyzed Particulate Filter System I (The CPF System Influence Assessment According to a Regeneration Condition)," *SAE Paper 2005-01-0661*, 2005.

[25] “Controlling Bus Emissions.” Calgary Transit.

[26] Wang, T. J., Baek, S. W., & Kim, S. J. "Re-evaluation of the Nusselt Number for Determining the Interfacial Heat and Mass Transfer Coefficients in a Flow-through Monolithic Catalytic Converter." *Chemical Engineering Science* 63 (2008): 3152-3159.

[27] Andersson, J., Antonsson, M., Eurenius, L., Olsson, E. et al., Deactivation of diesel oxidation catalyst: Vehicle – and synthetic aging correlations.” Applied Catalysis B: Environmental, 72 (2007): 71-81.

[28] Willems, F., Cloudt, R., van den Eijnden, E., van Genderen, M. et al., "Is Closed-Loop SCR Control Required to Meet Future Emission Targets?," SAE Paper 2007-01-1574, 2007.

[29] Seher, D., Reichelt, M., and Wickert, S., "Control Strategy for NOx - Emission Reduction with SCR," SAE Paper 2003-01-3362, 2003 .

[30] Van Helden, R., Verbeek, R., Willems, F., & van der Welle, R., "Optimization of Urea SCR deNOx Systems for HD Diesel Engines," SAE Paper 2004-01-0154, 2004.

[31] Devarakonda, M., Parker, G., Johnson, J., Strots, V. et al., "Model-Based Estimation and Control System Development in a Urea-SCR Aftertreatment System," *SAE Int. J. Fuels Lubr.* 1(1):646-661, 2009.

[32] Hsieh, M. F. & Wang, J., "NO And NO2 Concentration Modeling and Observer-Based Estimation Across a Diesel Engine Aftertreatment System," *ASME Journal of Dynamic Systems, Measurement and Control* 133/041005-1, 2011

[33] Fogler, H. Scott. *Elements of Chemical Reaction Engineering*. Prentice Hall PTR, 2006.

[34] Katare, S., Patterson, J., and Laing, P., "Aged DOC is a Net Consumer of NO_2: Analyses of Vehicle, Engine-dynamometer and Reactor Data," SAE Paper 2007-01-3984, 2007.

[35] Wiebenga, M. H., Kim, C. H., Schmieg, S. J., Oh, S. H. et al., "Deactivation mechanism of Pt/Pd-based Diesel Oxidation Catalyst," *Catalyst Today* 184: 197-204 (2012)

[36] Hauff, K., Tuttlies, U., Eigenberger, G., & Nieken, U., "A global description of DOC kinetics for catalysts with different platinum loadings and aging status," Applied Catalysis B: Environmental 100: 10-18, 2010.

[37] Sampara, C. S., Bissett, E. J., & Chmielewski, M., "Global kinetics for a Comercial Diesel Oxidation Catalyst with Two Exhaust Hydrocarbons," I*nd. Eng. Chem. Res.* 47: 311-322, 2008

[38] Beck, D. "A Study of Thermal Aging of Pt/Al2O3 Using Temperature-programmed Desorption Spectroscopy." *Journal of Catalysis* 110.2: 285-97, 1988.

[39] Schultz, R., "Light-Off Temperature Shift as a Detection Method of Catalyzed Diesel Particulate Filter Nonmethane Hydrocarbon Oxidation Efficiency Degradation," Unpublished M.S. Thesis. University of Purdue, 2010.

[40] Depcik, C., and D. Assanis. "One-dimensional Automotive Catalyst Modeling." *Progress in Energy and Combustion Science* 31.4: 308-69, 2005.

[41] Incropera, Frank P. *Fundamentals of Heat and Mass Transfer.* John Wiley, 2007.

[42] Li, J., Szailer, T., Watts, A., Currier, N. et al., "Investigation of the Impact of Real-World Aging on Diesel Oxidation Catalysts," *SAE Int. J. Engines* 5(3):985-994.

[44] Sampara, C. S., Bissett, E. J., Assanis, D., "Hydrocarbon storage modeling for diesel oxidation catalysts," Chemical Engineering Science 63 (2008): 5179-5192.

[45] Schultz, R. and Meckl, P., "Light-Off Temperature Shift for Catalyzed Diesel Particulate Filter On-Board Diagnostics," SAE Paper 2012-01-1248.

[46] Sutjiono, R., "Real-Time On-Board Indirect Light-Off Temperature Estimation as a Detection Technique of Diesel Oxidation Catalyst Effectiveness Level", Unpublished M.S. Thesis. Purdue University, 2012.

[47] Katare, S. R., Patterson J. E., Laing, P. M. (2007), "Diesel Aftertreatment Modeling: A Systems Approach to NO_x Control", *Ind. Chem. Res.* , 46, 2445-2454

[48] Zhou, K., "NO and NO_2 Modeling for Diesel Oxidation Catalyst at Different Thermal Aging Levels", Unpublished M.S. Thesis, Purdue University, 2014.

[49] Sutjiono, R., Tayal, P., Zhou, K., and Meckl, P., "Real-Time On-Board Indirect Light-Off Temperature Estimation as a Detection Technique of Diesel Oxidation Catalyst Effectiveness Level," SAE Technical Paper 2013-01-1517, 2013, doi:10.4271/2013-01-1517.

[50] Bernhard, A. M., Peitz D., Elsener, M. et. al. (2012), "Hydrolysis and thermolysis of urea and its decomposition byproducts biuret, cyanuric acid and melamine over anatase TiO_2", *Applied Catalysis B: Environmental*, 115-116 (129-137).

[51] Kolli, T., Kanerva, T., Lappalainen, P. et. Al. (2009), "The Effect of SO_2 and H_2O on the activity of Pd/CeO_2 and $Pd/Zr\text{-}CeO_2$ Diesel Oxidation Catalysts", *Topics in Catalysis*, 52(13-20), pp. 2025-2028.

[52] Bergeld, J., Kasemo, B., Chakarov, D. V. (2001), "CO Oxidation on Pt(111) promoted by coadsorbed H_2O". *Surface Science, 495*(3), pp. L815-L820.